2004

Effects of emphysema and chronic hypoxemia on skeletal muscle oxygen supply and demand

John D. Lowman Jr.
Virginia Commonwealth University

Virginia Commonwealth University

Medical College of Virginia Campus

School of Medicine

This is to certify that the dissertation prepared by John D. Lowman Jr., entitled “Effects of emphysema and chronic hypoxemia on skeletal muscle oxygen supply and demand,” has been approved by his committee as satisfactory completion of the dissertation requirement for the degree of Doctor of Philosophy.

_____

Roland N. Pittman, Ph.D., Dissertation Advisor, School of Medicine

_____

Mary Snyder Shall, Ph.D., P.T., School of Allied Health Professions

_____

Robert W. Barbee, Ph.D., School of Medicine

_____

Joseph J. Feher, Ph.D., School of Medicine

_____

Ross A. Arena, Ph.D., P.T., School of Allied Health Professions

_____

Margaret C. Biber, D.Phil., Physiology Department Chair, School of Medicine

_____

H. H. Newsome Jr., M.D., Dean, School of Medicine

_____

F. Douglas Boudinot, Ph.D., Dean, School of Graduate Studies

_____

Date

Effects of emphysema and chronic hypoxemia on skeletal muscle oxygen supply and demand

A dissertation submitted in partial fulfillment of the requirements
for the
Doctor of Philosophy degree
at the
Medical College of Virginia Campus,
Virginia Commonwealth University

by

John D. Lowman Jr.
M.S., Duke University, 1995
B.S.Ed., Virginia Tech, 1993

Advisor
Roland N. Pittman, Ph.D.
Professor
Department of Physiology

Virginia Commonwealth University
Richmond, Virginia
December 10, 2004

Dedication

This "product" of the last four and one-half years is dedicated to my wife, *Mary Elizabeth Lindsay (Beth)*, without whom I may neither have started nor finished this program. She has spent half of our married life with me as a full-time student at VCU, and she has been with me every step of the way. In every sense, this has been a collaborative effort.

Her support has been direct and indirect, physical and spiritual, fiscal and emotional. She quizzed me with biochemistry flash cards, and proof-read my papers; she took notes during experiments, chopped and ground up muscles, and pippetted muscle samples until her thumb was sore. She helped clean up the lab and equipment after my experiments. She brought me lunch in the lab on the weekend and dinners in the lab at night, and always made sure I had food and drinks in the fridge when she was out of town. She got me out of bed when I needed to leave for the lab at 5 am, and was often entering my hard-copy data into Excel and Access before I even got out of bed in the morning. She let me study when I needed to study and made me take breaks when I was too stubborn to admit that I needed one. Most importantly, despite all the new knowledge, skills and techniques I was learning, she always made sure that I didn't forget the important things in life. She is the kindest, most thoughtful person I know. She is a blessing to my life; she is my best friend.

Acknowledgements

I was attracted to Virginia Commonwealth University (VCU) because of *Dr. Roland N. Pittman's* extensive work and reputation in the field of skeletal muscle microcirculatory physiology. Since joining his lab four years ago, I have continually been impressed by his expertise, but especially by his teaching and mentoring style; he makes difficult concepts clear and understandable, and makes me feel as if I came up with the answer on my own. His door is always open, and he is happy and eager to address my questions and concerns. His mentoring style has encouraged my self-discovery and independence of thought. All of the professional encomiums that have been bestowed upon him cannot adequately express what he has done for me and others. Any success I have in academia will be in large part due to his tutelage, and I hope that I will be able to model his scientific and personal attributes.

Dr. Aleksander S. Golub has continually instructed, encouraged and assisted me since I joined Dr. Pittman's lab. His theoretical and practical knowledge of all-things-science inspires me to continually learn and never settle for the status quo. Much of the data colleted and analyzed for this study would not have been possible without his technical expertise and guidance.

Dr. Mary Snyder Shall welcomed me into her lab when I expressed an interest in classifying my muscles using both molecular biological and histological techniques. She, as well as her technician, *Shelley Jordan*, and graduate student, *Susan Van Cleave*, supported me with their knowledge, laboratory space and supplies, and patiently taught me many new techniques.

Dr. R. Wayne Barbee seemed to have all the right answers whenever I had issues related to either equipment or animal experimentation; without some of his suggestions, I might still be scratching my head. He and Dr. Ivo Torres also provided advice and consolation with regard to the presumed Rat respiratory virus affecting my animals.

Dr. Helena de Carvalho graciously shared her time, talents, and expertise with me. She patiently taught me most of what I know about animal care and handling, as well as how to perform invasive surgical cannulations and phosphorescence quenching microscopy P_{O_2} measurements.

Drs. Lane M. Smith and *Luciana N. Torres* taught me how to perform the rat spinotrapezius muscle preparation.

Dr. David C. Poole, Kansas State University, and *Dr. Gloria D. Massaro*, Georgetown University, provided technical advice regarding the elastase-instillation procedure for

inducing emphysema. Dr. Poole also provided technical expertise concerning spinotrapezius muscle force measurements.

Mike A. Tevald, a fellow graduate student of Dr. Pittman's, contributed to this study in many ways. Collaboratively, we learned new experimental techniques, designed and built or configured essential hardware and software, and even learned (or re-learned) some basic mathematics. In addition, he provided statistical consultation and editorial assistance. I expect our collaboration on like-minded projects will continue well after we leave VCU.

While Dr. Pittman's reputation attracted me to VCU's Department of Physiology, *Debbie Bohn's* cheerful spirit and helpfulness during our interstate telephone conversations during the admissions process assured me that this was a place I could spend the next four years. After matriculating here, I was not disappointed; Debbie's warm heart and friendly smile have made it a pleasure to study and work here; I will truly miss her when I leave.

Sally Brown's work behind the scenes has limited the financial concern of leaving a professional career to return to school full time. Her personal concern and sense professional duty were greatly appreciated.

Rishi Sood saved me countless hours by analyzing near all of the phosphorescence quenching microscopy microvascular P_{O_2} data. Without his help, I might still be analyzing this data.

Patty Gerber and *Dr. Ervin Baas* of VCU's Division of Animal Resources provided the knowledge, skill, and expertise required to perform the radiographic studies used in my project. *Dr. Baas* and *Dr. Mario E. Dance* also helped me try to resolve a string of experimental deaths and performed many necropsies of my sick animals.

Financial support for this study was provided in part by a Promotion of Doctoral Studies II scholarship by *The Foundation for Physical Therapy*, as well as by Dr. Pittman's VCU *A.D. Williams Fund Research Award*.

Table of Contents

Page

List of Tables

Page

List of Figures

Page

List of Abbreviations

2,3-DPG	2,3-diphosphoglycerate
α	aperture, or vertex angle
α_{O_2}	solubility coefficient for oxygen
A	1) surface area, or 2) fraction of the observed signal due to phosphorescence
ABG	arterial blood gas
AC	alternating current
ANOVA	analysis of variance
AP	systemic arterial pressure
ATP	adenosine triphosphate
ATPase	adenosine triphosphatase
B	bluntness profile
BE	base excess
bpm	1) breaths per minute, or 2) beats per minute
BSA	bovine serum albumin
C	Celsius
C/F ratio	capillary-to-fiber ratio
Ca^{+2}	calcium ion
CaO_2	oxygen content of arterial/arteriolar blood
CD	capillary density

C_{Hb}	oxygen binding capacity of hemoglobin
Cl^-	chloride ion
cm	centimeter
cmH_2O	centimeters of water
COHb	carboxyhemoglobin
COPD	chronic obstructive pulmonary disease
CS	citrate synthase
CSA	cross-sectional area
Cv_{O_2}	oxygen content of venous/venular blood
CVP	central venous pressure
d	diameter
D	depth of field
DC	direct current
DCLP	dichroic, long pass
deoxy-Hb	fraction of available hemoglobin to which oxygen is not bound
dl	deciliter
DMSO	Dimethyl sulfoxide
D_{O_2}	diffusion coefficient for oxygen
$\dot{D}_{O_2}$	tissue oxygen delivery
δ	half-width of the rectangular distribution of oxygen
ETT	endotracheal tube
F	force

FCSA	fiber cross-sectional area
FF	fast-twitch, fatigable
FG	fast-twitch glycolytic
FI	1) fast-twitch, intermediate fatigability, or 2) fatigue index
$F_{I_{O_2}}$	fraction of inspired oxygen
FOG	fast-twitch oxidative, glycolytic
FR	fast-twitch, fatigue resistant
FTI	force-time integal
g	gram
G	acceleration of gravity
H^+	hydrogen ion
H_2O	water
Hb	hemoglobin
[Hb]	concentration of hemoglobin
HCO_3	bicarbonate
hr	hour
Hz	hertz
i.e.	*id est*, that is
i.v.	intravenous
K^+	potassium ion
kDa	kilodalton
kg	kilogram

k_q	quenching coefficient of Pd-MTCPP
kV	kilovolt
λ	emission wavelength
l	liter
L_o	optimal muscle length
m	mass
m.	muscle
mA	milliamp
Mb	myoglobin
meq	milliequivalent
MetHb	methemoglobin
mg	milligram
MHC	myosin heavy chain
min	minutes
ml	milliliter
mm	millimeter
mmHg	millimeter meters of mercury
mmol	millimoles
msec	millisecond
mV	millivolt
n	1) Hill coefficient, 2) refractive index of water, or 3) number
N	Newtons

N.A.	numerical aperture
Na^+	sodium ion
nl	nanoliter
nm	nanometer
Ω	ohms
O_2	oxygen
OD	optical density
oxy-Hb	fraction of available hemoglobin bound to oxygen
P_{50}	partial pressure of oxygen at a S_{O_2} of 0.50
PAGE	polyacrylamide gel electrophoresis
Pa_{O_2}	partial pressure of arterial oxygen
Pb	barometric pressure
P_B	barometric pressure
PBS	phosphate buffered saline
PC	personal computer
P_{CO_2}	partial pressure of carbon dioxide
Pd-MTCPP	palladium meso-tetra (4-carboxylphenyl) porphyrin
PE	polyethylene
PFK	phosphofructokinase
$P_{I_{O_2}}$	partial pressure of inspired oxygen
P_{O_2}	partial pressure of oxygen
P_{O_2}	partial pressure of oxygen

ΔP_{O_2}	partial pressure difference of oxygen
PVP	polyvinyl pyrrolidone
$\dot{Q}$	cardiac output (total blood flow)
$\dot{Q}_{O_2}^{C}$	convective oxygen delivery
$\dot{Q}_{O_2}^{D}$	diffusive oxygen delivery
$\dot{Q}^{ST}$	spinotrapezius blood flow
$\dot{Q}_{a}^{ST}$	spinotrapezius arteriolar blood flow
$\dot{Q}_{v}^{ST}$	spinotrapezius venular blood flow
ρ	density
r	correlation coefficient
r^2	ratio of regression variance to total variance
r	1) radius, or 2) radial distance from the longitudinal axis of the vessel
Δr	radial diffusion distance
R	vessel radius
R_0	longitudinal axis of the vessel
RBC	red blood cell
RR	respiratory rate
RRV	Rat respiratory virus
S	slow-twitch, fatigue resistant
SD	standard deviation
SDS	sodium dodecyl sulfate

sec	seconds
sinh	hyperbolic sine function
SO	slow-twitch oxidative
S_{O_2}	fractional oxygen saturation of hemoglobin
ST	Spinotrapezius muscle
τ	phosphorescence lifetime
τ_0	phosphorescence lifetime in the absence of oxygen
τ_F	flash artifact lifetime
t	time
tHB	total hemoglobin concentration
T_m	muscle temperature
µg	microgram
µl	microliter
µm	micrometer
µs	microsecond
V	volts
VCR	video cassette recorder
VD	ventral dorsal
v_0	maximal blood velocity
v_p	particle velocity
$\bar{v}$	mean blood velocity
vs.	versus

$\dot{V}_{O_2}$	oxygen consumption
$\dot{V}_{O_2}^{ST}$	spinotrapezius muscle oxygen consumption
$\bar{x}$	mean
W	1) middle one-third of vessel width, or 2) work
W	watts

Abstract

EFFECTS OF EMPHYSEMA AND CHRONIC HYPOXEMIA ON SKELETAL MUSCLE OXYGEN SUPPLY AND DEMAND

By John D. Lowman Jr., Ph.D., P.T., C.C.S.

A dissertation submitted in partial fulfillment of the requirements for the Doctor of Philosophy degree at the Medical College of Virginia Campus, Virginia Commonwealth University.

Virginia Commonwealth University, 2004

Major Director: Dr. Roland N. Pittman, Professor, Department of Physiology

Skeletal muscle dysfunction in chronic obstructive pulmonary disease (COPD) is a condition in which peripheral skeletal muscle undergoes myopathic changes which impair muscle function, limit physical performance, and can lead to significant disability. While the etiology of the dysfunction is unknown, this study was conducted to test the hypothesis that chronic hypoxemia leads to alterations in oxygen transport and muscle function. A primary objective was to validate elastase-induced emphysema in rats as an animal model of skeletal muscle dysfunction in COPD.

Arterial blood gases were used to determine the severity of hypoxemia and sodium dodecyl sulfate- polyacrylamide gel electrophoresis was used to determine the proportions of myosin heavy chain isoforms I, IIa, IIx, and IIb. Measures of

microvascular oxygenation and blood flow in the spinotrapezius muscle allowed for determination of both convective and diffusive oxygen supply to the muscle, as well as calculation of muscle oxygen consumption at rest and during electrically stimulated three-minute muscle contractions. Muscle performance measures included peak force, force-time integral, and fatigue index.

Due to a presumed rat respiratory virus, which likely resulted in the control group being nearly as hypoxemic as the elastase-induced emphysema group, this study was not able to definitively test the hypothesis that chronic hypoxemia leads to both a diminished supply and demand of oxygen in skeletal muscle. Although many of the results of the present study were not statistically significant, they exhibited consistent trends over time and are likely of physiological significance. All measures of muscle performance were lower in the emphysema group. In addition, spinotrapezius muscle oxygen consumption and blood flow were lower in the emphysema group. The addition of supplemental oxygen during isolated, small-muscle mass exercise did increase the force-time integral by ~18% in both groups, suggesting that muscle work in these hypoxemic animals may be limited by oxygen supply.

Thus, the data on muscle fiber type, oxygen consumption and muscle performance suggest that elastase-induced emphysema in rats leads to a similar skeletal muscle dysfunction that is observed in humans with COPD, and indicates that it is a valid animal model of skeletal muscle dysfunction in COPD.

Introduction

COPD: definition and epidemiology

Chronic obstructive pulmonary disease (COPD), an umbrella term that primarily refers to *emphysema* and *chronic bronchitis* (West 1997), is the fourth leading cause of death in the U.S. (Anderson 2001), accounts for 1.7% of ambulatory care visits (NCHS 1999), and costs an estimated $30.4 billion per year (ALA 2001). While the overall death rate in the past 20 years has decreased 18%, COPD mortality has increased 42% (ALA 2001). The death rate is even higher in mountainous high-altitude states where the partial pressure of inspired oxygen ($P_{I_{O_2}}$) is lower (Anderson 2001); however, oxygen therapy, which increases $P_{I_{O_2}}$, also increases exercise tolerance and quality of life, and decreases dyspnea (shortness of breath) and mortality in chronically hypoxemic patients (NOTTG 1980; Eaton, Garrett et al. 2002).

Hypoxia vs. hypoxemia: definition and causes

Hypoxia refers to low oxygen (O_2) levels in general, and is often preceded by adjectives that describe its location: alveolar hypoxia, tissue hypoxia, or cellular hypoxia. Cellular hypoxia is functionally defined as the failure of convective or diffusive O_2 transport to meet the O_2 demand such that the rate of adenosine triphosphate (ATP) synthesis is

limited. Hypoxia can also be defined in terms of its etiology: 1) ischemic hypoxia, due to blood-flow limitations, 2) anemic hypoxia, due to low hemoglobin concentrations, 3) histotoxic or cytotoxic hypoxia, due to chemical poisoning of the cell, and 4) hypoxic hypoxia, due to *hypoxemia* (Schumacker 1991).

Specifically, hypoxemia refers to a decreased *arterial* oxygen partial pressure (Pa_{O_2}) below the normal range (80-100 mmHg) (Pierson 2000). Obviously, hypoxemia can be a cause of tissue or cellular hypoxia. Hypoxemia can be caused by: 1) hypoventilation, 2) impaired diffusion across the alveolar blood-gas barrier, 3) ventilation-perfusion mismatch, 4) intrapulmonary shunt, or 5) breathing a reduced $P_{I_{O_2}}$ (West 1997).

Clinically, acute hypoxemia refers to a short-term (minutes to days), reversible cause of hypoxemia (*i.e.*, a patient recovering from pneumonia or anesthesia), while chronic hypoxemia is a longer-term process (days to decades) and the cause is usually irreversible (*i.e.*, a patient with COPD or pulmonary fibrosis). Chronic hypoxemia in COPD is primarily caused by ventilation-perfusion mismatch (ventilation of under perfused lung tissue and/or perfusion of under ventilated lung tissue), but also by impaired diffusion (decreased surface area available for gas exchange due to destruction of alveoli) and hypoventilation (decreased minute ventilation due to an increased work of breathing) (West 1998).

Research on "chronic hypoxia" is usually based on human or animal studies lasting less than three months, what I shall refer to as "short-term chronic hypoxia." Studies using

patients with COPD or permanent high-altitude residents will be referred to as "long-term chronic hypoxia." In most of these studies, the term *hypoxia* is used as opposed to *hypoxemia*, because there were no measures to verify a low Pa_{O_2}.

Skeletal muscle dysfunction in COPD

COPD results not only in impaired pulmonary function, but also well known cardiovascular sequelae: pulmonary hypertension and right ventricular hypertrophy. In addition, there are more poorly understood secondary effects on skeletal muscle, such as impaired muscle strength and endurance. These impairments result in dyspnea (shortness of breath), leg fatigue, and poor exercise tolerance (Zattara-Hartmann, Badier et al. 1995; Serres, Gautier et al. 1998), and are the symptoms of the emerging syndrome "Skeletal muscle dysfunction in COPD" (ATS/ERS 1999).

Skeletal muscle dysfunction in COPD is a debilitating disease that often leaves patients anxious, homebound, and depressed because of their poor tolerance for physical activity, including basic activities of daily living. A significant amount of research has focused on characterizing this syndrome over the last 25 years, much of which will be reviewed subsequently. The etiology of skeletal muscle dysfunction in COPD is unknown, but the most likely causes include hypercapnia, inflammation, malnutrition, deconditioning (decline in physical performance due to inactivity), and hypoxemia. The evidence seems to favor deconditioning and/or hypoxemia (Richardson 1999), but uncoupling the two has proved difficult in human studies.

Oxygen transport in normal skeletal muscle

Oxygen transport to skeletal muscle by blood is regulated by adjusting *O_2 supply* (cardiac output, blood flow distribution, and the O_2 capacity of the blood) to the *O_2 demand* (metabolic consumption) of the muscle (Weibel 1984). As far as O_2 supply goes, I will focus on blood flow distribution to and in skeletal muscle, and O_2 capacity of the blood; for the current discussion it is sufficient to say that cardiac output generally increases as oxygen consumption increases.

Oxygen supply

Oxygen supply, or delivery, consists of both convective and diffusive flow of O_2. *Convective delivery* refers to the bulk flow of O_2 bound to hemoglobin (Hb) in red blood cells (RBCs) from the lung's microvascular network (O_2 source) to the muscle's microvascular network via the cardiovascular system, while *diffusive delivery* refers to the flux of O_2 out of the RBCs in the microcirculation to the mitochondria (O_2 sink) in the muscle fibers (Pittman 2000).

Convective O_2 delivery

Based on Fick's Principle, whole body convective O_2 delivery ($\dot{Q}_{O_2}^{C}$) is:

Equation 1

$$\dot{Q}_{O_2}^{C} = \dot{Q} \cdot Cao_2$$

where $\dot{Q}$ is total blood flow (cardiac output) and Cao_2 is arterial O_2 content (Pittman 2000). Tissue perfusion, and thus convective O_2 delivery, is regulated by both total blood flow and blood flow distribution. Altering blood flow distribution in response to changes in local metabolism allows the fraction of cardiac output increase to metabolically active tissues, while shunting blood away from less metabolically active tissue, and is altered by modulating vascular resistance, which is under both neural and local regulation (Weibel 1984).

Diffusive O_2 delivery

Diffusive O_2 delivery ($\dot{Q}^D_{O_2}$) is related to convective O_2 delivery ($\dot{Q}^C_{O_2}$) by:

Equation 2

$$\dot{Q}^D_{O_2} = \dot{Q}^C_{O_2(in)} - \dot{Q}^C_{O_2(out)}$$

where $\dot{Q}^C_{O_2(in)}$ and $\dot{Q}^C_{O_2(out)}$ are the convective flow of O_2 into and out of the muscle tissue, respectively (Pittman 2000). Equation 2 is related to Fick's first law of diffusion that can be expressed as:

Equation 3

$$\dot{Q}^D_{O_2} = Do_2 \cdot \alpha o_2 \cdot A \cdot \Delta Po_2 / \Delta r$$

where Do_2 and αo_2 are the diffusion and solubility coefficients for oxygen, A is the available surface area for diffusion, and $\Delta Po_2 / \Delta r$ is the radial P_{O_2} gradient (Pittman

2000). As indicted by Equation 3, O_2 will diffuse from one site to another provided the driving force (ΔP_{O_2} = blood P_{O_2} – intracellular P_{O_2}) is large enough and the diffusion distance (Δr) is not too great. In fact, contrary to traditional views, Swain and Pittman (1989) calculated that, in the hamster retractor muscle, about ⅔ of $\dot{Q}_{O_2}^{D}$ occurs in the arterioles and about ⅓ in the capillaries.

D_{O_2} and α_{O_2} are relatively constant. However, if the number of perfused capillaries per muscle fiber area increases, then A increases and diffusion distance decreases, causing O_2 flux to increase. Diffusion distance can also be altered by changing the quantity and location (subsarcolemmal vs. intermyofibrillar) of mitochondria, the O_2 sink, in the muscle (Weibel 1984). The other way to increase O_2 flux is by increasing ΔP_{O_2}; this can occur by: 1) shifts in the oxy-hemoglobin (Hb-O_2) dissociation curve, 2) myoglobin facilitated diffusion, and 3) increased consumption (see next section: Oxygen demand).

The *Hb-O_2 dissociation curve* (Figure 1) can shift to the left or right by changes in 1) muscle temperature, 2) carbon dioxide tension/pressure (P_{CO_2}), 3) hydrogen ion concentration [H^+], and 4) 2,3-diphosphoglycerate concentration [2,3-DPG] (Berne and Levy 1998). Exercise, or muscular work, increases the first three of these factors, shifting the curve to the right, which facilitates a higher blood P_{O_2} for a given O_2 saturation (SO_2) of hemoglobin and enhances O_2 flux by increasing ΔP_{O_2}.

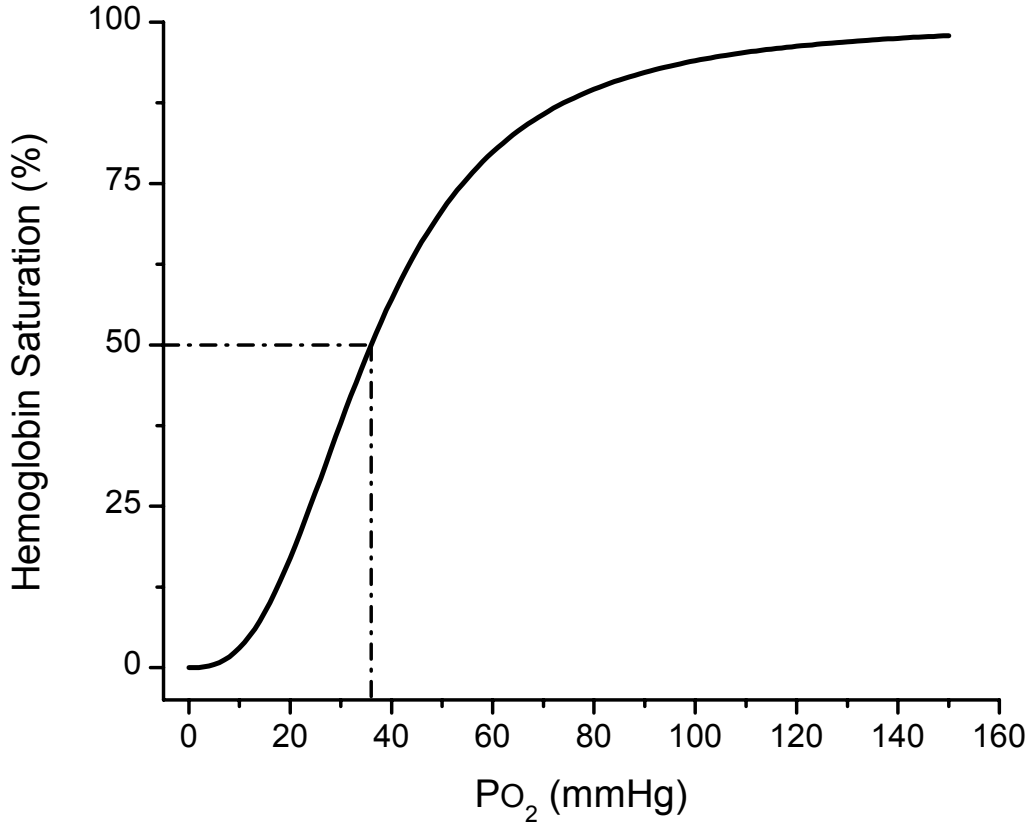

Figure 1. Hemoglobin-O_2 dissociation curve (P_{50} = 36 mmHg).

Myoglobin (Mb) facilitated diffusion increases O_2 flux by several mechanisms. By binding free O_2 inside the muscle fiber, myoglobin lowers subsarcolemmal P_{O_2}, thus increasing ΔP_{O_2} and enhancing O_2 flux. Myoglobin binding of O_2 inside the fiber decreases the diffusion distance for free O_2. Lastly, due to the shape of the Mb-O_2 dissociation curve (Figure 2) (Schenkman, Marble et al. 1997), myoglobin also buffers mitochondrial P_{O_2} by releasing bound O_2 as intracellular P_{O_2} decreases, which occurs during muscle contraction as O_2 is consumed, and intramuscular pressure compresses blood vessels and impairs convective O_2 supply (Honig, Gayeski et al. 1991).

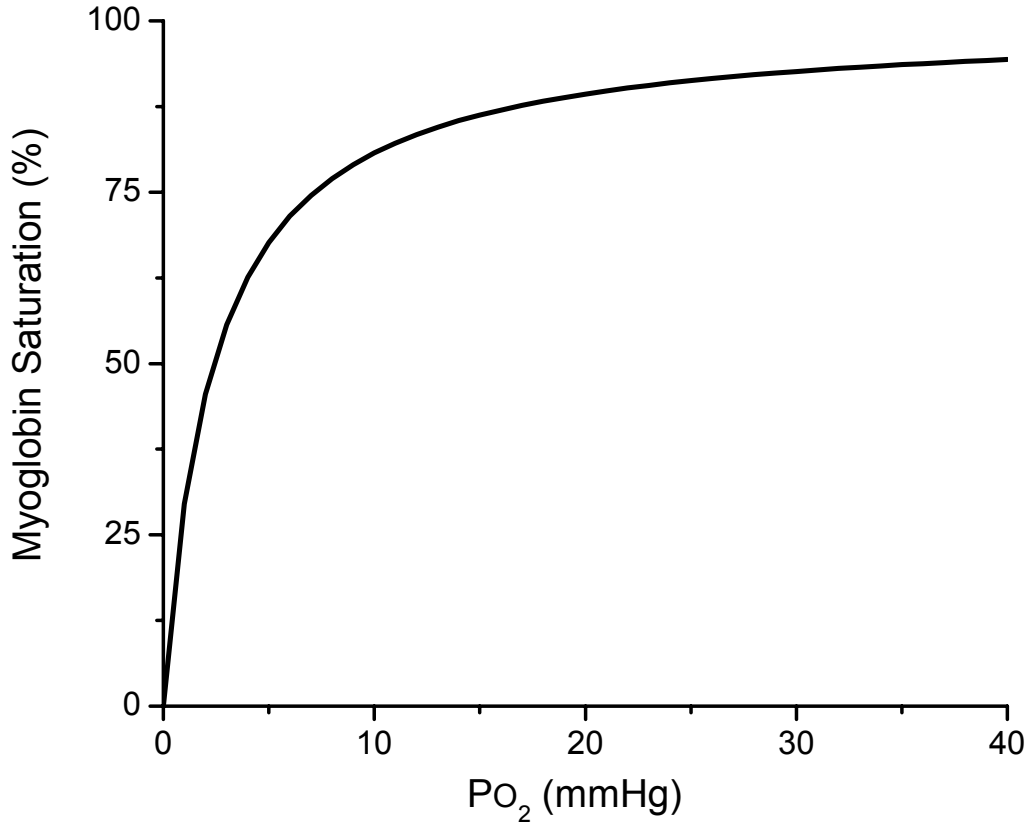

Figure 2. Myoglobin-O_2 dissociation curve (P_{50} = 2.4 mmHg).

Oxygen demand

Within the mitochondria, the process of oxidative phosphorylation consumes O_2 in proportion to the need to produce ATP and replenish high energy phosphate stores within the muscle. This O_2 consumption by the mitochondria depletes cellular O_2 stores, lowers intracellular P_{O_2}, increases ΔP_{O_2} and results in increased *O_2 demand*. In skeletal muscle, O_2 consumption ($\dot{V}_{O_2}$) can vary from 1.7 ml/min/kg at rest to over 70 ml/min/kg at $\dot{V}_{O_2\,max}$ (Weibel 1984; Aw and Jones 1990). This dramatic range of $\dot{V}_{O_2}$ requires complex regulation of the O_2 supply, but also provides a reserve capacity that is rarely utilized. Due to this large $\dot{V}_{O_2}$ reserve capacity as well as the ability of the muscle to increase oxygen extraction, minor impairments in O_2 supply do not pose a major threat to the organism under normal functional conditions (*i.e.*, the muscle tissue does not become hypoxic). However, a major impairment in O_2 supply (*i.e.*, chronic hypoxemia) does result in muscle tissue hypoxia, which has both cellular and systemic effects.

Effect of COPD and chronic hypoxemia on skeletal muscle

The effects of chronic hypoxemia on skeletal muscle are evident not only by cellular *changes* within the *muscle fibers* themselves, but also include systemic effects, including increased RBC production and *microvascular changes*. In the following literature review, hypoxemia is the result of either 1) chronic lung disease, or 2) reduced $P_{I_{O_2}}$. $P_{I_{O_2}}$ can be reduced by 1) lowering the fraction of inspired O_2 ($F_{I_{O_2}}$) below that of room air (0.21), and/or 2) decreasing the barometric pressure ((PB) hypobaric hypoxia); PB can be

lowered in the lab using a hypobaric chamber or in the field by going to high altitudes (normal $P_{I_{O_2}}$ of room air at sea level is 150 mmHg).

Muscle fiber changes

Muscle fiber type

Specific muscle fiber types have been classified using several schemes. One of the first was based on contractile speed (time-to-peak tension) and fatigability: slow-twitch, fatigue resistant (S), fast-twitch, fatigue resistant (FR), fast-twitch, intermediate fatigability (FI), and fast-twitch, fatigable (FF) (Burke, Levine et al. 1971). There are two histochemical methods, one based on metabolic enzyme staining: slow-twitch oxidative (SO), fast-twitch oxidative, glycolytic (FOG), and fast-twitch glycolytic (FG) (Peter, Barnard et al. 1972), and the other based on pH lability of myofibrillar adenosine triphosphatase (ATPase) staining: I, IIa, IIx, and IIb (Brooke and Kaiser 1970). More recently, myosin heavy chain (MHC) immunoreactivity has been developed using specific antibodies for different MHC isoforms: I, IIa, IIx, and IIb (Termin, Staron et al. 1989). Refer to Table 1 for a summary of how the classifications schemes compare.

Table 1. Muscle-fiber type classification schemes.

Classification Scheme	Muscle-Fiber Type			
Twitch	S	FR	FI	FF
Metabolic	SO	FOG		FG
ATPase	I	IIa	IIx	IIb
MHC	I	IIa	IIx	IIb

modified from ATS/ERS (1999)

The proportion of muscle fiber types from the vastus lateralis muscle of *asymptomatic* elderly men is: 48% type I, 34% type IIa, and 17% type IIb. It varies slightly for women: 54% type I, 41% type IIa, and 7% type IIb, but was only significantly different for type IIb (due to rounding, these values total slightly more or less than 100%) (Aniansson, Grimby et al. 1981). These numbers serve as reference values for the ensuing discussion of fiber types in COPD, primarily a disease of the aged.

In a group of 18 patients with advanced COPD, with and without hypercapnia (Pa_{CO_2} > 40 mmHg), Jakobsson *et al* (1990) looked at the percentage of type I muscle fibers in the vastus lateralis and found that patients with and without hypercapnia had abnormally low percentages of type I fibers, 17 and 22% respectively, which were positively correlated to Pa_{O_2}, 58 and 78 mmHg, respectively, and were more than 50% lower than reference values. A similar finding of decreased proportion of type I fibers, 29%, was found in nine patients with a Pa_{O_2} of 63 mmHg (Hildebrand, Sylven et al. 1991). More recently, Satta *et al* (1997) used the MHC classification in 22 borderline hypoxemic (mean Pa_{O_2} = 81 mmHg) patients with COPD (mean age 65). They reported a fiber transformation from MHC I to MHC II_{2A} to MHC_{2B}, and in particular report a MHC_{2B} proportion of 23% versus 7% for their control group (mean age 35). Using age matched controls (mean age 65), Whittom *et al* (1998) also reported reduced type I and increased type IIb fibers in patients with COPD. Even following lung transplantation (mean postoperative months = 12, range 3 to 24), essentially curing hypoxemia, patients continue to have a lower proportion of type I fibers, 25% vs. 56% for control (Wang, Williams et al. 1999).

Contrary to the consistent evidence of fiber type transformation in patients with COPD, the data are less conclusive regarding normal subjects exposed to hypobaric hypoxia. A study of permanent, high-altitude residents (P_{IO_2} ~90 mmHg), who did not regularly exercise, found normal fiber type proportions: type I 50.8%, type IIa 30.3%, type IIb 15.4%, and 2.9% type IIab (Desplanches, Hoppeler et al. 1996). Green *et al* studied mountaineers exposed to eight weeks of high altitude (5,000-8,484 m; P_{IO_2} = 43-78 mmHg) and saw no change in fiber-type distribution (Green, Sutton et al. 1989). However, in a later study he reported a 12% decrease in type I and a corresponding increase in type IIa and IIb fibers following only three weeks at 4,300 m (P_{IO_2} = 88 mmHg) (Green, Sutton et al. 1992).

Animal models of hypoxia are not conclusive either. Although Itoh *et al* (1990) found a decrease in type I and increase in type II muscle fibers of rats exposed to 10 weeks at 4,000 m (P_{IO_2} = 91 mmHg), Takahashi *et al* (1992) saw no fiber type transformation in rats exposed to P_{IO_2} of 71 mmHg for four weeks, a relatively short hypoxic period. van Ekeren *et al* (1992), using a more pronounced hypoxia (P_{IO_2} = 57 mmHg) in rats for almost seven weeks, also reported no change in fiber type proportions.

Muscle mass/Cross sectional area

Muscle tissue mass and fiber cross-sectional area (FCSA) provide indices of muscle force production or strength (Lieber 1992). Since a loss in lower extremity strength is a hallmark of skeletal muscle dysfunction in COPD (Hamilton, Killian et al. 1995; Zattara-

Hartmann, Badier et al. 1995), measurement of FCSA from vastus lateralis muscle biopsies in chronically hypoxemic patients provides a reliable index of muscle fiber atrophy.

Several studies found decreases in FCSA in patients with COPD (Hughes, Katz et al. 1983; Whittom, Jobin et al. 1998). Compared to age matched controls, Whittom reported a 36% smaller FCSA for type I fibers, an 18% decrease for type IIa, and no difference in type IIb.

Although some report no change in FCSA of human muscle in response to three weeks of hypobaric hypoxia (Green, Sutton et al. 1992), muscle fiber atrophy appears to be a consistent finding in most studies. Following up to two months at altitudes greater than 5,000 m ($P_{I_{O_2}} < 78$ mmHg), several investigators report a 20-25% decrease in both type I and type II muscle FCSA (Green, Sutton et al. 1989; Hoppeler, Kleinert et al. 1990; MacDougall, Green et al. 1991; Waynforth and Flecknell 1992).

Additional studies validate muscle atrophy as well as impaired hypertrophy in response to training under hypoxic conditions. Rats exposed to $P_{I_{O_2}}$ of 57 mmHg for 45 days had a decrease in FCSA of both extensor and flexor lower extremity muscles (van Ekeren, Sengers et al. 1992). Narici and Kayser (1995) compared the effects of strength training for one month on hypertrophy in humans at sea level versus at 5,050 m ($P_{I_{O_2}}$ ~77 mmHg); although they used elbow flexors and nuclear magnetic resonance imaging to

measure cross sectional area, they found approximately 33% lower values for both strength and muscle hypertrophy in the subjects trained at altitude.

Muscle fiber constituents

Several muscle fiber constituents are altered during chronic hypoxemia. *Myoglobin* assists in the flux of O_2 into and within the cell. *Metabolic enzymes* in the muscle fiber serve to catabolize substrates (*i.e.*, glucose and fatty acids) and produce ATP; the fate of many intermediary products depends on the presence of O_2. Many of these metabolic processes take place within the *mitochondria*.

Myoglobin

Despite its role in the diffusive flux of O_2 from the microvasculature to the mitochondria, few studies have looked at myoglobin content in either COPD or chronic hypoxia. The one study of patients with COPD and hypoxemia found a decreased myoglobin concentration compared to healthy, age matched controls (Moller, Hellstrom et al. 1984). However, the soleus muscle of guinea pigs exposed to 5,100 m ($P_{I_{O_2}}$ = 78 mmHg) for 14 weeks had increased myoglobin content when matched for body mass to normoxic animals (Sillau, Aquin et al. 1980).

Metabolic enzymes

Several groups have looked at metabolic enzyme activity in the vastus lateralis muscle of humans exposed to hypobaric hypoxia (Green, Sutton et al. 1989; Howald, Pette et al.

1990; Green, Sutton et al. 1992), with COPD (Jakobsson, Jorfeldt et al. 1995; Maltais, Simard et al. 1996; Maltais, LeBlanc et al. 2000), or following lung transplantation (Wang, Williams et al. 1999). Table 2 summarizes these results. In the hypobaric hypoxia studies, the results are the percent change after exposure to ≥ 4,300 m for three to six weeks. The results of the COPD and lung transplantation groups are percent change compared to age matched controls. Of particular interest is the study by Maltais *et al* in 2000, which compared 57 patients with COPD to sedentary controls.

The consistent finding is that processes taking place in the mitochondria (β oxidation, citric acid cycle and oxidative phosphorylation) are either diminished or unchanged. In all cases citrate synthase, the rate limiting step of the citric acid cycle, was reduced by an average of ~32%. Evidence to substantiate an increase in glycolytic activity is less conclusive. However, a decrease in the citrate synthase/phosphofructokinase ratio does suggest a shift from aerobic to anaerobic production of ATP, presumably due to cellular hypoxia, or insufficient O_2 to support oxidative phosphorylation. It is unfortunate that only two of these studies also looked at mitochondrial volume density; however, Howald *et al* (1990) concluded that there was no enzymatic functional impairment, but the diminished enzymatic activity was due to the loss of mitochondrial volume.

Mitochondria

Rats exposed to P_{IO_2} 57 mmHg for almost seven weeks exhibited a decrease in subsarcolemmal mitochondrial volume density of both the soleus and extensor digitorum longus muscles; however, the intermyofibrillar mitochondrial volume density of the

soleus increased (van Ekeren, Sengers et al. 1992). When mountaineers were exposed to ≥ 5,300 m ($P_{I_{O_2}} \leq 75$ mmHg) for up to two months, both their subsarcolemmal and intermyofibrillar mitochondrial volume density had decreased 43 and 13%, respectively, a 26% overall decrease (Hoppeler, Kleinert et al. 1990). A 30% lower mitochondrial volume density has also been reported in young permanent high-altitude residents, 4,000 m ($P_{I_{O_2}} = 91$ mmHg), compared to age matched lowlanders (Hoppeler and Vogt 2001). The only study of mitochondrial content in a patient population, expressed the yield of mitochondrial protein as grams of protein per kilogram of muscle mass, reported a 43% lower quantity in lung transplant patients when compared to healthy controls (Wang, Williams et al. 1999).

Table 2. Muscle enzyme activities.

Enzyme	Metabolic pathway	Hypobaric hypoxia		COPD				Lung Tx
		Green (1989)	Howald (1990)	Green (1992)	Jakobsson (1995)	Maltais (1996)	Maltais (2000)	Wang (1999)
Hexokinase	Glycolysis	↓ 53%		↑ 16%		No Δ		No Δ
Phospho-fructokinase (PFK)*	Glycolysis	No Δ	↑ 9%	↓ 14%	↑ 34%	No Δ		↑ 29%
β-Hydroxyacyl-CoA-dehydrogenase	*β* oxidation of fatty acids	No Δ	↓ 27%	No Δ	No Δ	↓ 44%	↓ 24%	↓ 43%
Citrate synthase (CS)*	Citric acid cycle	↓ 37%	↓ 23%		↓ 29%	↓ 38%	↓ 24%	↓ 45%
Succinate dehydrogenase	Citric acid cycle	↓ 21%		No Δ	No Δ			
Malate dehydrogenase	Citric acid cycle		↓ 19%					
Cytochrome oxidase	Oxidative phos-phorylation		↓ 23%					
CS/PFK ratio			↓ 38%		↓ 48%			↓ 58%
Mitochondrial content			↓ 26%					↓ 43%

* indicates rate limiting step

Microcirculatory changes

Due to the importance of the microcirculation to O_2 delivery in skeletal muscle and the potential for impaired O_2 flux in chronic disease, the following is a review of the anatomical (*capillarity*) and physiological (*perfusion*) changes in the microcirculation related to chronic hypoxia.

Capillarity

Muscle capillarity is a measure of the quantity of local microcirculation that can be measured by several different methods; each of these methods has advantages and disadvantages, and may give varying results. *Capillary density* (CD, number of capillaries per muscle FCSA), *capillary-to-fiber ratio* (C/F ratio), *number of capillaries around a fiber*, and *number of capillary contacts per FCSA* are all commonly used measures of capillarity, but do not take into account capillary tortuosity or sarcomere length, both of which change with muscle contraction (Mathieu-Costello, Ellis et al. 1991). Mathieu-Costello (1991) argues that the best measure to assess a muscle's structural capacity for O_2 flux is the *capillary-to-fiber perimeter ratio*, because it takes into account the amount of area available for diffusion and does not vary with muscle contraction; however, it has not become widely used and none of the subsequent articles cited used this measure.

Only one study looked at capillarity in patients with and without COPD (Whittom, Jobin et al. 1998). Although they saw a reduced number of capillary contacts per fiber, there was no difference after correcting for the lower FCSA due to atrophy. Despite the fact

that the 20 patients in the study had a moderately severe obstructive airway disease, they were only borderline hypoxemic (Pa_{O_2} 80 = mmHg), and thus may not have crossed the threshold for changes in capillarity.

The topic of muscle capillarity has been studied by several investigators using either a hypobaric chamber (Green, Sutton et al. 1989; MacDougall, Green et al. 1991), or field studies of mountaineers in the Himalayas (Hoppeler, Kleinert et al. 1990). Subjects were exposed to altitudes of 5,000 to 8,848 m (PI_{O_2} ~78 – 43 mmHg) for a period of up to 60 days. Investigators consistently found an increased CD due to muscle fiber atrophy, and an unchanged C/F ratio. However, permanent high-altitude residents have both a lower CD and C/F ratio (Desplanches, Hoppeler et al. 1996).

Rats have also been used extensively in studies of hypoxia. Fisher (1992), looking at the *in vivo* rat cremaster muscle after 50 days at ~6,000 m (PI_{O_2} ~68 mmHg), saw not only an increased capillary *length density*, but also increased number of perfused capillaries. In several well-designed studies (Smith and Marshall 1999; Deveci, Marshall et al. 2001), Marshall *et al* compared rats breathing a FI_{O_2} of 0.12 (PI_{O_2} ~86 mmHg) to controls breathing room air; they saw a decreased Pa_{O_2} (41 vs. 86 mmHg), increased hematocrit (50 vs. 43%), decreased body mass, and increased right ventricular mass (due to pulmonary hypertension) following only 18 to 21 days of hypoxemia. Compared to control animals, they also reported increased *angiogenesis*, evidenced by decreased *interbranch distance* between 1°, 2°, and terminal arterioles, and an increased proportion of 2° and terminal arterioles, from which O_2 flux occurs more easily. It is unfortunate

that these measures of capillarity, "length density," and "interbranch distance," cannot be compared to other studies.

Perfusion

Few studies have looked at the *in vivo* physiology of blood flow in skeletal muscle during chronic hypoxia. Cassin, in 1971, observed an increased perfusion of capillaries in rats exposed to 6,150 m ($P_{I_{O_2}}$ ~67 mmHg) for seven weeks that was not related to an increase in capillarity, but rather opening of preexisting vessels (Cassin, Gilbert et al. 1971). Nearly 20 years later, Fisher *et al* (1992), using the cremaster muscle, reported an increase in both the anatomic and perfused capillary "length-density" in rats after 7 weeks at 6,000 m ($P_{I_{O_2}}$ ~68 mmHg). They also saw an increased RBC flux and capillary hematocrit, even when normalized to systemic hematocrit. In all, they found more capillaries, increased perfusion of capillaries, and more RBCs in those capillaries; all factors that serve to increase O_2 flux into the muscle fiber.

Summary: Altered skeletal muscle O_2 transport in chronic hypoxemia

Due to the variance in method, intensity, frequency and duration of hypoxia in experimental studies and use of different assessment techniques, conclusive evidence does not exist regarding the precise effects of chronic hypoxemia on skeletal muscle fibers or their associated microcirculation. Another major problem is clinical relevance: most studies look at "short-term chronic hypoxia," while patients with COPD may be hypoxemic for decades, "long-term chronic hypoxia." The following is a summary of the

overall changes in O_2 supply and demand in skeletal muscle in response to both COPD and other modes of hypoxemia.

Supply changes

Both anatomical and physiological modifications occur *locally* in the microcirculation and muscle fibers, as well as *systemically*, to increase the *convective* and *diffusive* flow of O_2 from the blood to the mitochondria and help prevent cellular hypoxia. Since the systemic and pulmonary circulations are connected to the heart in series, pulmonary hypertension and right heart failure, which can develop due to chronic hypoxemia, impair systemic cardiac output and decrease convective O_2 delivery ($\dot{Q}^{C}_{O_2}$). In an effort to compensate for the hypoxemia, the hormone erythropoietin is upregulated to increase [Hb] and thus the quantity of O_2 able to be convectively carried in the blood (Ca_{O_2}). As for systemic effects that increase diffusive O_2 delivery, chronic hypoxemia increases [2,3-DPG] levels which shifts the O_2-Hb curve to the right, facilitating unloading; thus, for a lower S_{O_2}, there is a higher blood P_{O_2} and a larger driving force (ΔP_{O_2}) to facilitate O_2 flux into the cell. In addition, P_{CO_2} and $[H^+]$ increase with the severity of COPD further shifting the Hb-O_2 curve to the right.

It is debatable whether or not chronic hypoxemia promotes angiogenesis locally, or even if there is a loss of capillarity. Following short-term chronic hypoxemia there appears to be an increase in CD, while C/F ratio is maintained (Green, Sutton et al. 1989; Hoppeler, Kleinert et al. 1990; MacDougall, Green et al. 1991). This argues against the idea of capillary angiogenesis in humans exposed to hypoxia, because the increased CD is due to

a decrease in muscle FCSA (Hoppeler and Vogt 2001). With or without angiogenesis, an increased CD would mean a greater supply of O_2 to the muscle per unit of contractile mass due to increased capillary surface area per fiber area and decreased diffusion distances associated with smaller fiber diameters. However, the Desplanches *et al* (1996) study of permanent high-altitude residents reported that CD and C/F ratio were both reduced in proportion to the loss of mitochondria and oxidative potential, suggesting that O_2 supply does decline over time.

Regardless of the number of capillaries per muscle fiber, these capillaries must be perfused in order to participate in the diffusive flux of O_2 into the muscle fiber. Although few studies have looked at the *in vivo* perfusion of skeletal muscle following short-term chronic hypoxia, those that have suggest an increase in the number of perfused capillaries (Cassin, Gilbert et al. 1971; Fisher, Schrader et al. 1992). As mentioned above, this would enhance O_2 flux by increasing surface area and decreasing diffusion distance. Also, the increased RBC supply rate and capillary hematocrit reported by Fisher *et al* (1992) would potentially serve to increase convective O_2 delivery, raising blood P_{O_2}, thereby increasing the driving force for O_2 diffusion into the muscle.

Another factor that would enhance O_2 flux into the muscle fiber is an increase in muscle myoglobin. While short-term hypoxia (14 days) increased [Mb] (Sillau, Aquin et al. 1980), hypoxemic patients with COPD had decreased [Mb] concentrations (Moller, Hellstrom et al. 1984). Although traditionally regarded as consumers of O_2, muscle fibers can also improve the influx of O_2 by the position of their mitochondria.

Subsarcolemmal mitochondria decrease the diffusion distance for O_2 when compared to intermyofibrillar mitochondria. However, several studies report that there is a loss of subsarcolemmal mitochondria (Hoppeler, Kleinert et al. 1990; van Ekeren, Sengers et al. 1992), which would also decrease the diffusion conductance of O_2 by increasing diffusion distance.

Demand changes

In the mitochondria, the enzyme cytochrome oxidase contains the final binding site for O_2 before it is reduced to H_2O. Despite it's importance, only one study (Howald, Pette et al. 1990) has looked at cytochrome oxidase activity in short-term chronic hypoxia; they found that it had decreased 23% in mountaineers following six weeks of exposure to a P_{IO_2} of $\leq$ 75 mmHg. Not surprisingly, this reduction was in close proportion to the 26% decrease in mitochondrial volume density that they reported, and similar to the 30% reduction seen in long-term chronic hypoxia (Hoppeler and Vogt 2001).

Muscle fiber type is relevant to the topic of O_2 demand because different fiber types derive their supply of ATP preferentially from different sources, type I from oxidative phosphorylation and type IIb from glycolysis. Type I fibers not only require more O_2 than type II for ATP synthesis, but since they contract more often (they are the first to be activated and the last to fatigue), they consume more ATP and demand more O_2. Thus, it is not surprising that hypoxemic patients with COPD and permanent high-altitude residents demonstrated a muscle fiber type transformation from I to II, as this would decrease O_2 demand.

The consistent finding of muscle atrophy in nearly all studies of chronic hypoxia is also significant in regard to O_2 demand. Smaller cells contain fewer enzymes and contractile proteins that must be synthesized and maintained at the expense of ATP and O_2; thus, fiber atrophy could be an adaptive response to diminished resources.

Conclusion

Taken as a whole, there seem to be significant differences in the effects of short-term versus long-term chronic hypoxemia; however, the effects of both are attempts to maintain homeostasis. Although the time sequence of the changes is not known, it appears that short-term hypoxemia results in changes that increase *O_2 supply* to skeletal muscle. Despite these efforts to maintain normal tissue oxygenation, tissue P_{O_2} remains low and the muscle fibers undergo adaptive strategies in the first few months of hypoxemia to decrease *O_2 demand*: decreased fiber size, muscle fiber type transformation, and decreased oxidative capacity (loss of mitochondria and aerobic enzymes). Over the long-term, however, this decreased O_2 demand leads to a decreased O_2 supply to the muscle, but the mechanism by which this occurs remains to be discovered.

Therefore, the long-term changes seen in muscle fibers and their associated microcirculation in response to chronic hypoxemia could be intended to decrease O_2 conductance (supply and demand) in skeletal muscle in order to preserve blood P_{O_2} for more vital organs. This could explain why there is a persistent exercise limitation

following lung transplantation, where the hypoxemia is cured, but its long-term effects are not.

Animal model of COPD

The development of animal models of COPD, in particular *emphysema*, began in the mid-1960's with Eriksson's discovery of α 1-antitrypsin deficiency (Laurell and Eriksson 1963; Eriksson 1965), and simultaneous with Gross' finding of enzymatically produced pulmonary emphysema (Gross, Babjak et al. 1964; Gross, Pfitzer et al. 1965). Since 1973, porcine pancreatic elastase has been the primary enzyme used to reliably reproduce emphysema in animals (Kaplan, Kuhn et al. 1973; Lucey, Keane et al. 2002). Initially, studies in hamsters focused on model and technique development of elastase-induced emphysema (Kaplan, Kuhn et al. 1973), as well as documenting pulmonary histological, stereological, and physiological changes that occur following elastase instillation (Kuhn and Tavassoli 1976; Kuhn, Yu et al. 1976; Snider and Sherter 1977; Snider, Sherter et al. 1977). More recently, intratracheal elastase instillation has been validated as an experimental model of emphysema in rats (Damon, Mauderly et al. 1982; Busch, Buschbom et al. 1984; Busch, Lauhala et al. 1984; Sato, Kato et al. 1990; Finlay, O'Donnell et al. 1996).

Animals treated with a single intratracheal instillation of porcine pancreatic elastase exhibit the same characteristics as humans with emphysema (Snider, Lucey et al. 1986): altered pulmonary function tests (increased residual volume, functional residual capacity, and total lung capacity) (Snider and Sherter 1977; Snider, Sherter et al. 1977; Damon,

Mauderly et al. 1982), impaired gas exchange (decreased diffusion capacity and arterial blood oxygen levels) (O'Brien, Lucey et al. 1979; Lucey, O'Brien et al. 1980; Damon, Mauderly et al. 1982; Sexton and Poole 1998), and cardiovascular sequelae (pulmonary hypertension and right ventricular hypertrophy) (Icochea, Cooper et al. 1982; Sato, Kato et al. 1994).

While the morphogenesis of emphysema begins within hours of the elastase instillation (Kuhn, Yu et al. 1976; Busch, Lauhala et al. 1984), the structural changes in the lung are relatively stable after six weeks (Snider and Sherter 1977). However, it is not known how muscle morphology may change over time, or how oxygenation, blood flow, and muscle function may be altered in animals with "stable" emphysema and chronic hypoxemia.

To my knowledge, there are only two published investigations into the effects of chronic emphysema on *peripheral* skeletal muscle. Mattson and Poole reported similar activity levels between control and emphysematous hamsters (7 to 8 months old), but citrate synthase levels in the vastus lateralis and gastrocnemius muscles were 7% and 13% lower in the emphysematous hamsters (Mattson and Poole 1998). By contrast, in a different study they reported no difference in hindlimb blood flow, using 15 μm-diameter radiolabeled microspheres, but did find that blood flow to *respiratory* muscles in emphysematous hamsters was higher during exercise than in controls (Sexton and Poole 1998). This group also found that microvascular PO_2 in the diaphragm was ~35% lower in emphysematous versus control hamsters.

Spinotrapezius muscle

Gray originally described the spinotrapezius muscle preparation in 1973 as "an ideal preparation for the microscopic study of a skeletal muscle vascular bed;" it is easily accessible, thin enough for trans-illumination, and its neurovascular supply can remain intact (Gray 1973). The spinotrapezius' parallel muscle fibers originate from the spinous processes of the 4th thoracic through the 3rd lumbar vertebrae, as well as a small segment of the thoracolumbar fascia, and inserts onto the spine of the scapula. The muscle has dual innervation from both cranial and peripheral nerves (spinal accessory (cranial nerve XI), and 2nd and 3rd cervical nerves, respectively) (Gray 1973). Its main blood supply, from the large spinotrapezius feeding artery (via subscapular branch of axillary artery), enters near the scapula; a few other feeding arteries/arterioles enter the muscle either near the caudal or cephalad border of the muscle (Schmid-Schonbein, Firestone et al. 1986) (refer to Figure 3).

Since Gray's original article, nearly 40 articles have been published using the spinotrapezius muscle, either describing its anatomy (Engelson, Schmid-Schonbein et al. 1985; Engelson, Skalak et al. 1985; Engelson, Schmid-Schonbein et al. 1986; Schmid-Schonbein, Firestone et al. 1986; Skalak and Schmid-Schonbein 1986; Saltzman, DeLano et al. 1992), characterizing its contractile properties and fiber type (Taylor and Calvey 1977; Delp and Duan 1996), describing its normal microvascular physiology (Lash and Bohlen 1987; Lash 1994; Suzuki, Poole et al. 1995; Musch and Poole 1996; Poole, Musch et al. 1997; Kindig and Poole 1998; Lash 1998; Lash 1998; Kindig and Poole 1999; Richmond, Shonat et al. 1999; Bailey, Kindig et al. 2000; Behnke, Kindig et al.

2001; Bishop, Nance et al. 2001; Kindig and Poole 2001; McDonough, Behnke et al. 2001; Behnke, Kindig et al. 2002; Bishop, Popel et al. 2002; Kindig, Richardson et al. 2002; Smith, Golub et al. 2002; Kano, Padilla et al. 2004) as well as functional and microcirculatory changes associated with hypertension (Schmid-Schonbein, Firestone et al. 1986; Lash and Bohlen 1995; Smith, Barbee et al. 2004; Smith, Barbee et al. 2004), skeletal muscle ischemia (Suzuki, Poole et al. 1995), diabetes (Kindig, Sexton et al. 1998), chronic heart failure (Kindig, Musch et al. 1999; Richardson, Kindig et al. 2003; Behnke, Delp et al. 2004), and aging (Russell, Kindig et al. 2003). The fact that surgical exteriorization of the spinotrapezius does not alter microvascular P_{O_2} and blood flow when compared to the intact state (Bailey, Kindig et al. 2000) makes it an ideal tissue to measure oxygen transport and consumption. Surprisingly, no one has used the spinotrapezius muscle, or any other peripheral skeletal muscle, to investigate microvascular oxygen transport or muscle contractile changes related to chronic hypoxemia or COPD.

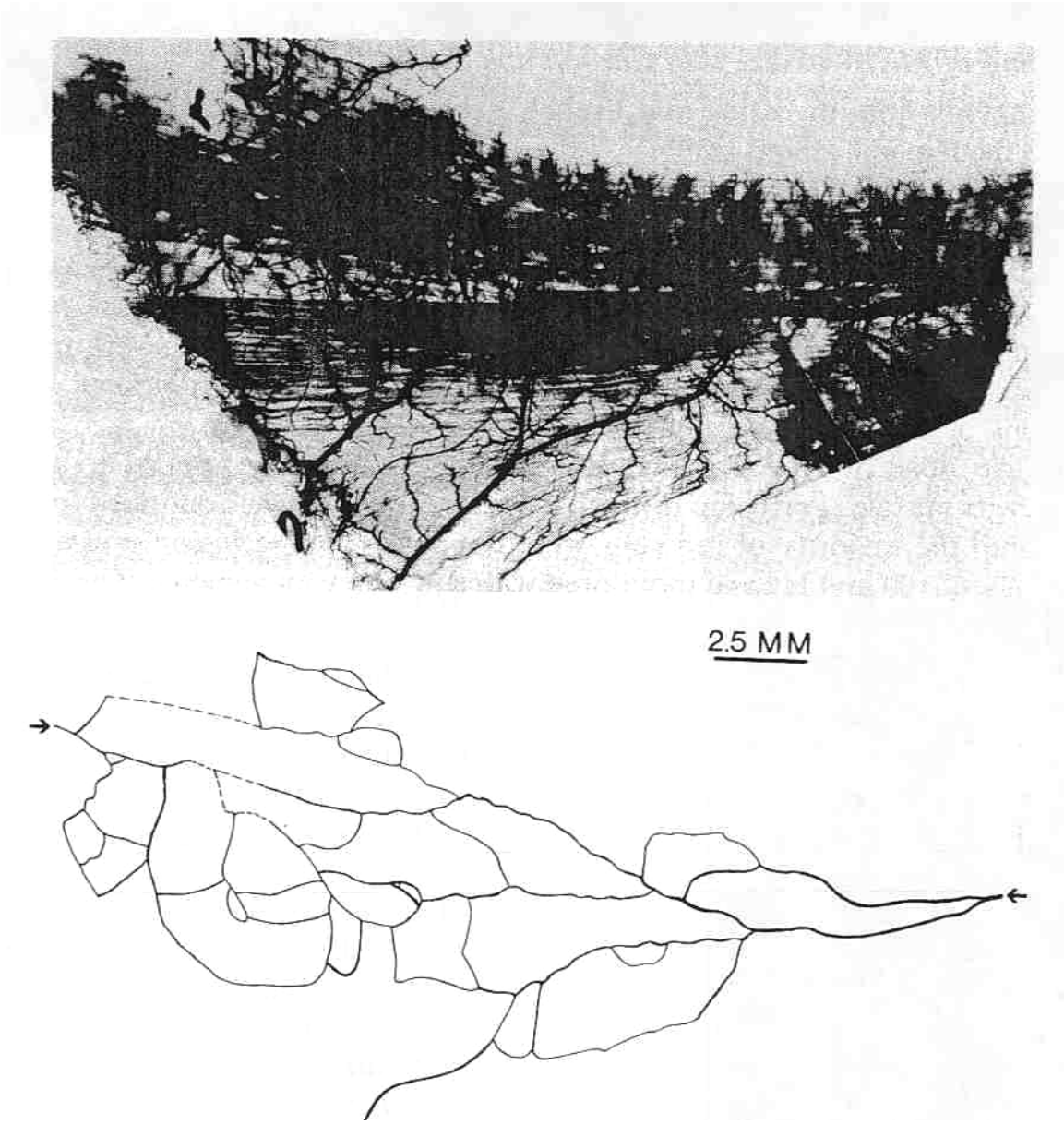

Figure 3. Microvascular network of rat spinotrapezius muscle (Engelson, Skalak et al. 1985).

Purpose of present study

The overall purpose of this series of investigations was to test the hypothesis that the principle of symmorphosis, regulated morphology "commensurate to functional needs" (Weibel 1984; 2000), is operative under conditions of chronic hypoxia. If it is, then one might expect that 1) chronic systemic hypoxemia leads to diminished *oxygen demand* from the muscle due to slow-to-fast fiber type transformations and reduced oxidative enzyme capacity, and 2) that this chronic reduction in tissue oxygen demand would remove the stimulus for angiogenesis (*i.e.*, vascular endothelial growth factor) and lead to vascular rarefaction, further diminishing *oxygen supply*, as has been seen in other chronic disease models (hypertension and heart failure) (Hansen-Smith, Greene et al. 1990; Nusz, White et al. 2003). This proposed negative-feedback loop is illustrated in Figure 4.

There is no animal model of "skeletal muscle dysfunction in COPD," but there is 1) an excellent animal model of emphysema, and 2) an ideal skeletal muscle for studying the microcirculation. Thus, the objectives of my study, in relation to the above hypothesis, were to:

1. validate elastase-induced emphysema in rats as an animal model of skeletal muscle dysfunction in COPD,
2. determine if there is a relationship during aging between severity of hypoxemia and transformations in muscle fiber type,
3. investigate differences in oxygen transport and skeletal muscle function in the spinotrapezius muscle of animals with and without COPD, and

4. determine if short-term supplemental oxygen improves oxygen supply and muscle performance of the spinotrapezius.

The independent measures included both *local* skeletal muscle O_2 supply and demand parameters, and muscle performance, as well as *systemic* measures of O_2 supply and evaluation of respiratory function.

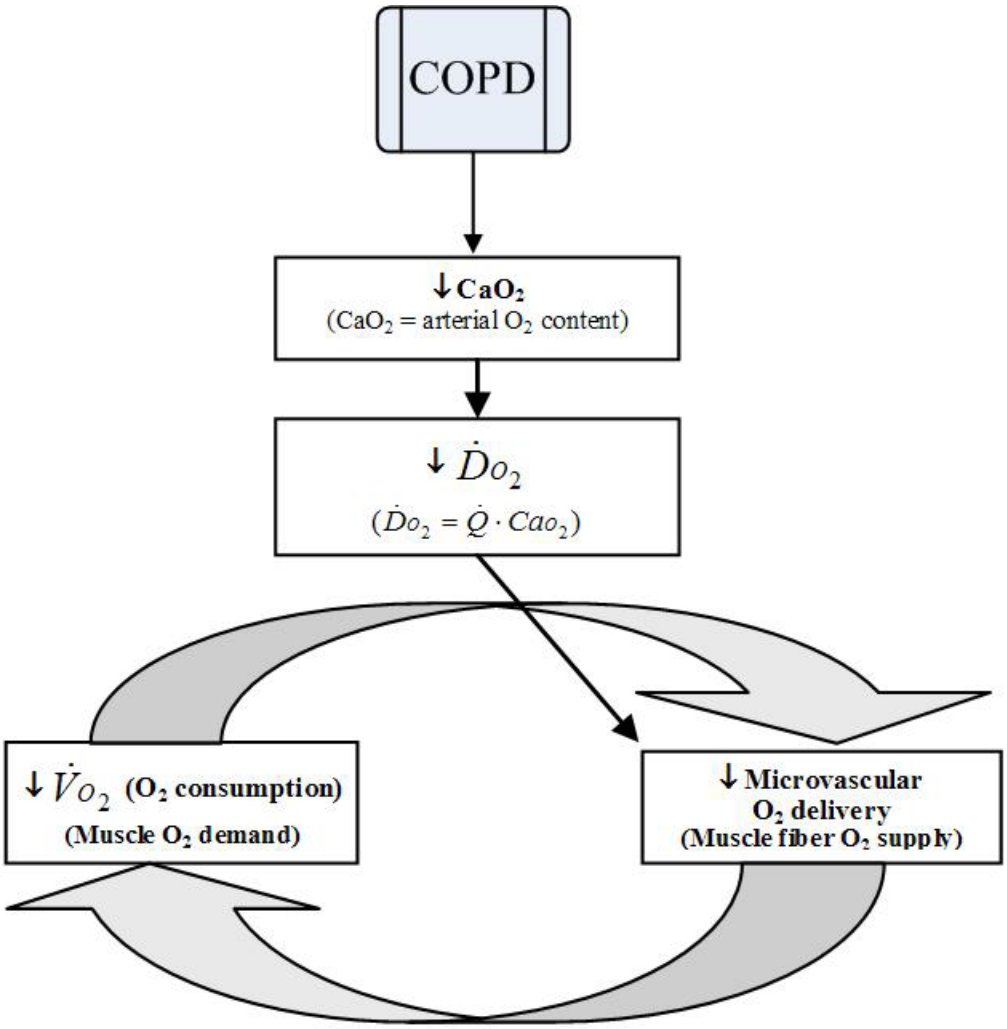

Figure 4. Proposed negative-feedback loop. As tissue O_2 delivery becomes impaired, so does muscle fiber O_2 supply, and consequently O_2 demand; likewise, as fiber O_2 demand decreases during chronic hypoxia, this may lead to a decrease in O_2 supply.

Materials, Methods, and Data Analysis

Based on the objectives of this study, there were two phases of this project:

I. validation of elastase-induced emphysema as an animal model of skeletal muscle dysfunction in COPD (*i.e.,* transformation of muscle fiber type with aging and hypoxemia) and
II. investigation of oxygen consumption and skeletal muscle performance differences in animals with and without COPD, and the effects of supplemental oxygen on these parameters.

Each phase was preceded by the initial intervention: endotracheal instillation of either elastase or saline. Many of the materials and methods were used in both phases of the study; others were unique to one phase or the other. For convenience of reference, the various experimental methods and techniques are described first, followed by the details of each protocol. Further details of some aspects are found in the appendices. This study was approved in advance by Virginia Commonwealth University's Institutional Animal Care and Use Committee (protocol # 0206-3081), and all animals were treated in accordance with the Institute for Laboratory Animal Research's *Guide for the Care and Use of Laboratory Animals* (1996).

Experimental Animals

Seventy-six Sprague-Dawley rats (Harlan, Indianapolis, IN) with a mean initial body mass of 215.5 g (SD 14.5, range 176 – 248) were used in these experiments. Since the spinotrapezius muscle of male rats is thicker and contains more connective tissue, giving poorer image quality for intravital microscopy, female rats, which have a lower maximal body mass (Figure 5), were used. Animals were housed in individual cages and maintained on a 12:12 hr light-dark cycle in a climate-controlled room (temperature 68-75° F, humidity 40-60%), with access to rodent chow and water *ad libitum*. Animals were delivered to the institutional animal care facility at 8.3 (SD 0.6) weeks of age, and were given two weeks for acclimatization. At a mean age of 10.6 (SD 0.7) weeks of age (range 9.6 – 12.0), the initial intervention (intratracheal instillation, described in "Initial intervention: Elastase/vehicle instillation," page 41) was performed. The terminal experiments were completed between 4 and 65 weeks after the initial intervention. Following a purported outbreak of Rat respiratory virus, the 16 animals used in phase II were housed in filter-top cages.

The influence of hypothermia, dehydration, infection, and pain were all addressed. To prevent hypothermia, all animals were kept at ~37° C, verified by rectal thermometer (Model 2018, Lumiscope, East Brunswick, NJ), using a homeothermic blanket system (Harvard Apparatus, Holliston, MA) and/or a thermostatic animal platform (Appendix I) (Golub and Pittman 2003). Due to the short duration of phase I experiments, dehydration was not an issue; during phase II experiments dehydration was prevented by intravenous administration of fluorescent and phosphorescent probes dissolved in phosphate buffered

saline (PBS), as well as a continuously infused anesthetic (Saffan, ~0.3 ml/hr). A prophylactic antibiotic, 60 mg tetracycline/L drinking water (Polyotic, Fort Dodge Animal Health, Fort Dodge, IA, Lot # 010805) was administered for seven days after the initial intervention to prevent mortality from suppurative pneumonia (Busch, Lauhala et al. 1984). To assess and prevent undue distress, discomfort, or pain, animals were monitored daily for one week after the intratracheal instillation, and scored using the "Modified distress scoring sheet" (Lloyd and Wolfensohn 1999) (Appendix II) a predictor of animal mortality; it was not necessary to euthanize any animal due to distress.

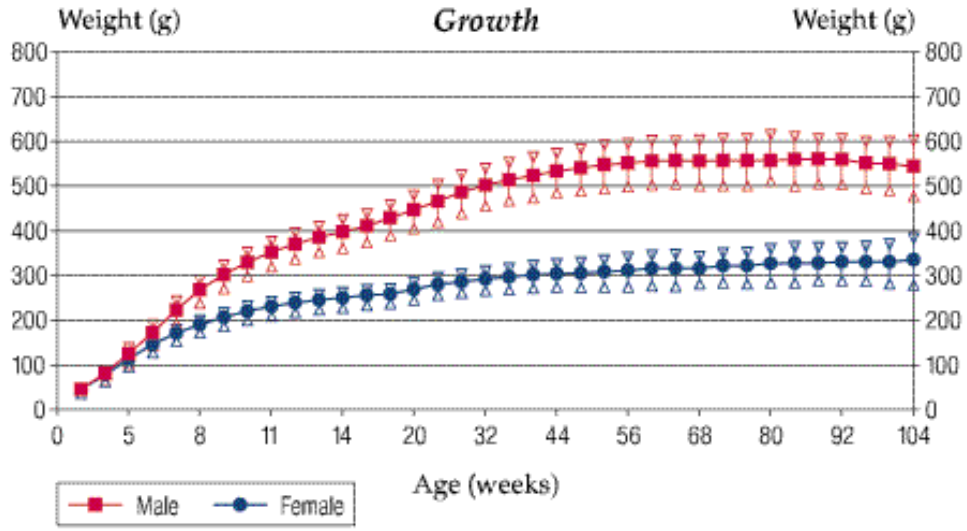

Figure 5. Sprague-Dawley male vs. female growth curve.

Anesthesia

Induction of anesthesia for the initial intervention and phase I experiments was accomplished by placing animals in an induction chamber (Anesthetizing box, Harvard Apparatus) with 4% Isoflurane (AErrane, Lot # N009B310, Baxter, Deerfield, IL) and 96% oxygen, administered with a gas vaporizer (Quantiflex VMC Small Animal Anesthesia Machine and VIP 3000 Veterinary Anesthesia Vaporizor, MDS Matrx, Orchard Park, NY). The animals were then orally intubated and placed on a small-animal pressure controlled ventilator (RSP1002, Kent Scientific Corp., Litchfield, CT), receiving maintenance anesthesia of 2% Isoflurane (Waynforth and Flecknell 1992) and 98% oxygen.

For the terminal microcirculatory experiments (phase II), animals were initially anesthetized with a combination of Ketamine (75 mg/kg) and Acepromazine (2.5 mg/kg) (Waynforth and Flecknell 1992). Maintenance of anesthesia throughout the experiment was accomplished using intravenous (i.v.) Saffan (Alphaxolone 9 mg/ml and Alphadolone 3 mg/ml, Schering-Plough Animal Health, Hertfordshire, England, Lot 20081) at an initial rate of 0.3 ml/hr (~0.2 mg/kg/min) (Waynforth and Flecknell 1992), which was titrated to maintain a mean arterial pressure of 95-105 mmHg.

Following the terminal experiments, animals were euthanized by administering Euthasol (Pentobarbital 390 mg/ml and Phenytoin 50 mg/ml, Delmarva Laboratories, Inc., Midlothian, VA) at a dose of 0.4 ml/kg (~150 mg/kg) (Goldberg and Henry 2000).

Tracheal and vascular cannulations

A set of vascular and tracheal cannulae were made from various sizes of polyethylene (PE) tubing (Figure 6). Endotracheal tubes (ETT) were made from PE 190 tubing, 6.5 cm long, with a teardrop shaped bulb placed ~2 cm from one end to seal the airway at the vocal cords, as described by Smith *et al* (2004). A tracheostomy tube was made from a 5 cm section of PE 240 tubing.

Both the initial intervention and phase I required oral endotracheal intubation. Following induction anesthesia, the vocal cords were visualized using a laryngoscope with a modified Miller # 0 fiber optic blade (Welch Allyn, Skaneateles Falls, NY), while the ETT with stylet was inserted into the trachea between the vocal cords during inspiration (Costa, Lehmann et al. 1986; Smith, Tiba et al. 2004). The laryngoscope and stylet were removed, the animal placed on mechanical ventilation, and correct ETT placement verified by observing the chest rise and fall in synchrony with the ventilator. A tracheostomy tube was placed during phase II experiments to maintain a patent airway, decrease work of breathing, and allow port of entry for inspiratory gases.

The right femoral artery was cannulated for arterial blood gas (ABG) samples during phase I experiments (Waynforth and Flecknell 1992). In phase II experiments, the right external jugular vein and left common carotid artery were cannulated and used for measurements of central venous pressure (CVP) and systemic arterial pressure (AP), respectively. The measurements were collected at 100 Hz using pressure transducers connected to a high-speed data acquisition system (MP150, BIOPAC Systems, Inc.,

Goleta, CA) via a RJ-11 cable, transducer connector interface (TCI-105, BIOPAC), and general purpose transducer amplifier (DA100C, Biopac). This acquisition system was connected to a personal computer (PC) equipped with a digital chart recorder (Acq*Knowledge* software, v3.7.3, BIOPAC). In addition, the jugular venous line was used for continuous infusion of i.v. Saffan, and the carotid arterial line was used for ABG sampling. The right femoral vein was also cannulated during phase II experiments for i.v. injections of various experimental solutions. Patency of vascular cannulae was maintained with either a heparin lock (20 units of heparin/ml of normal saline) or continuous infusion.

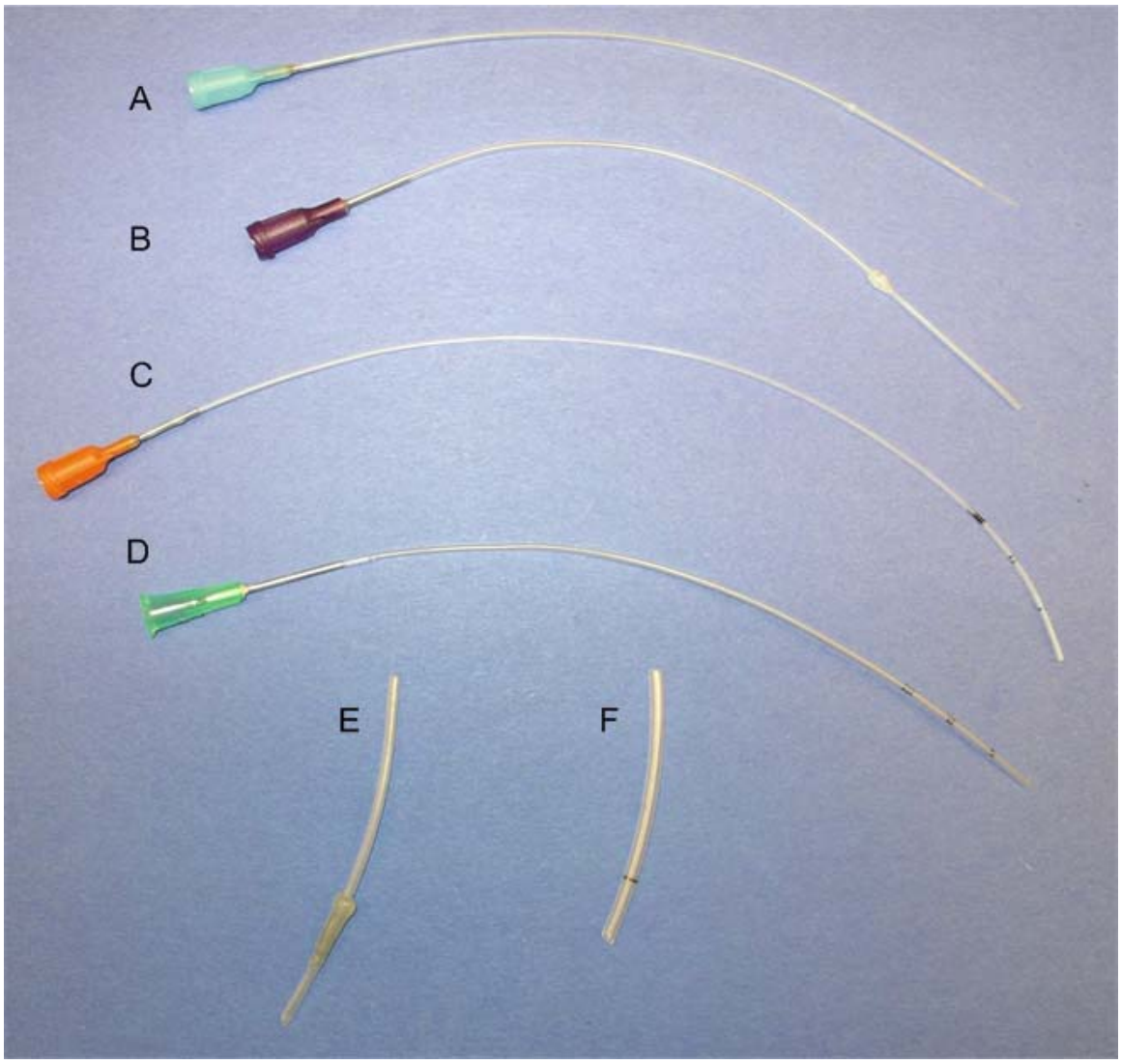

Figure 6. Vascular and tracheal cannulae (A. Femoral arterial (PE 50-20-10), B. Carotid artery (PE 90-50), C. Femoral venous (PE 50), D. External jugular venous (PE 90), E. Endotracheal (PE 190 with "bulb"), and F. Tracheostomy (PE 240)).

Initial intervention: Elastase/vehicle instillation

Lyophilized porcine pancreatic elastase (Elastin Products Company, Inc., Owensville, Missouri, EC134, 135 units of activity/mg of protein, Lot 52669) was dissolved in normal saline to give a concentration of 400 international units/ml of saline, and was administered at a dose of 80 units/100 g body mass (0.2 ml/100 g). Animals in the vehicle control group received an equivalent volume of normal saline (0.2 ml/100 g)

Following placement of an ETT, the animals remained hanging on the intubation board and were allowed to rest for three minutes on the ventilator. At that point, they were positioned on their left side at 60°, were temporarily removed from the ventilator, and half of their total dose was instilled into the ETT via a 1-ml syringe equipped with a sterile 20-gauge needle (Busch, Lauhala et al. 1984; Sato, Kato et al. 1990). The animals were placed back on the ventilator for two minutes in order to 1) maintain anesthesia, 2) ensure adequate ventilation and oxygenation, and 3) to assist in the distribution of the elastase. Following rotation to the right, and instillation of the remaining dose of elastase/vehicle, they were, again, placed on the ventilator for two minutes. At this point they were taken off the ventilator, and thus anesthesia. The ETT was removed as the animal awakened, and it was returned to its housing following a resumption of normal activity and no signs of respiratory distress, as determined by a score of $\geq$ 12/19 on the "Modified distress scoring sheet" (Lloyd and Wolfensohn 1999) for three hours. Prophylactic antibiotics (60 mg tetracycline/L drinking water; Polyotic, Fort Dodge Animal Health) were administered for seven days to prevent mortality from suppurative pneumonia (Busch, Lauhala et al. 1984).

Radiography

Ventral-dorsal (VD) and lateral chest radiographs were made of two animals, one experimental and one control, in the Department of Animal Resources with the assistance of a veterinary technologist and a veterinarian. These radiographs were made, approximately 19 weeks after the initial intervention, on living animals while intubated and anesthetized with Isoflurane, as previously described ("Anesthesia," page 39), during a "sigh" breath from the ventilator (with a maximal inspiratory pressure of 10 cmH_2O). Radiographs were taken using a Universal MP 300 X-ray unit used at a 40-inch distance set at 2 milliamp-seconds as well as 50 and 48-kV peak, respectively, for VD and lateral radiographs, resulting in an exposure time of 0.006 sec (Snider and Sherter 1977).

MHC isoform determination

The relative proportions of myosin heavy chain isoforms I, IIa, IIx/d, and IIb from each muscle were determined using the sodium dodecyl sulfate-polyacrylamide gel electrophoresis (SDS-PAGE) technique of Talamadge and Roy (1993), as modified by Kinirons (2002).

Muscle biopsy and tissue processing

After being euthanized, the left vastus lateralis, gastrocnemius, soleus, and spinotrapezius muscles were isolated and removed from the animals by open biopsy, weighed, placed in a microcentrifuge tube, quickly frozen in liquid nitrogen and stored at -70° C. The frozen muscles were later lyophilized, minced with scissors, homogenized with a mortar and pestle, and placed in a cold extraction buffer (see Appendix IV, MHC extract solution)

(Zhang, Wright et al. 1997). Following agitation every ten minutes, at 4° C for 60 minutes, the samples were centrifuged at 10,000 G for 10 minutes. A small portion of the supernatant, containing extracted MHC, was pipetted into microcentrifuge tubes and stored at -70° C.

At a later time, the extracted muscle samples were brought to room temperature, mixed in a vortex mixer, and the protein concentration assayed, based on the method of Bradford (1976) using a microplate absorbance reader at a wavelength of 595 nm (Tecan Sunrise, Phenix Research Products, Hayward, CA) calibrated with known concentrations of bovine serum albumin (Figure 7). If necessary, samples were diluted with additional extract solution to achieve a protein concentration of ~0.25 mg/ml and stored at -70° C.

On the day in which the SDS-PAGE was run, the diluted muscle samples were again brought to room temperature, mixed in a vortex mixer, and combined with an equal volume of sample buffer (see Appendix IV), yielding a final protein concentration of ~0.125 mg/ml. This sample was boiled for five minutes to help denature the protein, and then cooled to room temperature prior to loading into the gel.

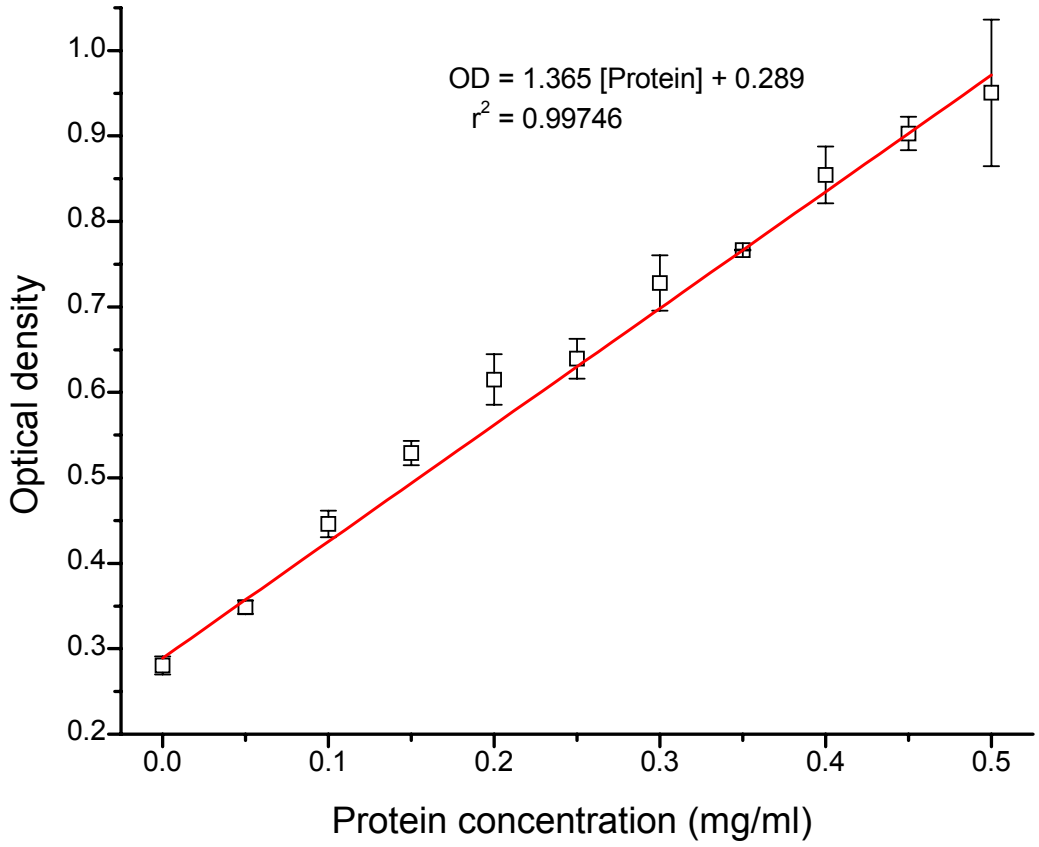

Figure 7. Protein assay calibration curve.

SDS-PAGE

The SDS-PAGE procedure, briefly described below, is detailed in the *PROTEAN II xi Cell Instruction Manual*, section 4.1: "Casting Discontinuous (Laemmli) Gels" (Bio-Rad Laboratories, Hercules, CA).

The 8% SDS separating gel solution (see Appendix IV), immediately after addition of the polymerizing agents, was injected between two glass plates in a casting stand to a height of ~13 cm. This 0.75 mm thick gel was layered with ~1 cm 10% ethanol, and allowed to set for at least 45 minutes. At this point, the ethanol was poured off, and Whatman #1 filter paper was used to dry between the glass plates. A 15-space comb was inserted between each plate prior to injecting the 4% SDS stacking gel solution (Appendix IV) to form the "wells" into which the muscle samples were injected. The stacking gel was allowed to set for at least 60 minutes; the comb was gently removed, and each well was individually and gently cleaned by an injection of the upper running buffer from a 5-ml syringe and 23-gauge needle.

Twenty µl of each sample were slowly injected into a separate well, yielding ~2.5 µg of protein per lane. The first and last wells were not used, and a standard (Precision Plus Protein Standard, 161-0374, Bio-Rad) was placed in the middle to help identify the bands of interest. The glass plate sandwich was then locked into a cooling core, and the upper and lower buffer chambers were filled with their respective buffer solutions (see Appendix IV), respectively. The central cooling core was placed in the lower buffer chamber, and 400 µl of 2 β-mercaptoethanol were added to the upper buffer chamber.

The lower buffer chamber, with the lid in place, was placed in the refrigerator, leveled, and the electrodes plugged into the electrophoretic system power supply (Power Pac 1000, Bio-Rad). The electrophoresis unit ran at a constant voltage of 275 volts for ~30 hours (maximal current of 20 mA per gel for 90 minutes, followed by a maximum of 15 mA per gel for the remaining time).

Gel staining and analysis

Immediately after removal from the glass plates, each gel was placed in a fixative solution (Appendix IV) for 20 minutes, rinsed twice with deionized water for 10 minutes, and stained with silver (Silver Stain Plus Kit, 161-04149, Bio-Rad). After adequate staining, the gels were placed in a stop solution (5% acetic acid) for 15 minutes, and rinsed for again for five minutes. In each of the above steps, the gels were gently agitated on a platform shaker (Innova 2000, New Brunswick Scientific Co., Inc., Edison, NJ).

Gels were removed from the rinse solution and immediately scanned with a high-resolution scanner (Duoscan HiD, AGFA, Belgium). These images were saved onto a PC and later analyzed offline with Gel-Pro Analyzer, MediaCybernetics, Silver Spring, MD), which was used to determine the relative fraction of total MHC isoform expression. Since each band, containing a different MHC isoform, was evaluated relative to other bands in the same lane (muscle), differences in protein concentrations and staining intensity between different lanes was not an issue. In addition, to make staining more uniform, only one type of muscle was analyzed on a single gel, and the protein content

per lane was uniform. Determination of MHC type from the stained gels was based on the migration order, I > IIb, IIx, > IIa (Figure 8) (Talmadge and Roy 1993).

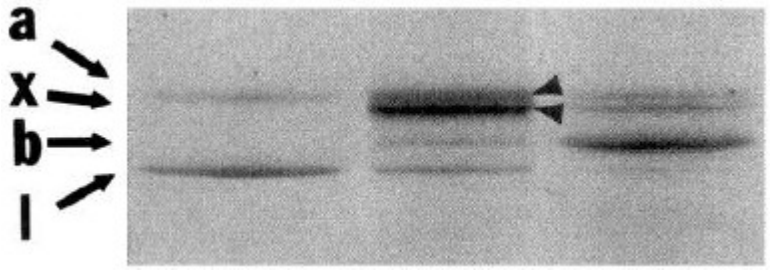

Figure 8. MHC bands after SDS-PAGE and silver staining. MHC I has the greatest electrophoretic mobility, followed by IIb, IIx and then IIa, with the least.

Spinotrapezius muscle preparation

The spinotrapezius muscle was prepared as previously described (Gray 1973; Lash and Bohlen 1987; Suzuki, Poole et al. 1995). After exposing the muscle through a dorsal, midline incision, the layer of subcutaneous fat and connective tissue was gently removed, while taking care not to damage the underlying muscle. Bleeding was prevented or controlled by using a cautery, and the tissue was keep moist with frequent applications of normal saline. Muscle length was measured on the lateral border of the spinotrapezius muscle, from the origin on the thoracolumbar fascia to its insertion on the spine of the scapula.

After the entire lateral border of the spinotrapezius muscle was gently separated from the underlying latissimus dorsi muscle, and the penetrating vessels at the caudal end were cauterized, an 8 cm, 28-gauge wire (~60 mg), in the shape of a horseshoe (Suzuki, Poole et al. 1995), was sutured to the lateral border at 8-10 mm intervals using 5-0 silk sutures. This "horseshoe" was then sutured to the muscle at 8-10 mm intervals as it was cut from its caudal, and then medial origins; in this process, a medial feed arteriole was cauterized as well. The wire horseshoe served as a rigid interface to attach the muscle to the force transducer (Figure 9), and also kept the muscle flat, near its *in situ* position, on the platform before and after muscle contractions.

Figure 9. Spinotrapezius muscle on pedestal connected to force transducer and covered by Saran film.

Intravital microscope

During the data collection phase of the experiment, both transmission and episcopic illumination images of the spinotrapezius preparation were continuously recorded from an upright Zeiss ACM microscope (Carl Zeiss, Inc., Göttingen, Germany). Transillumination and epifluorescent images were continuously recorded onto a video cassette recorder (VCR; Panasonic AG 7350) using a charge-coupled device camera (CCD-72, Dage MTI, Michigan City, IN); these images were visualized on a 20" video monitor (Panasonic WV 5490). The light source for both fluorescence and phosphorescence excitation was a Xenon flash lamp (Model FX-249, EG&G Optoelectronics, Salem, MA), with an output of 0.5 J, duration of 3 μs, used at a frequency of 100 Hz and 20 Hz, respectively.

For epifluorescence microscopy, used for blood velocity measures, a fluorescence filter cube was used (Figure 10) (11001v2, Chroma Technology Corp., Rockingham, VT) with an 1) excitation filter with a center wavelength at 470 nm and full bandwidth of 40 nm, 2) dichroic, longpass beamsplitter with a cut-on wavelength of 495 nm, and 3) longpass emission filter with a cut-on wavelength of 515 nm (Figure 11).

For phosphorescence microscopy, used for microvascular P_{O_2} measures, a filter cube was used with a 1) 430 nm bandpass excitation filter (430BP100, Omega Optical Inc., Brattleboro, VT), 2) dichroic, longpass beamsplitter with a cut-on wavelength of 510 nm (FT510, Zeiss), and 3) an emission filter with a cut-on wavelength of 650 nm (Oriel Corp., Stratford, CT).

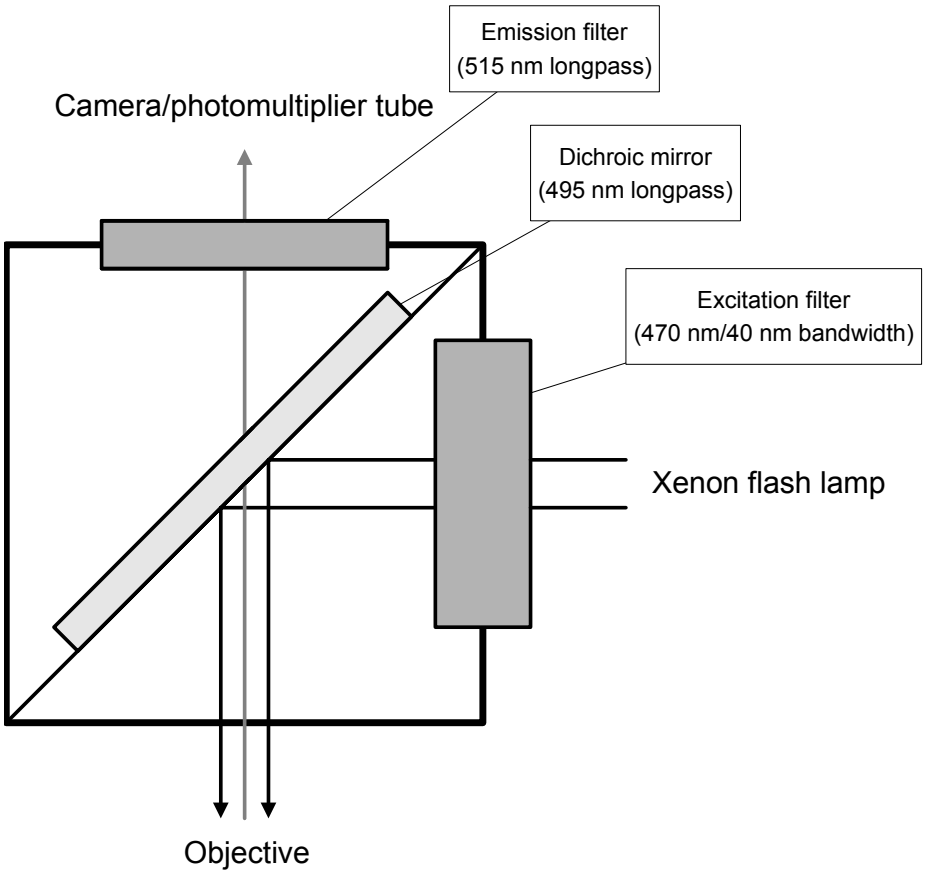

Figure 10. Flourescence filter cube (Chroma 11001v2).

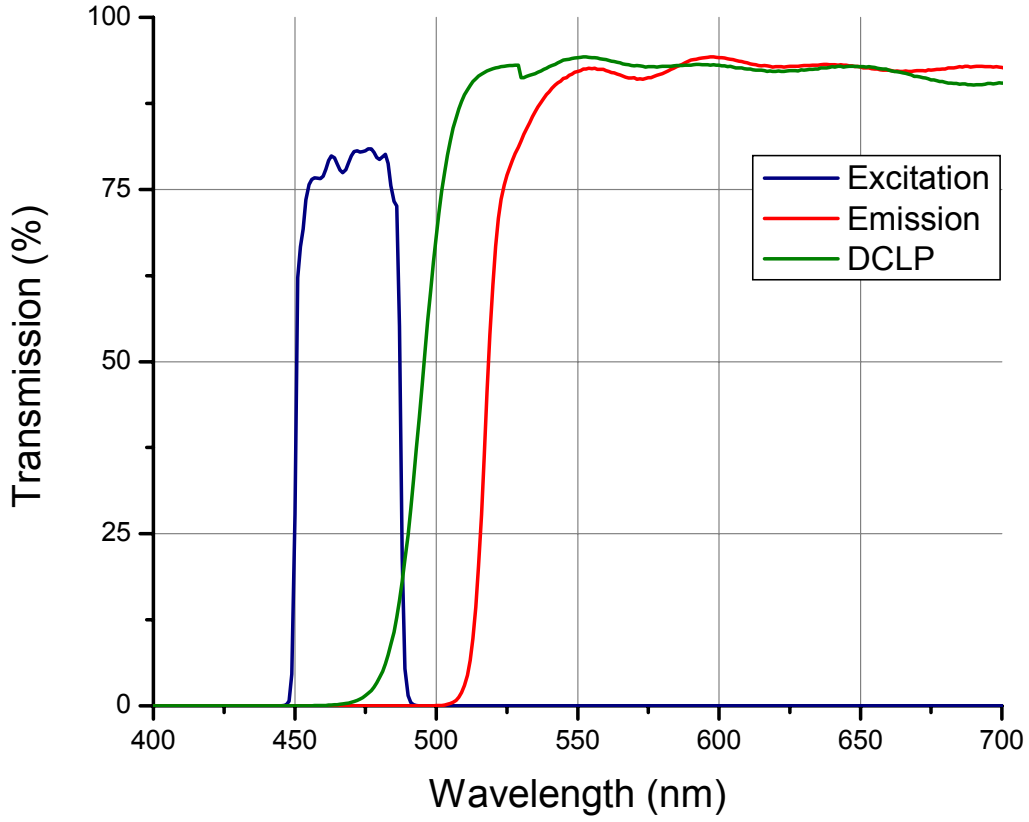

Figure 11. Chroma flouresence filter cube's (11001v2) excitation filter, dichroic mirror, and emission filter characteristics.

Phosphorescence quenching microscopy

Hardware

The microscope, excitation source and filter set were described above. Following excitation at 10 Hz through a 32 μm square diaphragm, the emitted phosphorescence signal from the spinotrapezius muscle was sent to a photomultiplier tube (model R1617, Hamamatsu, Middlesex, NJ). Output from the photomultiplier was sent to a low-noise current-to-voltage converter (model OP27EP, Analog Devices, Norwood, MA). That signal was sent to both an analog-to-digital converter (AT MIO/6F5, National Instruments, Austin, TX) in a PC, and it was monitored on an oscilloscope (model 72-3060, Tenma Test Equipment, Springboro, OH) to ensure that the signal was approximately 8 volts (near the maximal input voltage of 10 V for the analog-to-digital converter); this setup is diagramed in Figure 12 (Zheng, Golub et al. 1996).

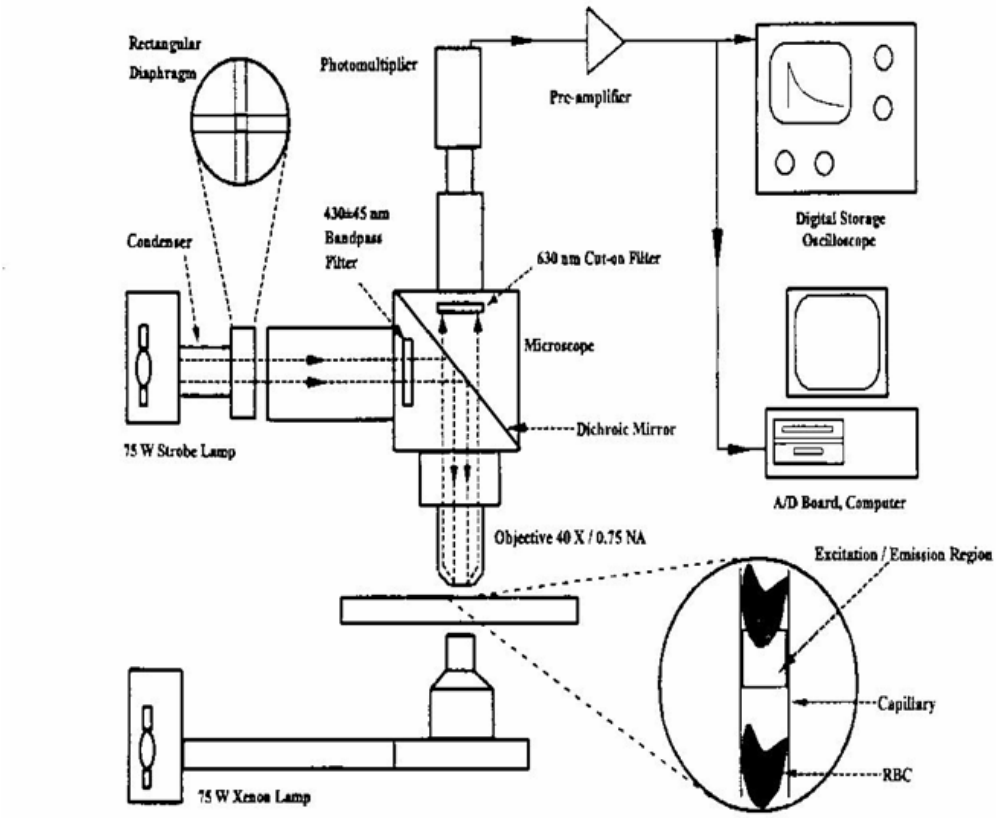

Figure 12. Schematic diagram of phosphorescence quenching microscopy setup.

Palladium-porphyrin phosphorescence probe preparation

Preparation of the albumin-bound Palladium-porphyrin phosphorescence probe (10 mg/ml) was a multi-step process, whose details are included in Appendix III. In brief, it included preparing a solution of bovine serum albumin, fraction V (Sigma-Aldrich, Inc., St. Louis, MO), to which palladium meso-tetra (4-carboxylphenyl) porphyrin (Pd-MTCPP; Oxygen Enterprises, Ltd., Philadelphia, PA) was bound. This solution was dialyzed in polyvinylpyrrolidine (Sigma-Aldrich, Inc.) for ~24 hours to remove any unbound Pd-MTCPP from the solution. The pH was adjusted to 7.3 – 7.5 with the addition of Trizma base (Sigma-Aldrich, Inc.). The final product was filtered using a sterilization filter unit (NALGENE Labware, Rochester, NY), pipetted into 0.5 ml microcentrifuge tubes, immediately frozen in liquid nitrogen, and stored at -80° C.

Data acquisition and microvascular P_{O_2} analysis

LabVIEW 4.01 (National Instruments) was used to acquire and process the signal from the analog-to-digital converter at a sampling rate of 100 kHz. Twenty decay curves per measurement, 400 points per decay curve, were normalized, averaged, and saved in LabVIEW for off-line analysis.

Measuring P_{O_2} using the phosphorescence quenching method is based on the relationship between phosphorescence lifetime, τ, and P_{O_2}, using the Stern-Volmer equation:

Equation 4

$$1/\tau = 1/\tau_0 + k_q P_{O_2}$$

where τ_0 is the lifetime in the absence of oxygen (546 μs), and k_q is the quenching coefficient ($3.06 \cdot 10^{-4}$ $\mu s^{-1} \cdot mmHg^{-1}$). Normalized, averaged phosphorescence decay curves were analyzed using Origin 7.05 (OriginLab). Each curve was plotted on a semi-logarithmic scale, and analyzed using a non-linear curve fitting equation, based on the rectangular (R) distribution model of oxygen as developed by Golub *et al* (1997):

Equation 5

$$Y(t) = A \cdot Y_R(t) + (1 - A)\exp(-t / \tau_F)$$

where A is the fraction of the observed signal due to phosphorescence, (1-A) is the fraction contributed by the tail of the excitation flash, τ_F is the lifetime of the residual flash contribution, t is time in μs, and $Y_R(t)$ Equation 6 is the relationship between phosphorescence decay rate and P_{O_2} (k_0 is $1/\tau_0$, and δ is the half-width of the rectangular distribution) (Golub, Popel et al. 1997).

Equation 6

$$Y_R(t) = \exp\left[-\left(k_0 + k_q P_{O_2}\right) t\right] \sinh\left(k_q \delta\, t\right) / k_q \delta\, t$$

A representative plot, Figure 13, illustrates this relationship.

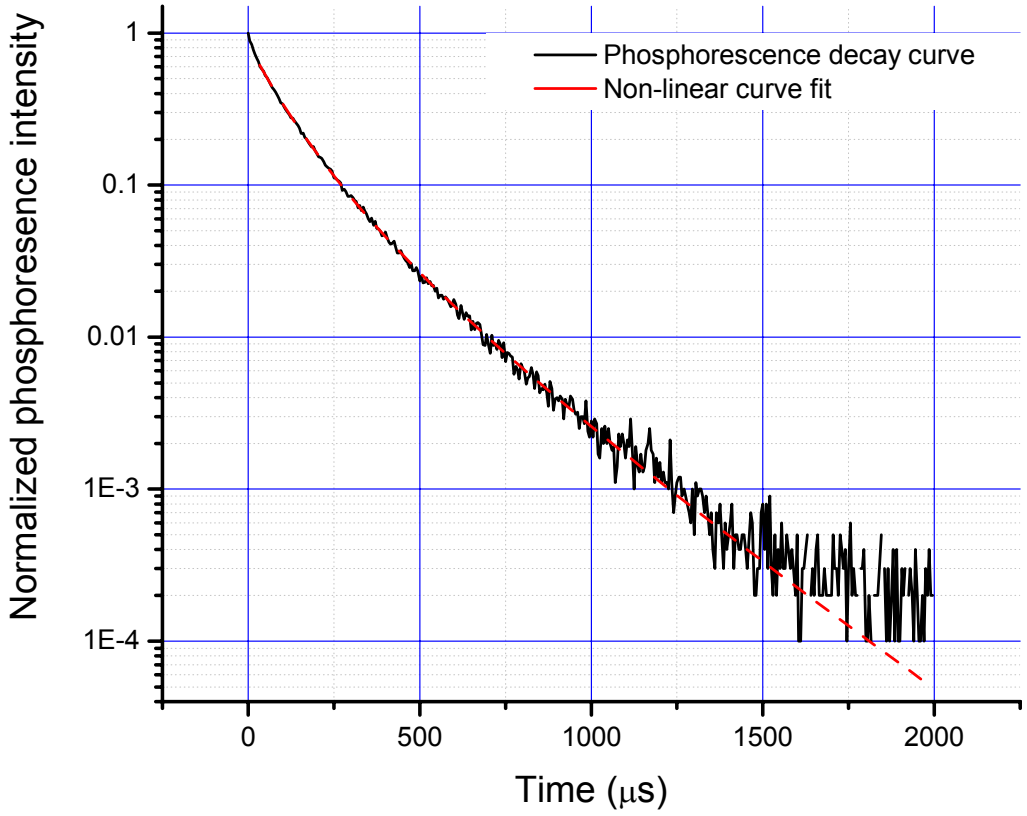

Figure 13. Representative phosphorescence decay curve.

Spinotrapezius oxygen consumption

Oxygen consumption of the spinotrapezius muscle was calculated based on Fick's principle, using spinotrapezius blood flow $\dot{Q}^{ST}$, and the arteriolar-venular oxygen content difference (Ca_{O_2}-Cv_{O_2}) as described in Equation 7:

Equation 7

$$\dot{V}_{O_2}^{ST} = \dot{Q}^{ST}\left(Ca_{O_2} - Cv_{O_2}\right),$$

where C_{O_2} is the oxygen content of blood (ml of O_2/dl of blood), and the subscripts "*a*" and "*v*" refer to arteriolar and venular blood, respectively. Measurement of blood flow is discussed in the following section "Blood flow."

Oxygen content

C_{O_2} includes oxygen both bound to hemoglobin and dissolved in blood, as defined in Equation 8:

Equation 8

$$C_{O_2} = S_{O_2}[Hb]C_{Hb} + \alpha_{O_2} \cdot P_{O_2},$$

where S_{O_2} is the fractional oxygen saturation of hemoglobin, *[Hb]* is hemoglobin concentration (g/dl), C_{Hb} is the oxygen binding capacity of hemoglobin (1.39 ml of O_2/g of Hb), α_{O_2} is the solubility coefficient of oxygen in whole blood (0.003 ml of O_2/dl·mmHg), and P_{O_2} is the partial pressure of oxygen (mmHg), which was determined using phosphorescence quenching microscopy.

Hemoglobin concentration, *[Hb]*, was calculated from Equation 9:

Equation 9

$$[Hb] = tHb - [tHb \cdot (COHb + MetHb)]$$

where *tHB* is total hemoglobin concentration, *COHb* and *MetHb* are the fraction of *tHb* that is either carboxyhemoglobin or methemoglobin, respectively. It was assumed that spinotrapezius arteriolar and venular [Hb] were equivalent to carotid artery [Hb]. This end result is the quantity of hemoglobin available for binding to oxygen.

S_{O_2} was calculated from microvascular P_{O_2}, based on the rat oxyhemoglobin dissociation curve (

Figure 1, page 7) using the Hill model and Mathcad 2000 (MathSoft, Inc., Cambridge, MA):

Equation 10

$$S_{O_2} = So_2^{\max} \cdot \frac{\left(P_{O_2}^{virtual}\right)^n}{P_{50}{}^n + \left(P_{O_2}^{virtual}\right)^n}$$

where $So_2^{\max}$ is 100, the Hill coefficient, *n*, is 2.7 (Kunert, Liard et al. 1996), and the P_{50} for rat blood, based on previous studies (Hall 1966; Lahiri 1975; Teisseire, Soulard et al. 1984; Kunert, Liard et al. 1996; Eichelbronner, Sielenkamper et al. 1999; Zinchuk and Dorokhina 2002), is 36 mmHg. "Virtual" P_{O_2} ($P_{O_2}^{virtual}$), which is based on standard temperature, *pH* and P_{CO_2} (via base excess, *BE*), was calculated from microvascular P_{O_2} measures ($P_{O_2}^{measured}$) according to Equation 11:

Equation 11

$$P_{O_2}^{virtual} = 10^{\left(\log_{10} Po_2^{measured} + 0.48(pH - 7.4) - 0.024(T_m - 37) - 0.0013 \cdot BE\right)}$$

that combines the equations of Severinghaus (1966). Based on the work of Lash and Bohlen (1987), arteriolar pH was assumed to be equivalent to that of carotid arterial blood, and venular pH was assumed to be 0.06 (the mean arterial-venous pH difference) (Teisseire, Soulard et al. 1984; Powell, Machiedo et al. 1991) less than arterial pH. Spinotrapezius muscle temperature was used as spinotrapezius blood temperature (T_m). Base excess (BE), which has only a minor impact on the oxyhemoglobin dissociation curve, was assumed to be equivalent in both arterial and venous blood.

Blood flow

Spinotrapezius blood flow ($\dot{Q}^{ST}$), of both the primary arteriole and venule, was calculated from Equation 12, which relates cross-sectional area of the blood vessel and average blood velocity:

Equation 12

$$\dot{Q}^{ST} = \pi\left(\frac{d}{2}\right)^2 \bar{v}$$

where d and $\bar{v}$ are the diameter and mean blood velocity, respectively. The diameter was determined during off-line analysis by measuring the internal width, perpendicular to the direction of blood flow, of the vessel on a video monitor, which was calibrated with a stage micrometer (Bausch & Lomb, Rochester, NY). Using a Neofluar 40X/N.A 0.75

water immersion objective (Model 46-07-52, Carl Zeiss, Inc.), 1.0 mm on the video monitor was equivalent to 0.51 μm on the microscope stage. The microscope was focused on the median plane of the vessel.

Blood velocity

As the velocity profile (Figure 14) demonstrates, blood velocity decreases away from the longitudinal axis of the vessel (R_0). Pittman and Ellsworth described red blood cell velocity with Equation 13 (Pittman and Ellsworth 1986),

Equation 13

$$v(r) = v_0\left[1 - B\left(\frac{r^2}{R^2}\right)\right]$$

where r is the radial distance from the axis, v_0 is maximal blood velocity ($r = 0$), B describes the bluntness of the profile, which ranges from 0 (plug flow) to 1 (Poiseuille parabolic flow), and R is the vessel radius. This equation forms the basis for deriving many of the equations used below for both venular and arteriolar velocity calculations.

To help determine blood velocity, a 0.1 ml solution (concentration $4.5 \cdot 10^8$ particles/ml) of 2.0 μm FluoSpheres, fluorescent microspheres (F-8827, lot 69A1, Molecular Probes, Inc., Eugene, OR), were injected via the jugular venous catheter for each time point measured (Rovainen, Wang et al. 1992; Vovenko, Golub et al. 2002). To prevent hypotensive episodes due to the anti-aggregate compound, Tween-20, the FluoSpheres were prepared as described in Appendix V. For blood velocity measurements, these

FluoSpheres were briefly excited by a 100 Hz flash illumination. Since the VCR captures video frames at a rate of 30 Hz, each microsphere produced a train of approximately three particle images on a single video frame.

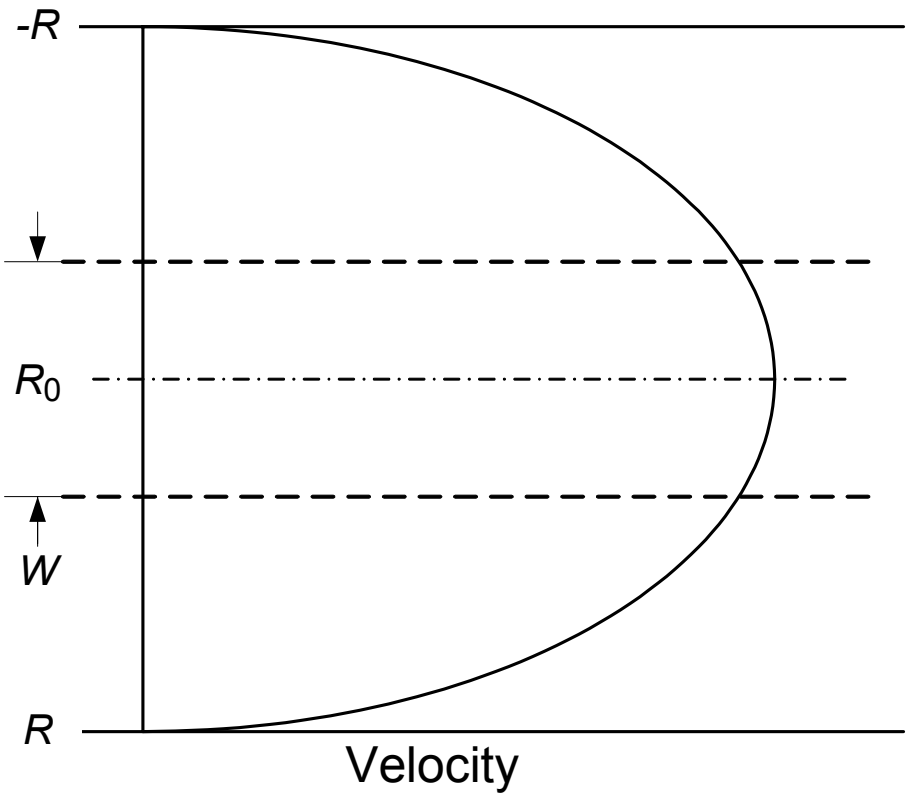

Figure 14. Longitudinal section of vessel, demonstrating bluntness of the velocity profile (B), vessel radius (R), longitudinal axis of vessel (R_0), and middle one-third of vessel (W).

Depth of field

The depth of field (*D*) for the objective was calculated to be 0.62 μm using Equation 14 and Equation 15, from Slayter (1970),

Equation 14

$$D = \frac{0.61\lambda \cos\alpha}{n \sin^2 \alpha}$$

Equation 15

$$\alpha = \sin^{-1}\left(\frac{\text{N.A.}}{n}\right)$$

where λ is the emission wavelength from the FluoSphere, 515 nm, α is the aperture, or vertex angle, 34°, and n is the refractive index of water, 1.337 (Figure 15). Thus, microspheres within ± 0.31 μm of the image plane will appear in focus. Whether the 2-μm diameter fluorescent particles were in focus was determined subjectively by the quality of the image, and objectively by the size of the microsphere image on the video monitor; "in-focus" microspheres have an on-screen diameter of ~4 mm (see above). This method of determining if RBCs or microspheres are in the median plane has been validated by Bishop *et al* (2001) and Tangelder *et al* (1986).

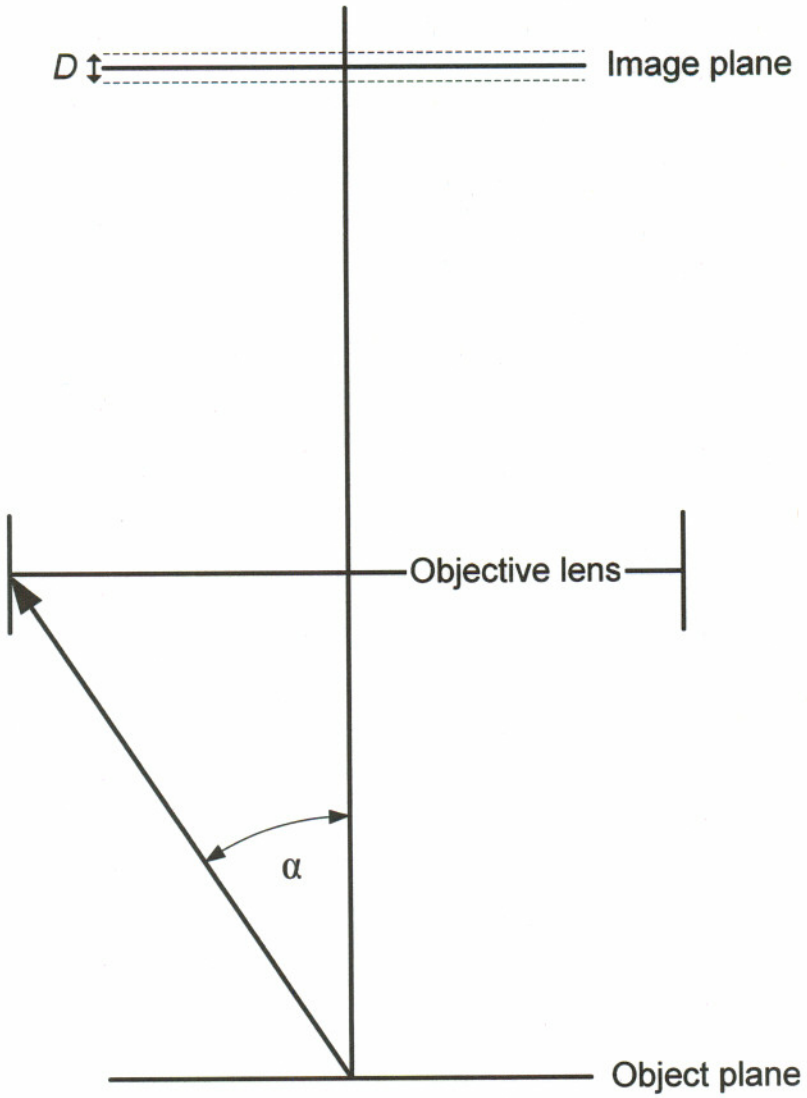

Figure 15. Depth of field (*D*) and aperture angle (*α*).

Venular blood velocity

In venules, where velocity is slower, maximal blood velocity was determined. The distance between in-focus microspheres on the median plane of the vessel and within the middle one-third of the vessel (*W*) (Figure 16) allowed for determination of particle (fluorescent microsphere) velocity (v_p) during off-line analysis, using Equation 16:

Equation 16

$$v_p = \frac{\left(\frac{d_t}{n-1}\right)}{t}$$

where d_t is the total distance between the first and last image of a single particle captured in a video frame, n is the number of times a microsphere appears in that frame, and t is 0.01 seconds (the time between flashes for 100 Hz excitation). The average velocity, weighted by particle frequency ($\bar{v}^*$), was determined by averaging the velocities of approximately 10 different particles (v_p). The result of the arithmetic average of the particle velocities is a value that is weighted by particle velocity, since the number of particles passing through the observation region is proportional to their individual velocities.

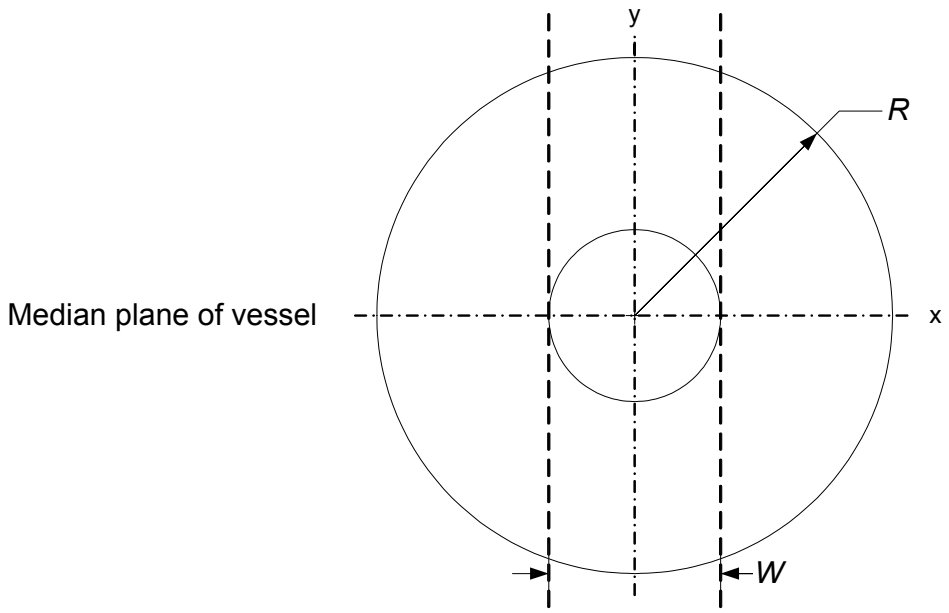

Figure 16. Cross section of vessel, demonstrating median plane, vessel radius (R) and the middle one-third of vessel (W).

Mean blood velocity ($\overline{v}$) was calculated from $\overline{v}^*$ using Equation 17 (Pittman 2004),

Equation 17

$$\overline{v} = \overline{v}^* \left(\frac{\left(1-\frac{B}{2}\right)\left(1-\frac{B}{3}\left(\frac{W}{2R}\right)^2\right)}{1-\frac{2B}{3}\left(\frac{W}{2R}\right)^2+\frac{B^2}{5}\left(\frac{W}{2R}\right)^4} \right)$$

Observing venules in the rat spinotrapezius muscle, Bishop *et al* (2001) reported values for *B* ranging from 0.9 to 1.1; thus, my calculations will assume that *B* is 1, Poiseuille flow. In addition, *W/2R* (Figure 16) was arbitrarily set to be 0.33.

Arteriolar blood velocity

In arterioles, the blood velocity was often so fast that, at a 100-Hz flash rate, centerline microspheres often appeared only once, and thus, their velocity could not be calculated. When this occurred, a slightly different methodology and equation were used. Instead of measuring central particle velocities, individual particle velocities (v_p) were determined on the median plane *outside* of the center one-third of the vessel, the area excluding *W* (Figure 16). Again, averaged velocity, weighted by particle velocity ($\overline{v}^*$) was determined by averaging the velocities of approximately 10 different particles.

In this case, assuming $B = 1$, mean blood velocity was calculated using Equation 18 (Pittman 2004),

Equation 18

$$\bar{v} = \bar{v}^{*}\left(\frac{\left[\frac{1}{3} - \frac{1}{4}\left(\frac{W}{2R}\right) + \frac{1}{6}\left(\frac{W}{2R}\right)^{2}\right]}{\left[\frac{8}{15} - \frac{W}{2R} + \frac{2}{3}\left(\frac{W}{2R}\right)^{3} - \frac{1}{5}\left(\frac{W}{2R}\right)^{5}\right]}\right)$$

This equation assumed that the depth of field was much less than the radius of the vessel; this was an appropriate assumption given that the depth of field was 0.62 μm and the radius was approximately 50 μm.

Muscle Contraction and Contractile Measures

The muscle contractions were initiated via a muscle stimulator (A310 Accupulser pulse generator and A360 high voltage stimulus isolator, World Precision Instruments, Inc., Sarasota, FL) connected to the exteriorized spinotrapezius muscle by two silver/silver chloride electrodes. The electrodes were fabricated from thin strips of an electrically conductive polymer coated film (114-26 B, Creative Materials, Inc., Tyngsboro, MA) and insulated 20-gauge wire connected by an electrically conductive epoxy (GPC 251, Creative Materials, Inc.).

Muscle force was measured with a Grass force-displacement transducer (model FT03C, Grass Instrument Co.), which has a linear sensitivity of 2 mg to 10 kg and a resonant frequency of 85 Hz; the transducer previously demonstrated a linear relationship between voltage and mass (Figure 17). Twenty-gauge wire was used to connect the wire support of the spinotrapezius muscle directly to the force transducer (Figure 9). The force transducer was attached to a tension adjuster mounted on the animal platform, which was used to optimize muscle length (L_o) during whole muscle isometric twitch contractions. During preliminary tests, it was determined that L_o occurred at a preload of ~3 g, which is in agreement with the results of Suzuki *et al* (1995).

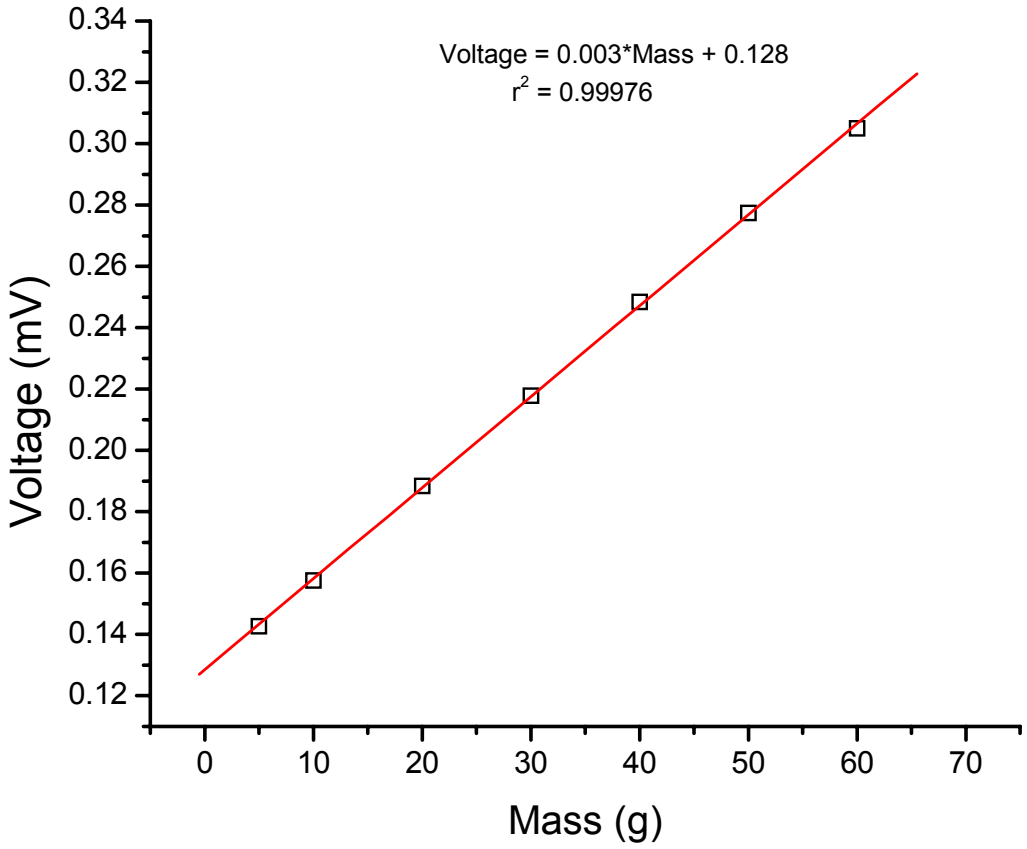

Figure 17. Force transducer calibration curve

Signals from the force transducer were sent to a general purpose transducer amplifier (DA-100C, BIOPAC Systems, Inc., Goleta, CA; gain of 200 and with a 10 and 100 Hz low pass filter) and high-speed data acquisition system (MP150, BIOPAC) via a six-pin Grass cable and transducer connector interface (TCI-100, BIOPAC), and then to a desktop computer for continuous on-line data acquisition at a rate of 100 Hz (Acq*Knowledge* software, v3.7.3, BIOPAC).

Peak force measurements were obtained during 200 msec stimulation at 80 Hz. In addition, muscle force was continuously acquired during a three-minute muscle stimulation protocol. This protocol involved contractions at a rate of one contraction per second; each contraction was stimulated by a 9-pulse (0.5 msec pulse duration) constant-frequency train delivered over 200 msec (40 Hz) (Figure 18), which was verified using a digital oscilloscope (TDS 2002, Tektronix, Beavertown, OR). From this recording, isometric muscle "work" and fatigue index were calculated.

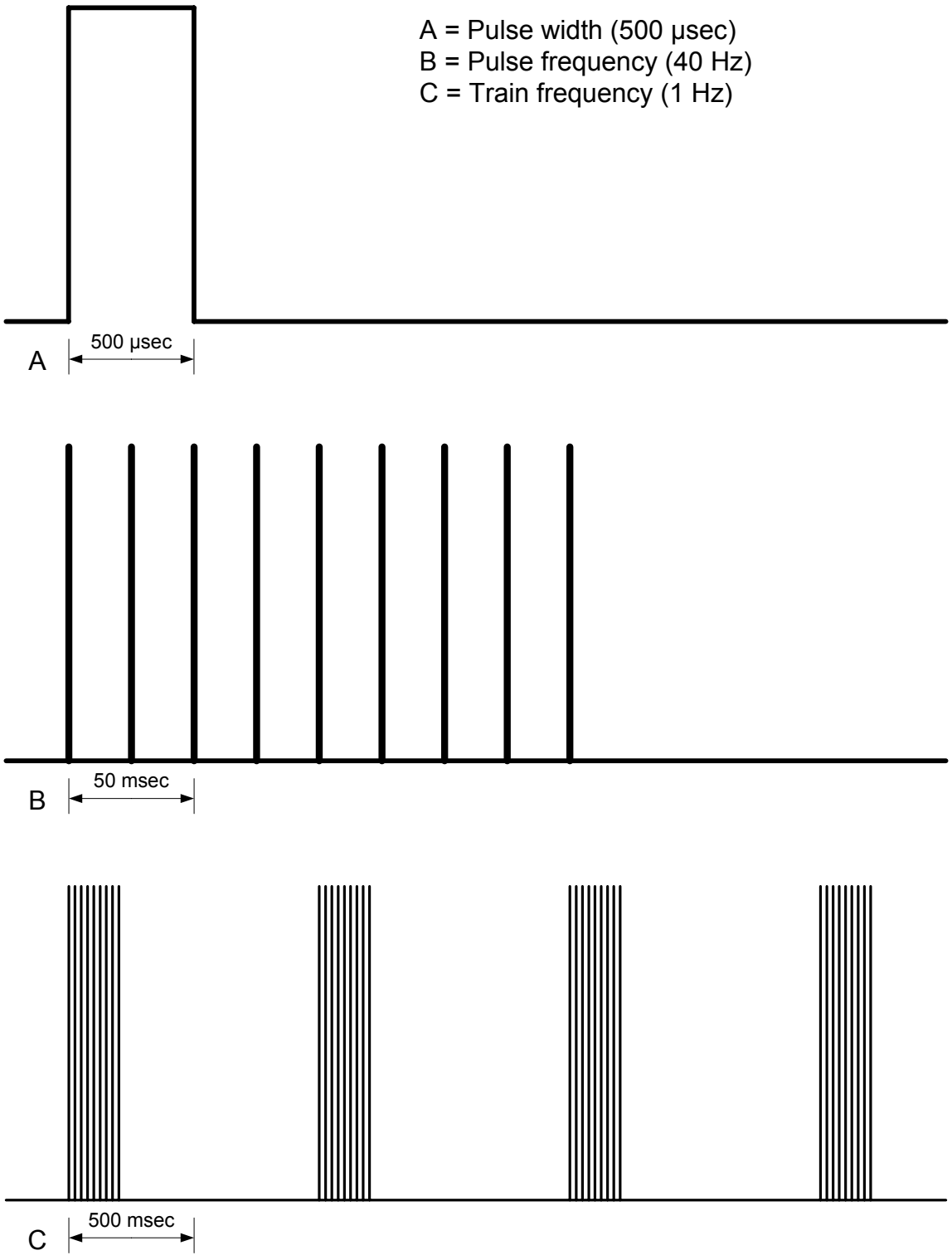

Figure 18. Stimulation protocol, where A) is an individual pulse, B) is a train of nine individual pulses, and C) is series of pulse trains (note the different time scales).

The force-time integral (FTI):

Equation 19

$$W = \int_{0}^{180} F \cdot dt$$

was used to quantify isometric muscle work (*W*) based on force (*F*) and time (Rome and Kushmerick 1983; Russ, Elliott et al. 2002). FTI was calculated from the force curves (Figure 19) using Origin 7.05 (OriginLab Corp., Northhampton, MA), and normalized to the estimated muscle cross-sectional area (*CSA*) in cm^2:

Equation 20

$$CSA = \frac{m}{\rho \cdot L_0}.$$

where *m* is mass in grams, ρ is density, assumed to be 1.05 $g \cdot cm^{-2}$ (Rome and Kushmerick 1983), and L_0 is muscle length in centimeters, to give a final quantity in $N \cdot s/cm^2$.

Fatigue index (FI) (Burke, Levine et al. 1973) was calculated as the percent decline in force from its peak to the last contraction of the three-minute protocol (Equation 21) (higher values mean less fatigue).

Equation 21

$$FI = 100 \cdot \frac{F_{\text{terminal}}}{F_{\text{peak}}}$$

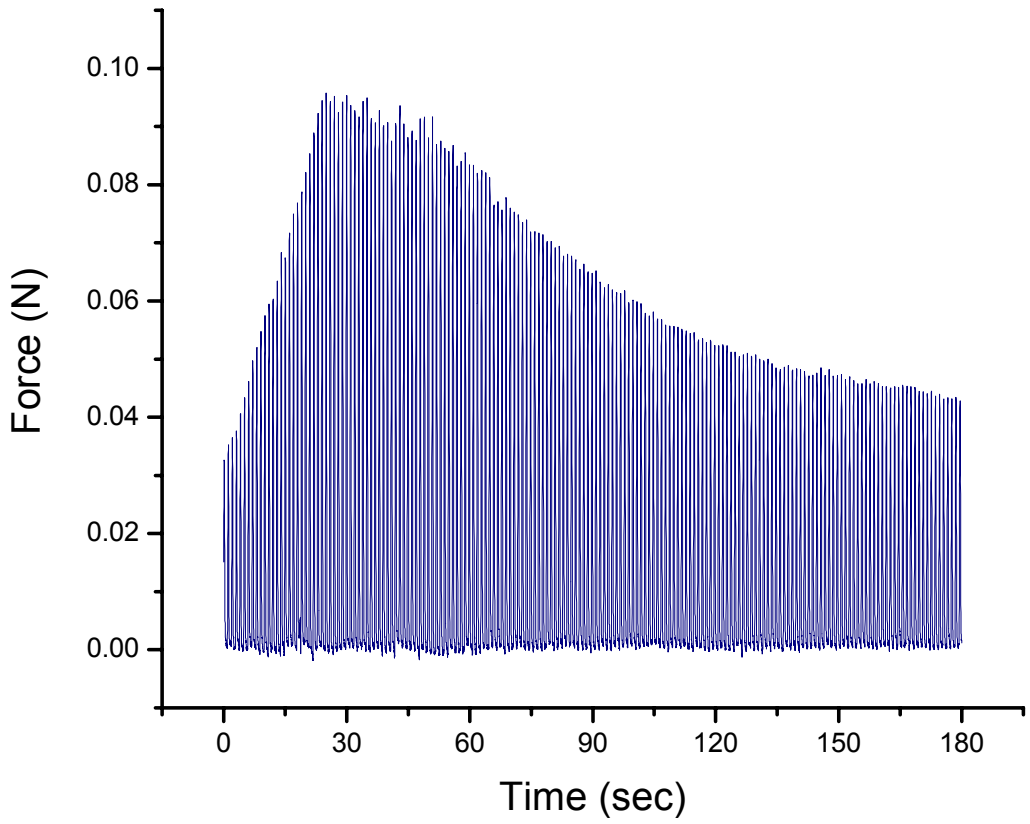

Figure 19. Representative spinotrapezius force tracing, from which force-time integral and fatigue index were calculated.

Specific protocols

The following details the experimental protocol for each phase. For all animals, Pa_{O_2} and Pa_{O_2}/FI_{O_2} ratio, an index of respiratory function (Sheridan, Zapol et al. 1999), was used to assess the degree of hypoxemia and indirectly quantify the severity of emphysema or other respiratory pathology. While a normal Pa_{O_2}/FI_{O_2} ratio should be ~500 (100/0.21), values of less than 300, 200, or 100 indicate a mild, moderate, or severe gas exchange impairment, likely due to intrapulmonary shunting and lung injury (Artigas, Bernard et al. 1998).

Phase I

Experiments were conducted on groups of animals 4, 8, 12, 16, or 20 weeks following the initial instillation of either elastase or saline to help determine the time course of any changes in arterial blood gases or transformation of muscle fiber types. After initial anesthesia and oral endotracheal intubation (described on pages 39 and 40, respectively), the animal was placed on a small animal ventilator set for a FI_{O_2} of 0.21 (room air), respiratory rate (RR) of 60 breaths per min (bpm), and inspiratory pressure of 10-12 cmH_2O. Pilot testing revealed that these settings resulted in normal ventilation as determined by arterial pH and P_{CO_2}.

Following 20 minutes of recovery and equilibration on the ventilator, and after femoral arterial cannulation, a *normoxic* arterial blood sample was withdrawn into a 100 µl capillary tube and analyzed in both a blood gas analyzer (ABL 705, Radiometer,

Denmark) to measure blood gas values (pH, Pa_{O_2}, Pa_{CO_2}), electrolytes (K^+, Na^+, Ca^{+2}, and Cl^-) and metabolites (glucose and lactate), and a co-oximeter (OSM 3 Hemoximeter, Radiometer) to measure tHb, COHb, MetHb, oxy-Hb, deoxy-Hb, and S_{O_2}. To simulate a fall in Pa_{O_2} (hypoxic condition), as occurs during whole body exercise in patients with emphysema, the FI_{O_2} was reduced to 0.15 and the animal given 20 minutes to equilibrate before withdrawing a *hypoxic* arterial blood sample.

At this point the animal was euthanized and the right spinotrapezius and soleus muscles were immediately removed and processed as previously described (page 44).

Phase II

For microcirculatory and muscle physiology experiments, animals were randomized approximately 62 weeks after elastase or saline instillation. The force transducer and pressure transducers were calibrated at two points prior to each experiment. After initial anesthesia and cannulations, the spinotrapezius muscle was prepared as previously described (page 10), and the animal was transferred to the thermostatic animal platform. The spinotrapezius muscle was positioned, ventral surface facing up, on the viewing pedestal of the platform, connected to the force transducer, moistened with normal saline and the covered with Saran film (S.C. Johnson & Sons, Inc. Racine, WI) to prevent desiccation and minimize atmospheric gas exchange.

After the platform was securely placed on the microscope, carotid arterial and jugular venous cannulae were connected to their respective pressure transducers, and muscle

tension adjusted to L_o; these parameters were continuously recorded on an electronic chart recorder (Biopac), as previously described, for the duration of the experiment. After peak force was measured from a twitch contraction (80 Hz for 200 msec), capped Tygon tubing was placed over the tracheostomy tube to deliver a $F_{I_{O_2}}$ of either 0.21 or 0.40 at a rate of 0.4 liters per minute. The animal was given at least 15 minutes to recover from surgery and equilibrate to its $F_{I_{O_2}}$. In the meantime, the Pd-MTCPP and FluoSphere solutions (Appendices III and V, respectively) were warmed to greater than room temperature, and the primary feed arteriole and venule were located under the microscope. Prior to baseline microvascular measures and the muscle contraction protocol, an arterial blood gas sample was drawn from the carotid artery and immediately analyzed (as described above), the Pd-MTCPP solution was injected via the femoral vein, and vital signs (body temperature, heart rate, systolic and diastolic blood pressure, and mean arterial pressure were measured. A continuous video recording of the microcirculation was made.

Baseline arteriolar and venular P_{O_2} measurements were made using the phosphorescence quenching method (page 54), followed by a 0.1-0.2 ml injection of FluoSpheres via the femoral vein, and blood velocity and diameter recorded as described above ("Blood flow," page 63). Immediately after a three-minute stimulation protocol, as described above ("Muscle Contraction and Contractile Measures," page 73), another 0.1-0.2 ml injection FluoSpheres was administered and blood velocity, vessel diameter, and microvascular P_{O_2} measurements were made, as well as five minutes after the end of the

contraction. The F_{IO_2} was then changed to either 0.21 or 0.40, and the animal given 15 minutes to recover and equilibrate. Baseline vital signs and microvascular measures were taken again, and the stimulation protocol and microvascular measures were repeated as previously described.

After the animal was euthanized, the spinotrapezius muscle was removed and weighed, a thoracic necropsy was performed, and the heart and lungs removed *en bloc*, inflated and photographed.

Statistical Analysis

Data in text and tables are presented as mean ($\bar{x}$) and standard deviation (SD), and graphic data are presented as mean values with bars or bands representing a 95% confidence interval. JMP version 4.0.4 (SAS Institute, Inc., Cary, NC) was used to perform significance tests (analyses of variance on multiple factors and t-tests on two independent means); actual p values are reported with the level of significance set at 0.05. Reporting in this manner is in accordance with established recommendations (Streiner 1996; Curran-Everett, Taylor et al. 1998), as well as the American Physiological Society's guidelines (Curran-Everett and Benos 2004).

Results

Phase I

Experimental animals

During pilot studies, as the instillation technique was being developed, five consecutive animals died during or immediately after the instillation procedure (one elastase, four saline); Poole (2002) had warned of this possibility. However, for no known reason, these were the last procedure-related fatalities. No other animals died prior to the final experiment.

Sixty-one animals were used in phase I, and data were available for 56 (two were taken by the Division of Animal Resources for testing, two died during the terminal experiment, and one animal is unaccounted for). As seen in Table 3, Student's t-test found no differences between elastase and saline groups with regard to age at instillation ($p = 0.57$), initial or final body mass ($p = 0.75$ and 0.78, respectively), or weight gain ($p = 0.96$) between initial instillation and the terminal experiment. Likewise, a two-way analysis of variance (ANOVA) found no effect ($p = 0.18$) for baseline body mass with respect to experimental group (elastase vs. saline) and time after instillation (weeks) (Table 4).

Figure 20 illustrates the change in mass between groups over time. In addition, soleus and spinotrapezius muscle masses were equivalent between experimental groups ($p = 0.31$ and 0.74, respectively). Over time, the only difference was found in the spinotrapezius muscle, which was lighter at four weeks after instillation than at eight, 12, 16, or 20 weeks (Figure 21) ($p < 0.01$ to 0.04).

Table 3. Baseline characteristics.

Group	n	Age at instillation (weeks)	Initial mass (g)	Final mass (g)	Difference (g)
Elastase	30	10.8 (SD 0.7)	213.7 (SD 16.2)	266.4 (SD 31.9)	52.8 (SD 32.8)
Saline	25	10.7 (SD 0.7)	214.9 (SD 11.3)	268.5 (SD 22.8)	53.6 (SD 24.5)
Total	55	10.8 (SD 0.7)	214.2 (SD 14.1)	267.4 (SD 27.9)	53.2 (SD 29.0)

Table 4. Final body mass (g) for each time interval.

Group	4 weeks	8 weeks	12 weeks	16 weeks	20 weeks
Elastase	234 (SD 10.9)	275 (SD 12.0)	268 (SD 10.1)	280 (SD 10.9)	278 (SD 12.0)
Saline	267 (SD 10.9)	257 (SD 15.4)	276 (SD 12.0)	265 (SD 12.0)	273 (SD 10.9)
Total	250 (SD 7.7)	266 (SD 9.8)	272 (SD 7.8)	272 (SD 8.1)	275 (SD 8.1)

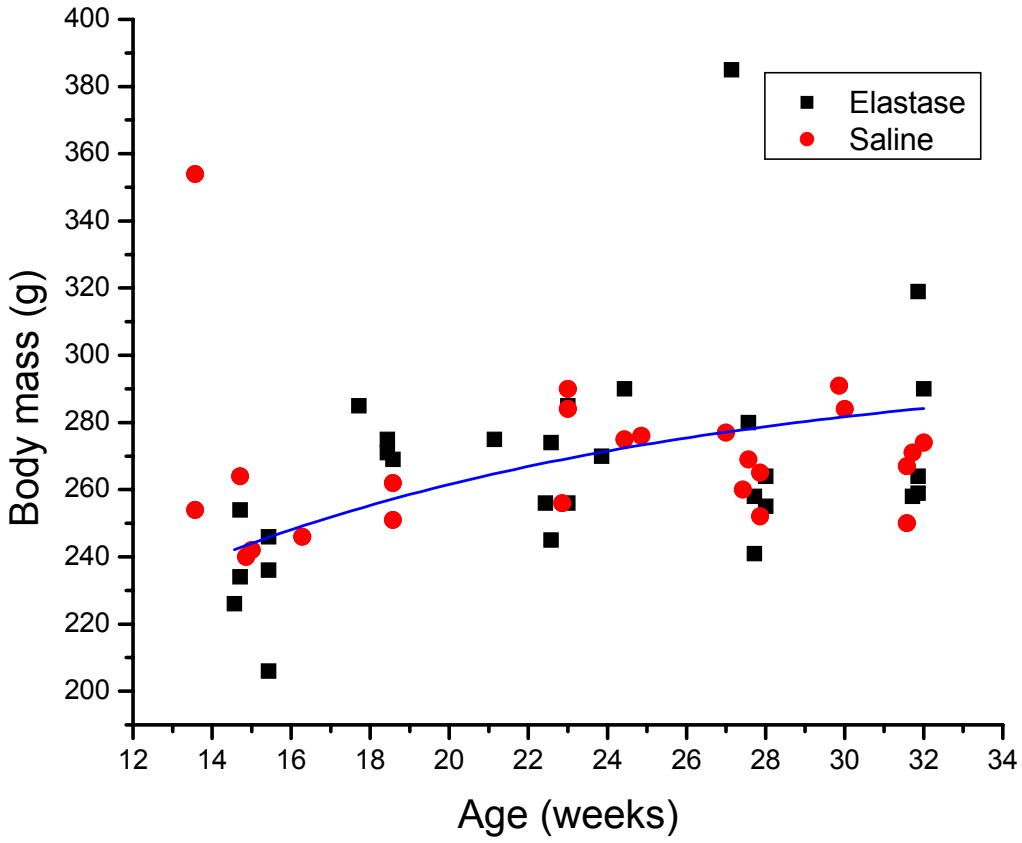

Figure 20. Growth curve.

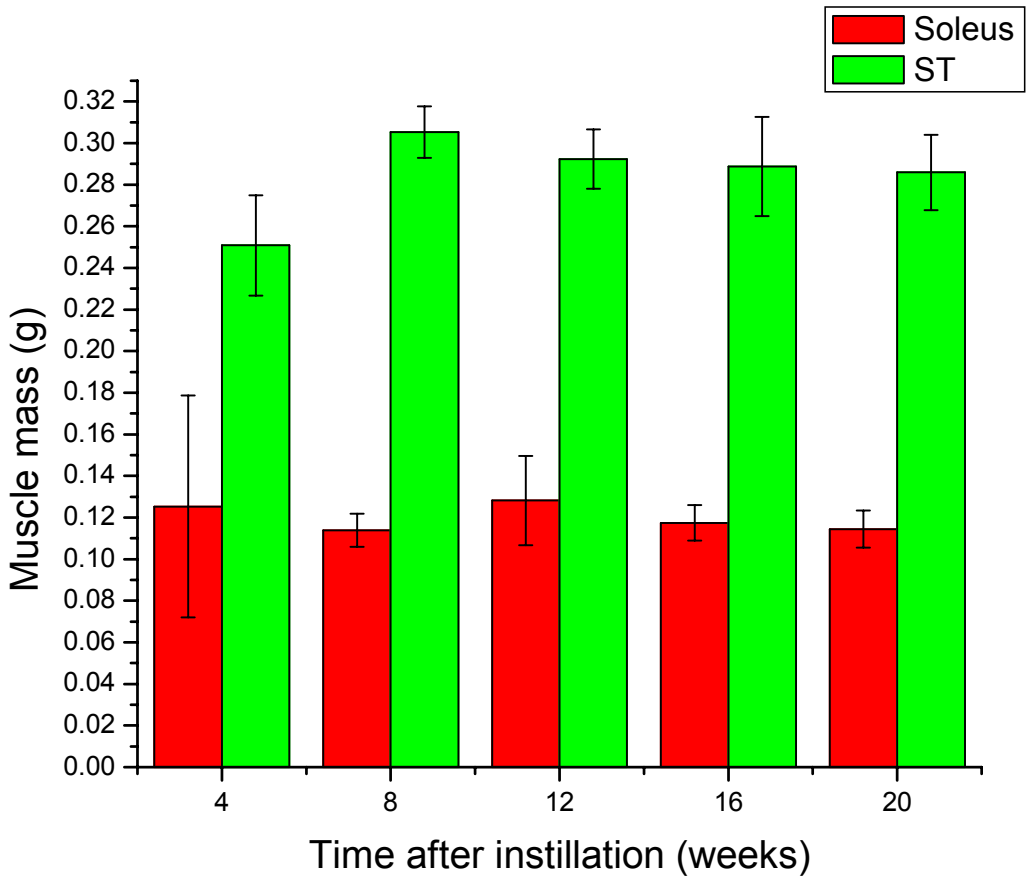

Figure 21. Soleus and spinotrapezius muscle masses over time.

To qualitatively assess whether or not the elastase instillation was producing emphysema, two animals had ventral-dorsal (Figures 22 and 23) and lateral chest radiographs (Figures 24 and 25) taken approximately 19 weeks after the instillation of either elastase or saline; it is fairly obvious that the rostral-caudal, lateral, and ventral-dorsal dimensions are larger in the elastase instilled animal, consistent with emphysema. Arterial Pa_{O_2} and Pa_{O_2}/FI_{O_2} ratio were used to quantitatively determine the severity of emphysema and the resulting hypoxemia (refer to "Arterial blood gases," page 91).

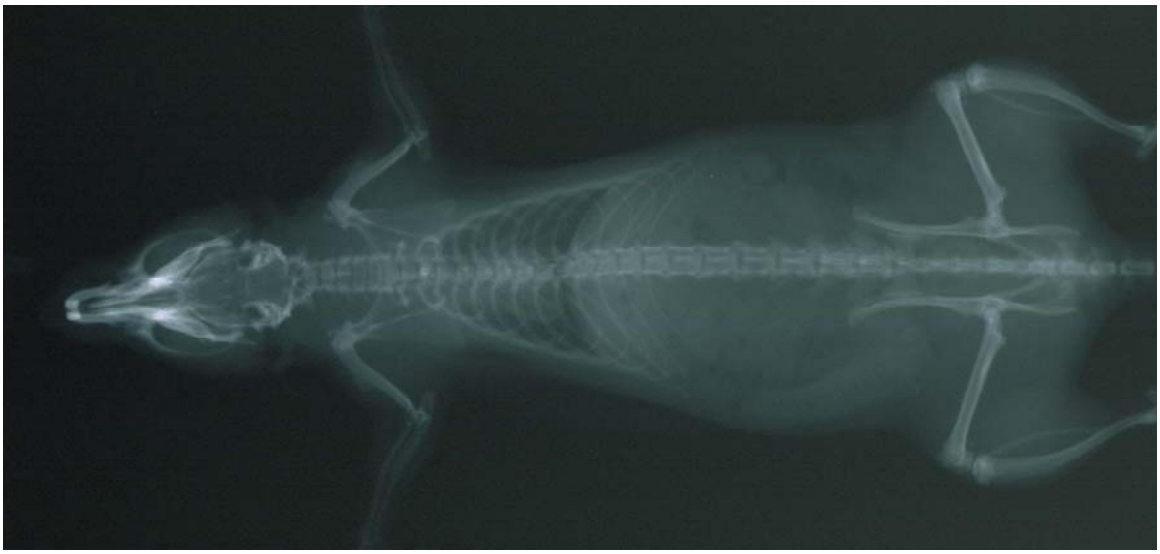

Figure 22. Ventral-dorsal chest radiograph of saline instilled rat.

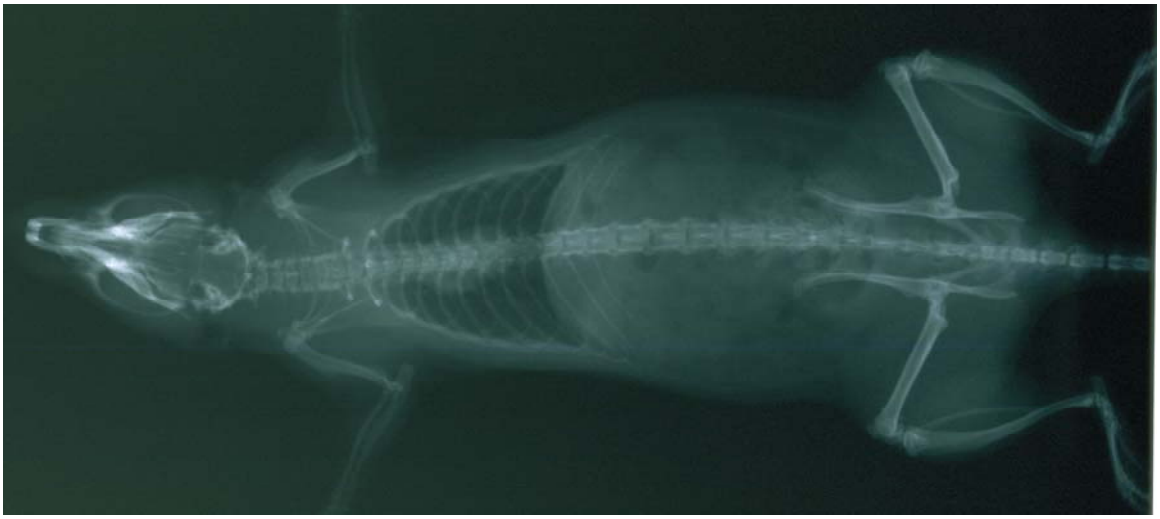

Figure 23. Ventral-dorsal chest radiograph of elastase instilled rat.

Figure 24. Lateral chest radiograph of saline instilled rat.

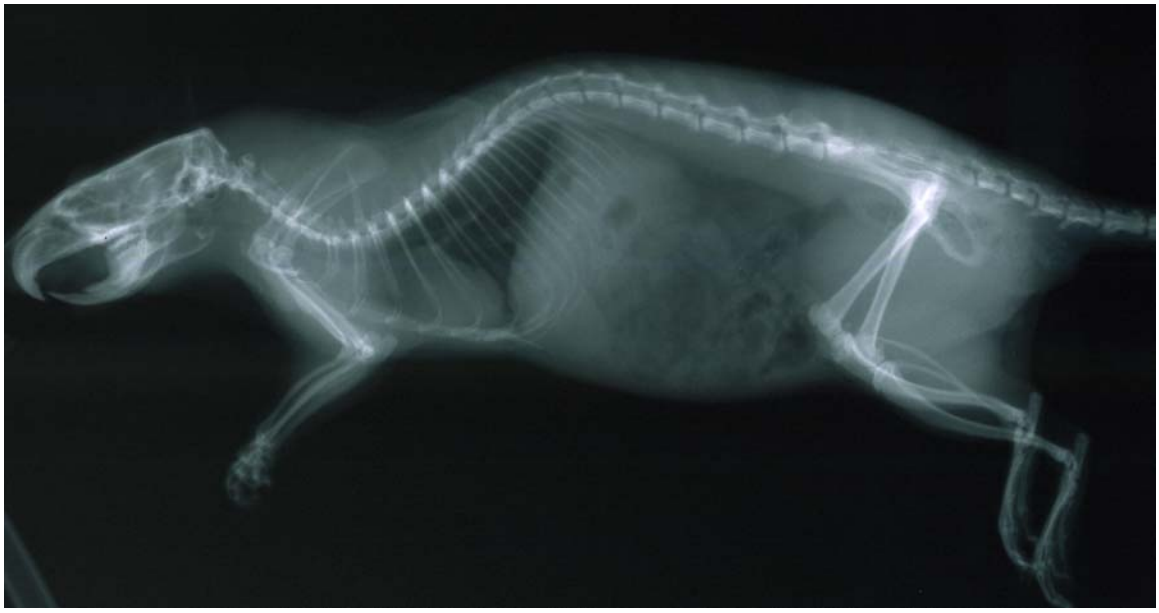

Figure 25. Lateral chest radiograph of elastase instilled rat.

Arterial blood gases

With the exception of arterial P_{O_2}, Pa_{O_2}/FI_{O_2} ratio, and glucose and lactate concentrations, arterial blood gas analysis revealed no differences between groups (elastase vs. saline) with regard to blood gases, acid-base status, hemoglobin, or electrolytes breathing either FI_{O_2} 0.21 (Table 5, Figure 26), or FI_{O_2} 0.15 (Table 6, Figure 27).

Table 5. Phase I arterial blood gas data on FI_{O_2} 0.21.

	Elastase	Saline	p value
pH	7.43 (SD 0.03)	7.44 (SD 0.03)	0.49
Pa_{CO_2} (mmHg)	40 (SD 3.4)	38.5 (SD 4.3)	0.07
Pa_{O_2} (mmHg)	77 (SD 10.7)	90 (SD 21.6)	**<0.01**
Pa_{O_2}/FI_{O_2}	365 (SD 51)	427 (SD 103)	**<0.01**
HCO_3^- (mmol/l)	26 (SD 0.9)	26 (SD 1.5)	0.08
Sa_{O_2} (%)	93 (SD 4.3)	94 (SD 6.7)	0.51
tHb (g/l)	140 (SD 7.4)	142 (SD 6.8)	0.19
K^+ (meq/l)	3.8 (SD 0.3)	3.8 (SD 0.2)	0.78
Na^+ (meq/l)	137 (SD 1.6)	136 (SD 1.4)	0.40
Ca^{+2} (meq/l)	2.2 (SD 0.2)	2.1 (SD 0.2)	0.57
Cl^- (meq/l)	99 (SD 2.4)	99 (SD 1.8)	0.71
Glucose (mg/dl)	224 (SD 31.2)	250 (SD 59.6)	**0.04**
Lactate (mmol/l)	1.0 (SD 0.4)	1.5 (SD 1.2)	**0.04**

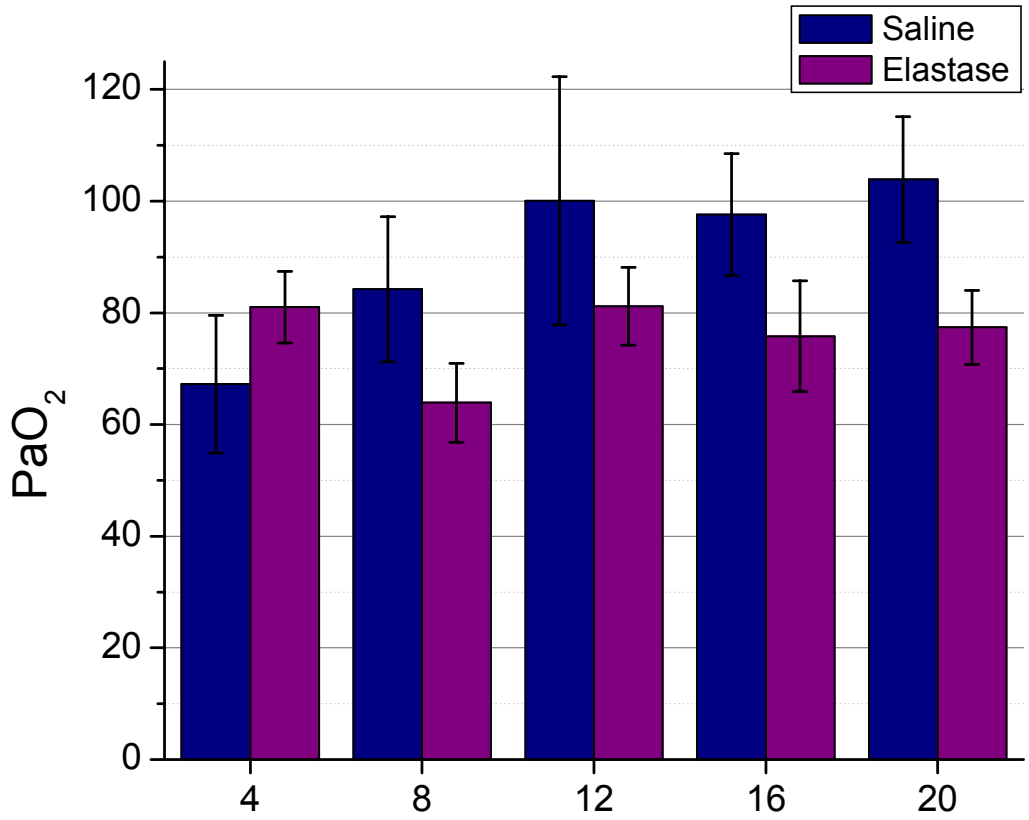

Figure 26. Arterial P_{O_2} at 4, 8, 12, 16, and 20 weeks; FI_{O_2} = 0.21.

Table 6. Phase I arterial blood gas data on FI_{O_2} 0.15.

	Elastase		Saline		p value
pH	7.42	(SD 0.07)	7.44	(SD 0.04)	0.31
Pa_{CO_2} (mmHg)	41	(SD 8.2)	39	(SD 4.3)	0.22
Pa_{O_2} (mmHg)	57	(SD 9)	67	(SD 12)	**<0.01**
Pa_{O_2}/FI_{O_2}	377	(SD 61)	449	(SD 77)	**<0.01**
HCO_3^- (mmol/l)	26	(SD 2.1)	26	(SD 1.3)	0.75
Sa_{O_2} (%)	84	(SD 12.3)	90	(SD 7.7)	0.06
tHb (g/l)	139	(SD 7)	142	(SD 7)	0.12
K^+ (meq/l)	4.0	(SD 0.3)	4.1	(SD 0.2)	0.31
Na^+ (meq/l)	136	(SD 2)	136	(SD 2)	0.65
Ca^{+2} (meq/l)	2.2	(SD 0.2)	2.2	(SD 0.2)	0.51
Cl^- (meq/l)	99	(SD 2)	99	(SD 2)	0.51
Glucose (mg/dl)	225	(SD 58)	233	(SD 74)	0.66
Lactate (mmol/l)	1.3	(SD 0.9)	1.0	(SD 0.5)	0.30

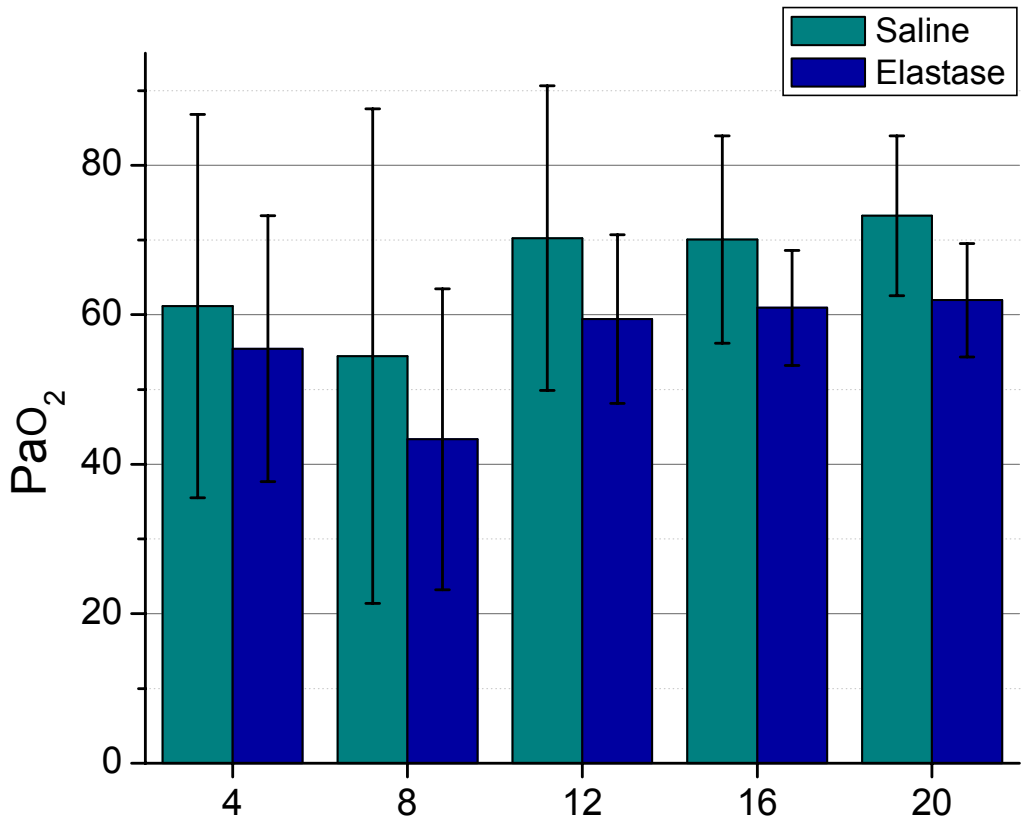

Figure 27. Arterial P_{O_2} at 4, 8, 12, 16, and 20 weeks; FI_{O_2} = 0.15.

MHC isoforms

SDS-PAGE (Figure 28**)** was used to differentiate the various MHC isoforms, and a densitometric analysis (Figure 29) was used to determine the relative proportions of each. The only statistically significant difference in MHC isoforms between experimental groups was a decrease in spinotrapezius MHC IIx, which was lower in the elastase group ($p = 0.01$); however, the slight increases in other MHC isoforms were not significant (Table 7). A two-way ANOVA for each MHC isoform found no interaction between *experimental group* (elastase vs. saline) and *age* (14, 18, 22, 26, or 30 weeks old) ($p = 0.08$ to 0.83). However, it did reveal differences in *soleus* muscle MHC expression with age for types I, IIa, and IIb ($p = 0.0002$, 0.05, and 0.006, respectively), but not IIx ($p = 0.58$) (Figure 30). In addition, *spinotrapezius* muscle MHC expression of type I, IIa, and IIx changed with age ($p = 0.03$, <0.01, and 0.02, respectively); there were no differences in IIb expression between age groups ($p = 0.25$) (Figure 31).

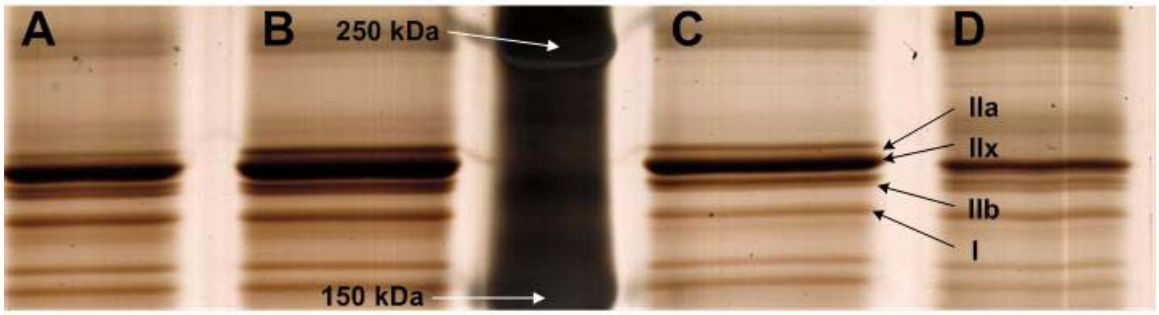

Figure 28. Representative soleus SDS-PAGE with arrows at reference molecular weights and MHC bands (~200 kDa). A, C, and D are 22, 18, and 26 wk old saline instilled animals, B is a 22 wk old elastase instilled animal.

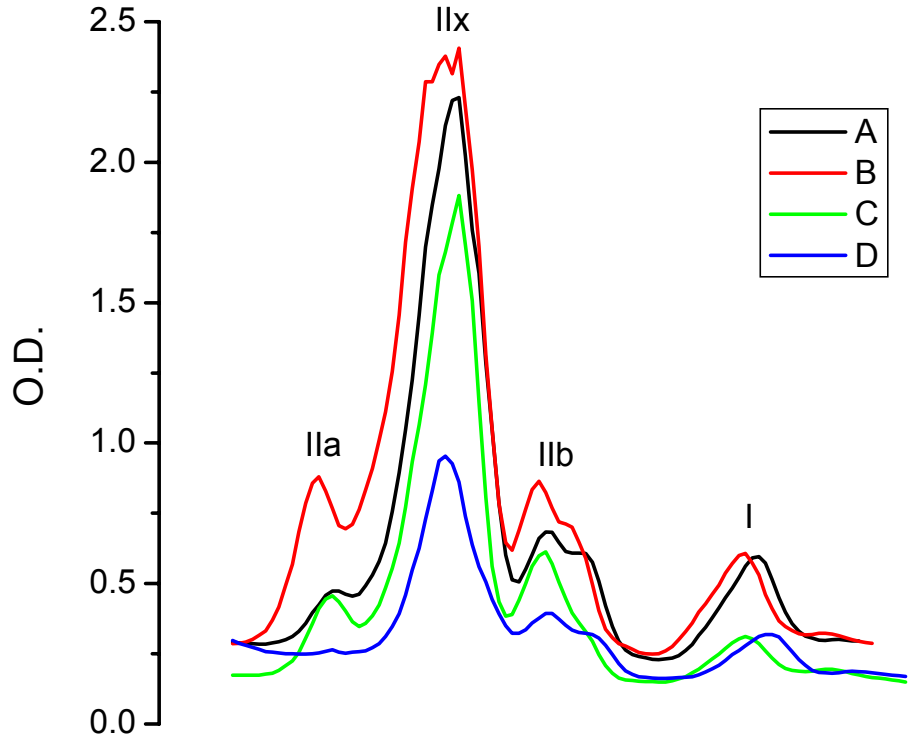

Figure 29. Representative densitometric analysis used to determine proportions of MHCs I, IIa, IIb, and IIx. Curves A – D correspond to the lanes labeled A – D in Figure 28.

Table 7. Percentage of MHC isoforms in elastase vs. saline instilled animals for all age groups.

	Elastase (n = 21)	**Saline (n = 13)**	**p value**
Soleus m.			
I	9% (SD 1)	9% (SD 1)	0.69
IIa	10% (SD 6)	11% (SD 9)	0.86
IIx	63% (SD 7)	62% (SD 10)	0.77
IIb	18% (SD 6)	18% (SD 4)	0.88
Spinotrapezius m.			
I	17% (SD 7)	16% (SD 7)	0.55
IIa	10% (SD 12)	6% (SD 4)	0.35
IIx	40% (SD 12)	51% (SD 9)	**0.01**
IIb	33% (SD 9)	27% (SD 7)	0.07

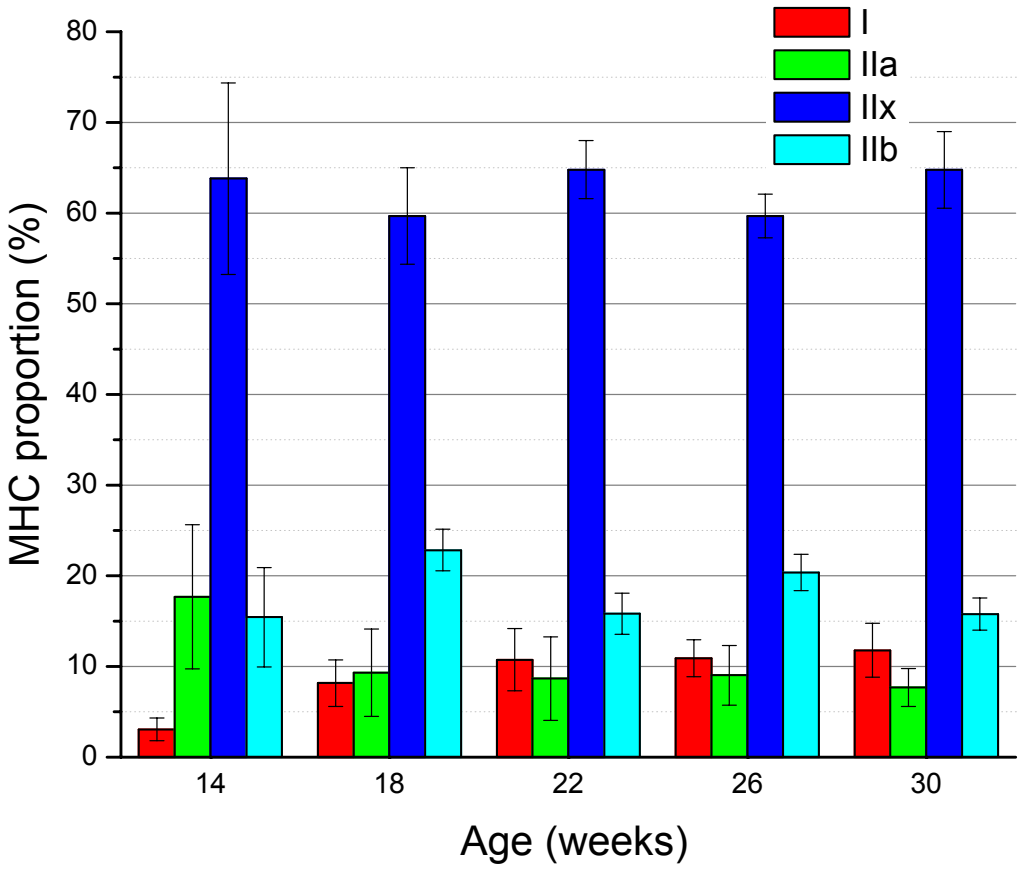

Figure 30. Soleus muscle MHC proportions by age.

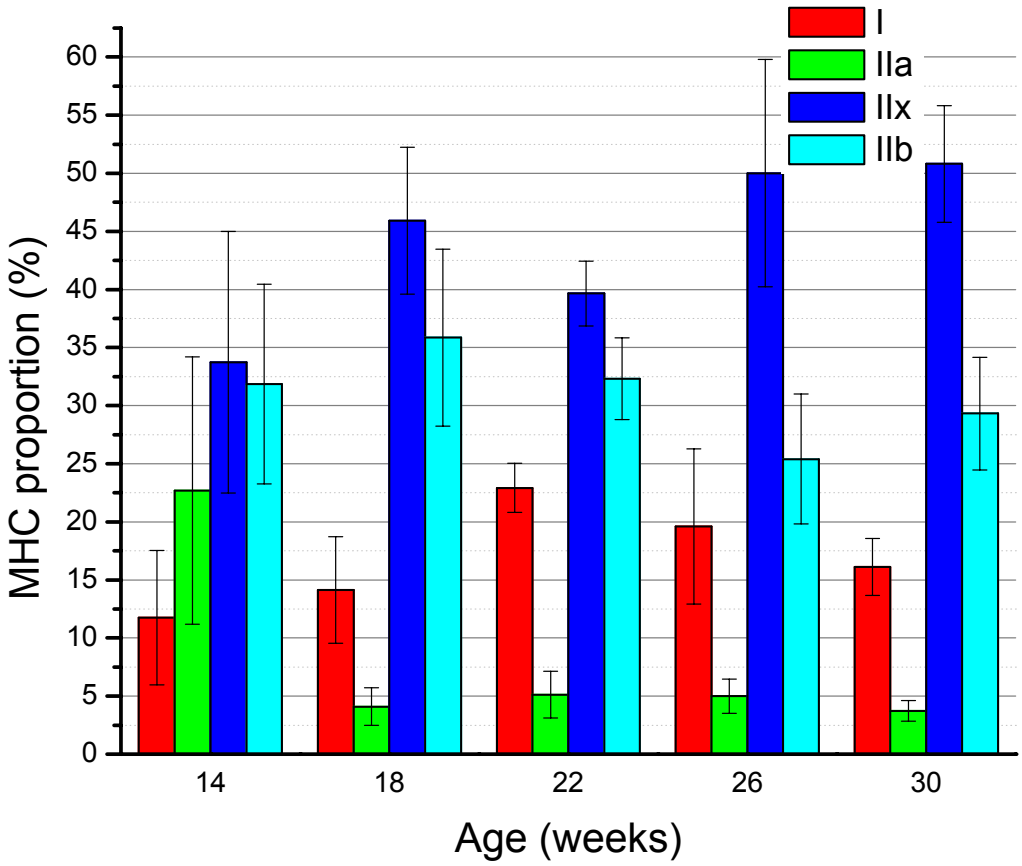

Figure 31. Spinotrapezius muscle MHC proportions by age.

Phase II

Experimental animals

There was no difference in body mass between elastase and saline groups ($\bar{x}$ = 294 g (SD 37) vs. 296 g (SD 22), respectively; p = 0.15). In addition, there were no differences in baseline vital signs between groups (Table 8). A matched pairs analysis also revealed no differences in heart rate (HR), respiratory rate (RR), mean arterial pressure (MAP), or body temperature between the exercise bouts on $F_{I_{O_2}}$ 0.21 versus 0.40 (p = 0.87, 0.42, 0.71, and 0.57, respectively), which indicates that the physiological conditions under which the animals performed each exercise bout were similar.

Initially, injection of 0.5 ml FluoSpheres caused a rapid and dramatic drop in blood pressure, severe enough to lead to death in a few preliminary experiments. Smaller doses (0.1 ml) still led to a substantial decline in blood pressure, which took several minutes to return to baseline (Figure 32). Eventually, it was determined that the anti-aggregation agent, Tween-20, was responsible (Figure 33).

Table 8. Baseline vital signs on FI_{O_2} 0.21 and 0.40.

	Elastase				**Saline**				**p value**
FI_{O_2}	0.21		0.40		0.21		0.40		E vs. S 0.21
HR (beats/min)	297	(SD 51)	285	(SD 66)	333	(SD 59)	327	(SD 65)	0.29
RR (breaths/min)	81	(SD 28)	57	(SD 12)	63	(SD 31)	67	(SD 10)	0.35
MAP (mmHg)	92	(SD 14)	92	(SD 15)	97	(SD 11)	97	(SD 15)	0.51
Body temp. (° C)	37.1	(SD 0.9)	37.1	(SD 0.7)	36.5	(SD 1.0)	36.5	(SD 0.9)	0.32

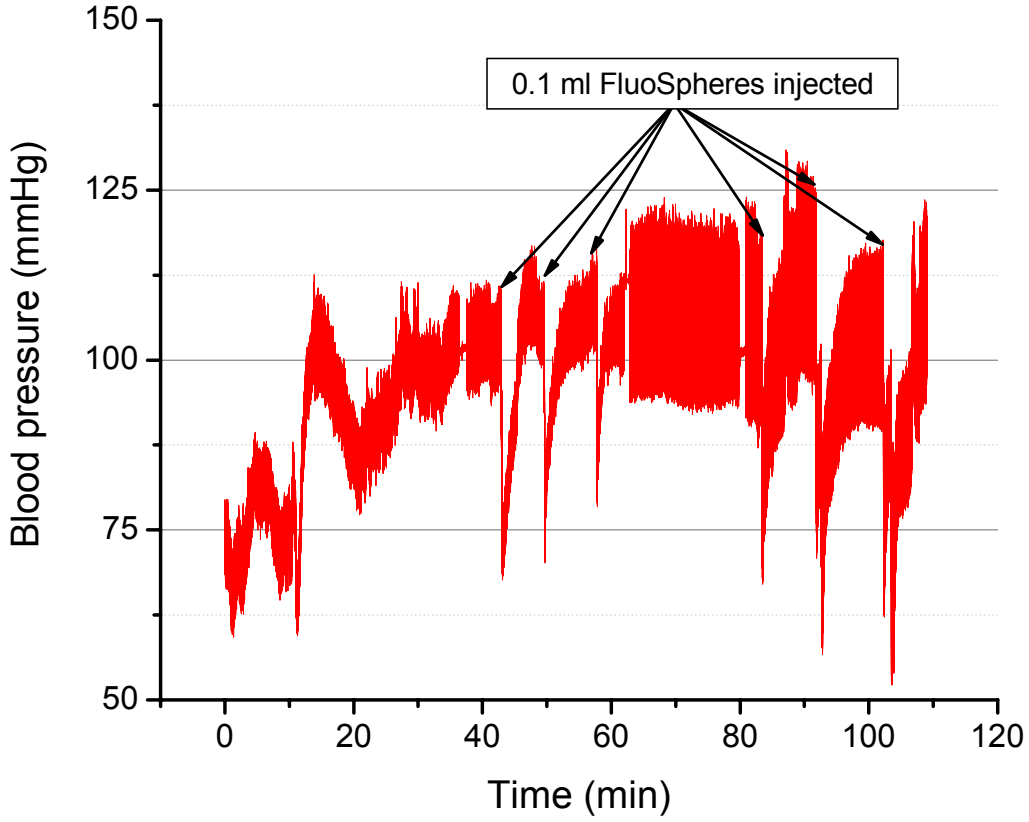

Figure 32. Arterial blood pressure tracing, demonstrating a dramatic hypotensive episode with each injection of FluoSpheres without Tween removed.

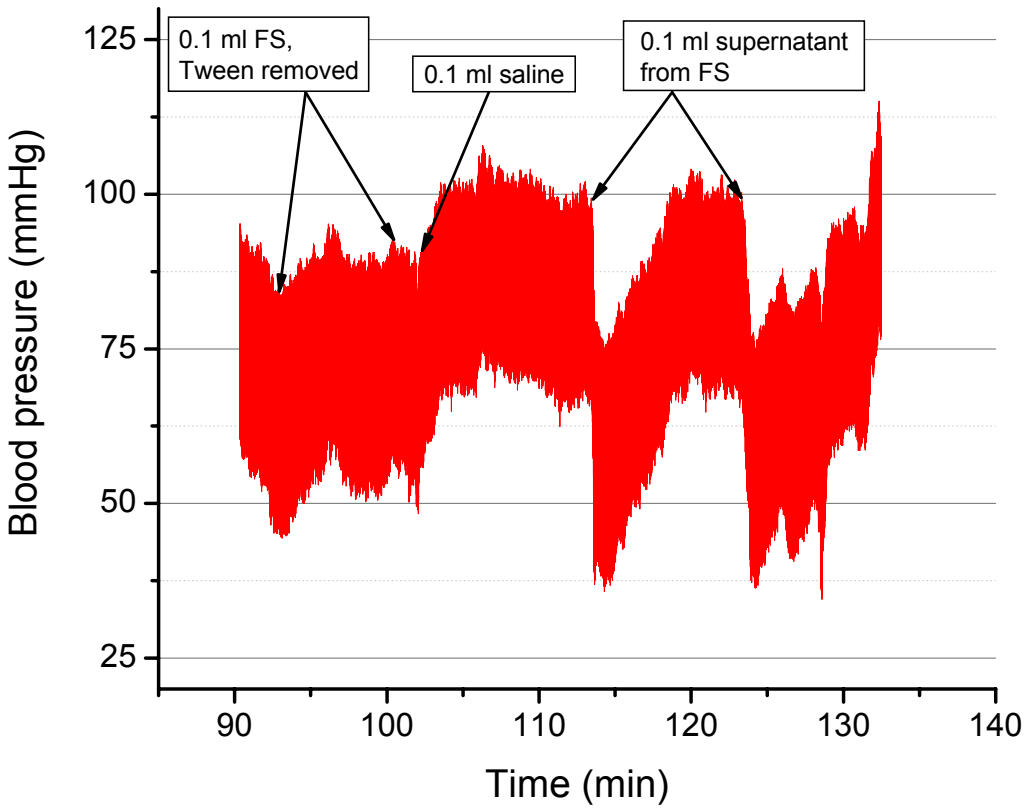

Figure 33. Arterial pressure tracing, demonstrating no hypotension after injection of either 1) FluoSpheres with Tween removed, or 2) normal saline, but significant hypotension when supernatant from diluted and centrifuged FluoSpheres is injected.

Lung pathology

Due to the surprisingly low systemic Pa_{O_2} values from phase I as well as anecdotal reports throughout this and other research universities, the lungs from each animal were grossly necropsied to determine if the animal had a lung pathology (*i.e.*, Rat respiratory virus) other than elastase-induced emphysema. No animal had normal looking lungs, and, if anything, the lungs from the saline group (Figure 34) looked even "less healthy" than those from the elastase group (Figure 35).

There does not appear to be a close relationship between severity of lung injury and Pa_{O_2}, although the animal with the highest Pa_{O_2} (Figure 35, B) appears to have a segmental (dorsal caudal and dorsal cranial) pattern of consolidation as opposed to the other lungs which show a more diffuse infiltration. Although not entirely obvious from these figures, there did appear to be a consistent pattern in which the right dorsal-caudal and dorsal-cranial segments demonstrated more infiltrate, with relative sparing of the left lung, and more medial and ventral segments of both the cranial and caudal lobes.

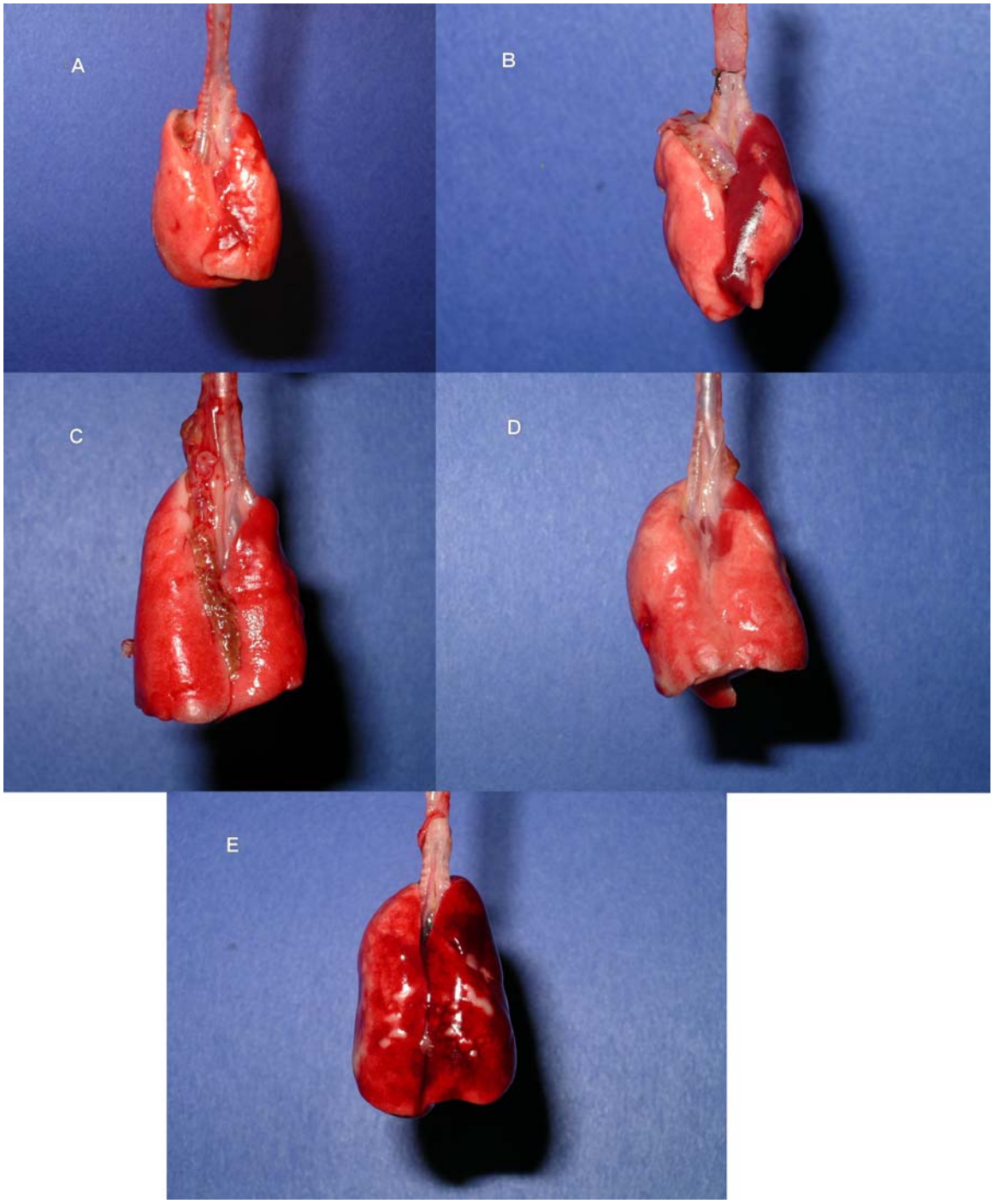

Figure 34. Lungs from necropsy of saline instilled animals, which had the following Pa_{O_2}'s (mmHg): A) 70, B) 96, C) 49, D) 79, and E) 62.

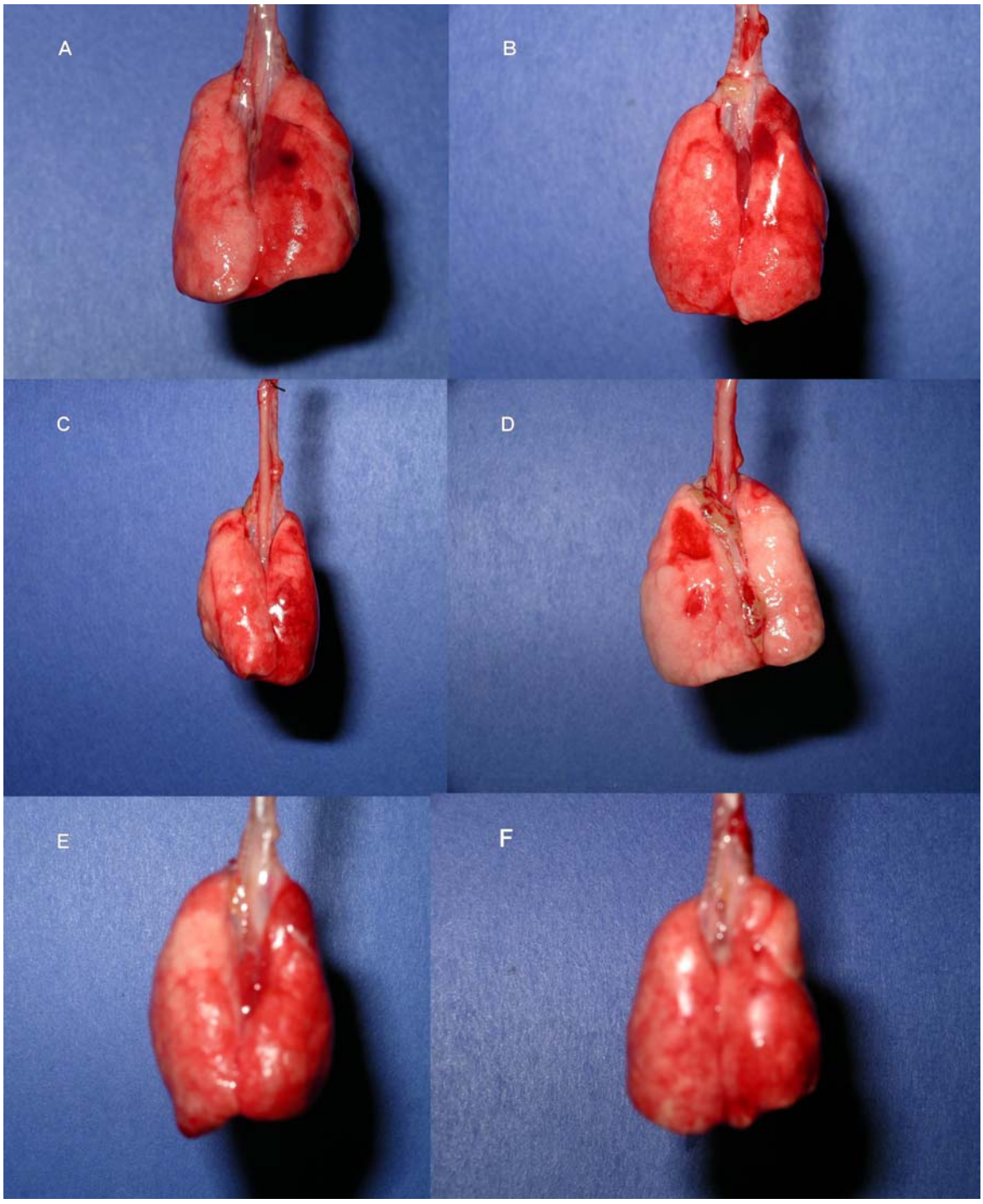

Figure 35. Lungs from necropsy of elastase instilled animals, which had the following Pa_{O_2}'s (mmHg): A) 64, B) 66, C) 66, D) 59, E) 49, and F) 72.

Arterial blood gases

Unfortunately, due to the lung pathology so prevalent in the animals in this study, both the elastase and saline groups were almost equally hypoxemic ($\bar{x}$ Pa_{O_2} 62 (SD 6.6) vs. 69 (SD 17.1), respectively with FI_{O_2} 0.21, $p = 0.36$), although on room air, only the elastase group had a $Pa_{O_2}/FI_{O_2} < 300$ (Table 9). However, both groups had a $Pa_{O_2}/FI_{O_2} < 300$ when breathing FI_{O_2} 0.40 (Table 10), indicating a mild gas exchange impairment. In fact, only one animal out of the 14, from the control group, had a room air Pa_{O_2} of > 80 mmHg.

Table 9. Phase II arterial blood gas data on FI_{O_2} 0.21.

	Elastase (n = 8)	**Saline (n = 6)**	**p value**
pH	7.44 (SD 0.04)	7.40 (SD 0.07)	0.17
Pa_{CO_2} (mmHg)	35 (SD 6.1)	43 (SD 10.1)	0.12
Pa_{O_2} (mmHg)	62 (SD 6.6)	69 (SD 17.1)	0.36
Pa_{O_2}/FI_{O_2}	297 (SD 31.3)	327 (SD 82)	0.36
HCO_3^- (mmol/l)	25 (SD 0.9)	25 (SD 1.5)	0.63
Sa_{O_2} (%)	87 (SD 5.3)	88 (SD 7.1)	0.81
tHb (g/l)	121 (SD 5.9)	123 (SD 6.5)	0.52
K^+ (meq/l)	3.6 (SD 0.3)	3.8 (SD 0.6)	0.58
Na^+ (meq/l)	142 (SD 2.3)	140 (SD 2.5)	0.16
Cl^- (meq/l)	107 (SD 2.3)	104 (SD 2.4)	**0.04**
Glucose (mg/dl)	228 (SD 58)	278 (SD 88)	0.23
Lactate (mmol/l)	1.7 (SD 0.4)	1.9 (SD 0.9)	0.59

Table 10. Phase II arterial blood gas data on FI_{O_2} 0.40.

	Elastase	Saline	p value
pH	7.39 (SD 0.03)	7.35 (SD 0.08)	0.24
Pa_{CO_2} (mmHg)	43 (SD 3.2)	49 (SD 11.0)	0.14
Pa_{O_2} (mmHg)	89 (SD 11)	107 (SD 8)	**0.01**
Pa_{O_2}/FI_{O_2}	224 (SD 28)	268 (SD 20)	**0.01**
HCO_3^- (mmol/l)	25 (SD 1.0)	24 (SD 1.0)	0.59
Sa_{O_2} (%)	96 (SD 2.8)	98 (SD 2.0)	0.24
tHb (g/l)	126 (SD 4.6)	126 (SD 8.0)	0.93
K^+ (meq/l)	3.7 (SD 0.3)	3.7 (SD 0.4)	0.75
Na^+ (meq/l)	141 (SD 2.1)	141 (SD 1.9)	0.87
Cl^- (meq/l)	105 (SD 2.1)	104 (SD 2.7)	0.44
Glucose (mg/dl)	228 (SD 72)	230 (SD 64)	0.97
Lactate (mmol/l)	1.2 (SD 0.4)	1.6 (SD 0.6)	0.25

Oxygen delivery to and consumption by the spinotrapezius muscle

Microvascular P_{O_2}

Using phosphorescence quenching microscopy, arteriolar and venular P_{O_2} were measured in the spinotrapezius (ST) muscle at rest, immediately after a three-minute contraction, and five minutes after contraction (time 0, 3, and 8, respectively, on the subsequent graphs) with the animal breathing a FI_{O_2} of 0.21 (Figures 36 and 37) or 0.40 (Figures 38 and 39). With the exception of first post-contraction venular P_{O_2} on FI_{O_2} 0.21, and both the baseline arteriolar and venular P_{O_2} on FI_{O_2} 0.21 ($p = 0.04$, 0.02, and 0.03, respectively), P_{O_2} was equivalent between groups. In addition, a repeated measures analysis revealed statistically equivalent arteriolar and venular P_{O_2} across all time points, for both FI_{O_2} 0.21 and 0.40 ($p = 0.15 – 0.92$).

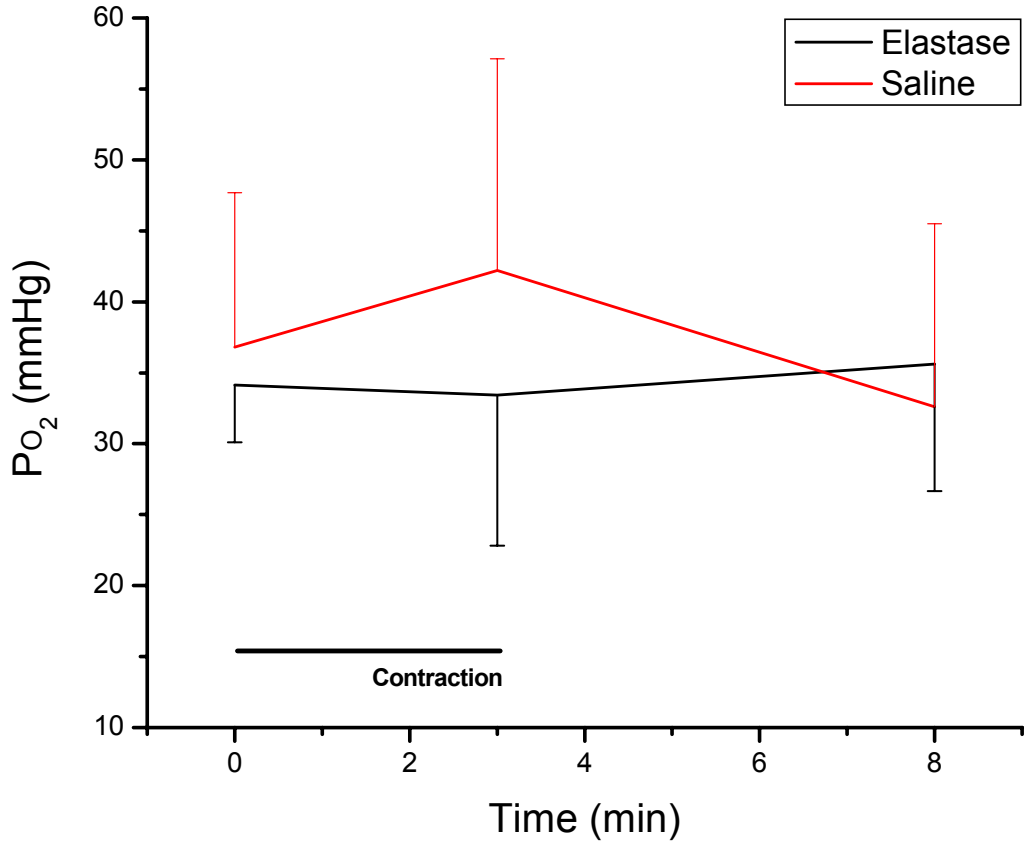

Figure 36. Arteriolar P_{O_2} before (time = 0) and after a three-minute contraction (time = 3 and 8); FI_{O_2} = 0.21.

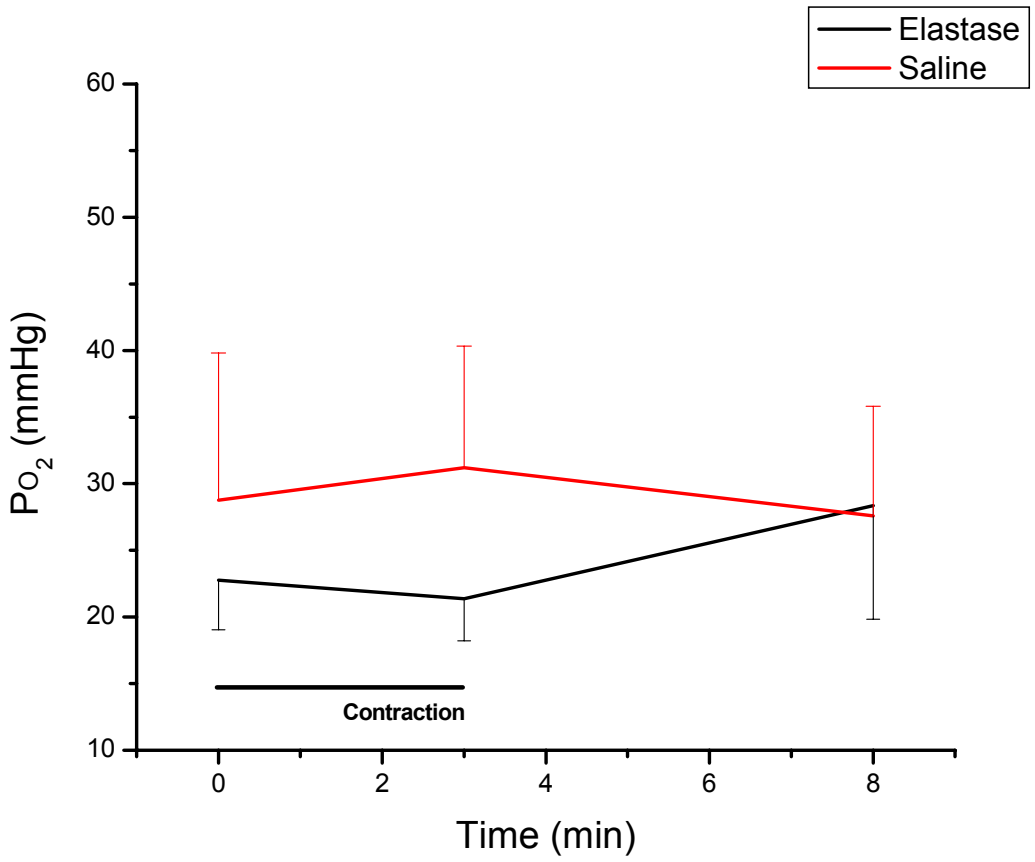

Figure 37. Venular P_{O_2} before (time = 0) and after a three-minute contraction (time = 3 and 8); FI_{O_2} = 0.21.

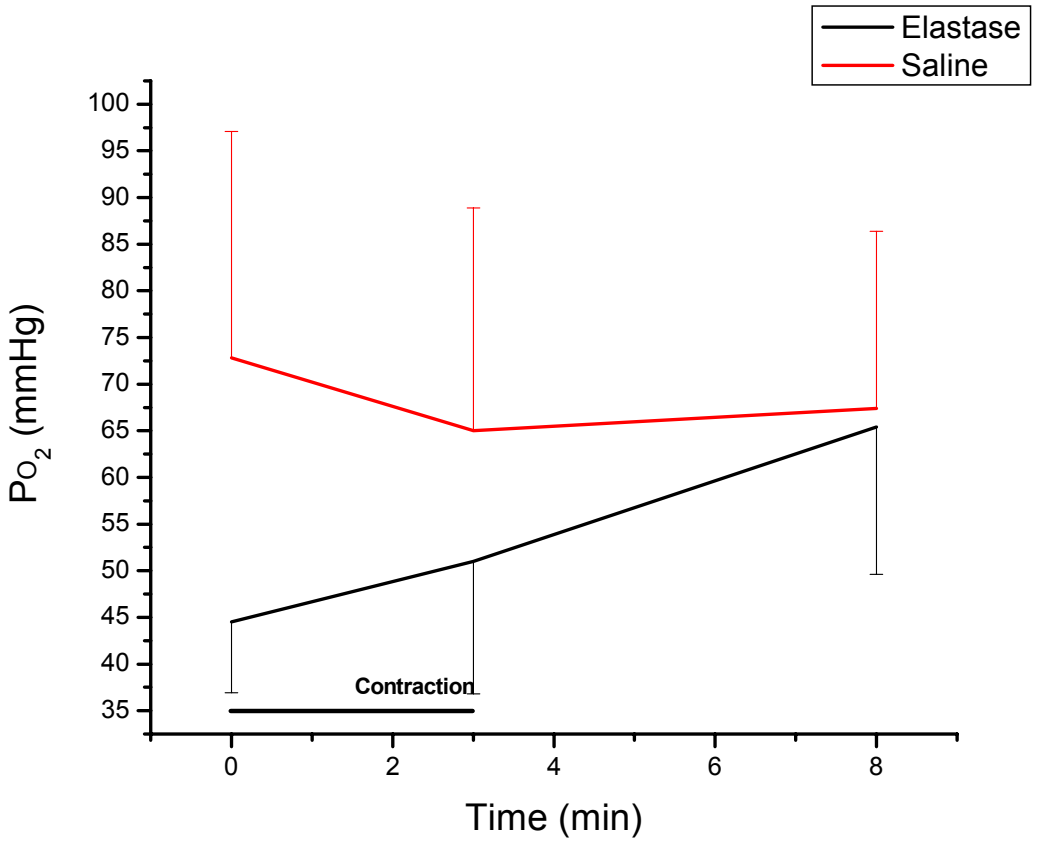

Figure 38. Arteriolar P_{O_2} before (time = 0) and after a three-minute contraction (time = 3 and 8); FI_{O_2} = 0.40.

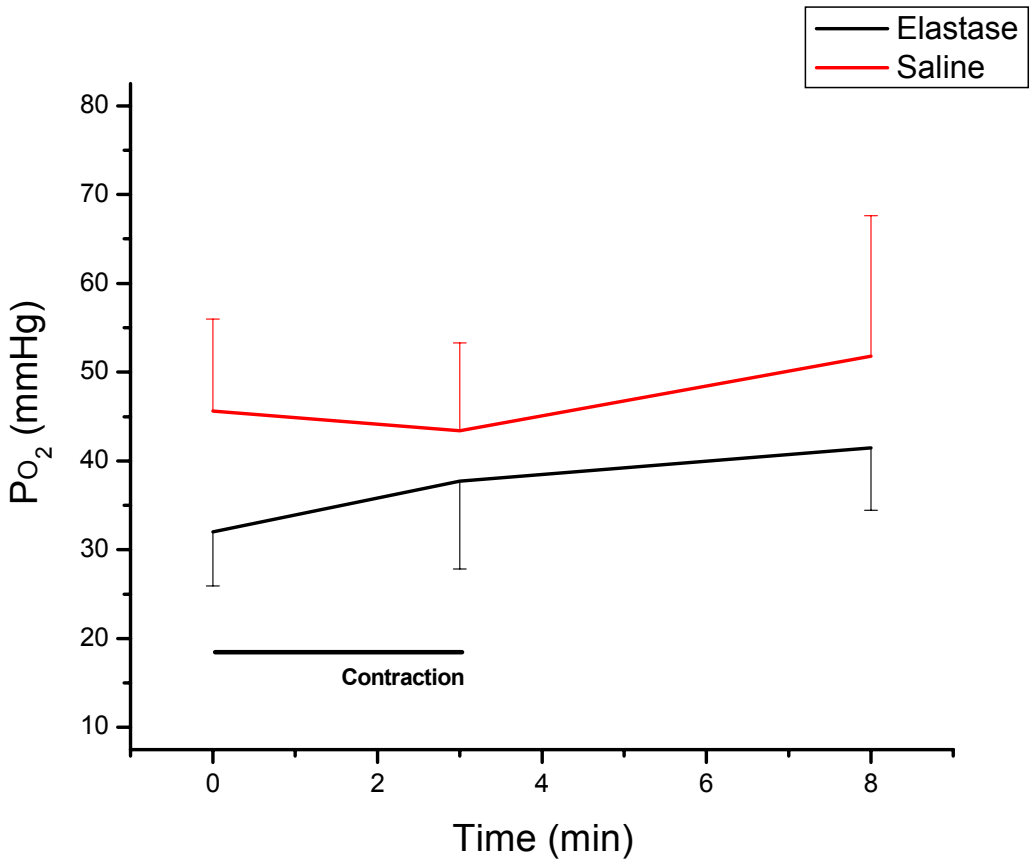

Figure 39. Venular P_{O_2} before (time = 0) and after a three-minute contraction (time = 3 and 8); FI_{O_2} = 0.40.

Spinotrapezius blood flow

Linear regression of all time matched arteriolar flow ($\dot{Q}_a^{ST}$) and venular flow ($\dot{Q}_v^{ST}$) measurements (n = 42) revealed a relatively strong correlation (r = 0.68, $p < 0.01$) (Figure 40). Because arteriolar flow had a greater number of complete data sets compared to arteriolar flow (n = 54 vs. 43), as well as a lower degree of variability ($\bar{x}$ = 25 nl/sec (SD 15.7) vs. 26 nl/sec (SD 18.2), arteriolar flow was used as ST blood flow in hypothesis testing, and for calculating oxygen consumption.

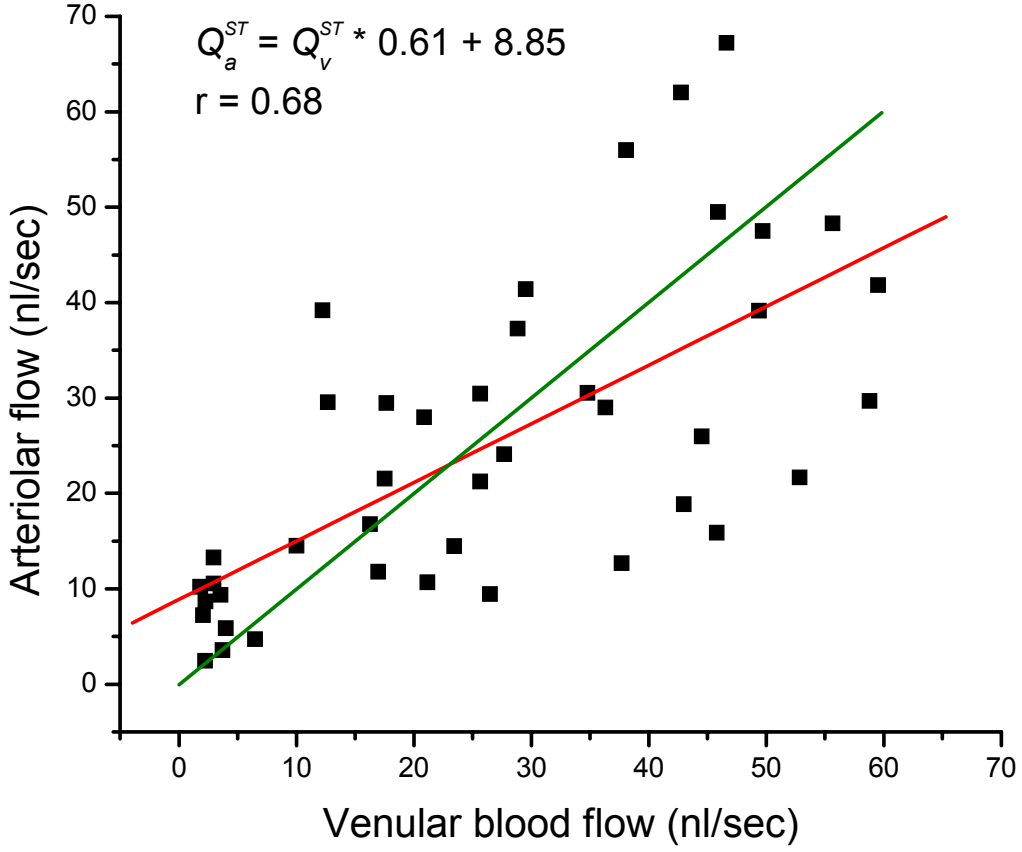

Figure 40. Scatterplot and regression line (red) of spinotrapezius arteriolar vs. venular flow for all matching time points (n = 42), which demonstrates a slope of 0.61 and correlation of 0.68 ($p < 0.01$) compared to the identity line (green), where $Q_a^{ST} = Q_v^{ST}$.

Tables 11 and 12 report the measured (diameter and blood velocity) and calculated (blood flow) arteriolar parameters at baseline, and immediately following a three minute contraction, respectively; there were no differences between experimental groups. Blood velocity was also unchanged when comparing *baseline* to *post-contraction* measures ($p = 0.57$), thus making increased diameter ($p = 0.04$) almost solely responsible for the increase in flow ($p = 0.08$).

There were no statistical differences in *ST arterial* (Figure 41) or *venular flow* (Figure 42) between groups (elastase vs. saline) at any time point (time = 0, 3, and 8 minutes) while breathing FI_{O_2} 0.21 ($p = 0.81$, 0.20 and 0.92, and $p = 0.83$, 0.37 and 0.68, respectively). In addition, breathing FI_{O_2} 0.40 (Figure 43) did not have an effect on flow, either between groups at any time point ($p = 0.32$, 0.48, and 0.63) or when compared to the same group breathing FI_{O_2} 0.21 ($p = 0.31$, 0.99, and 0.08). However, there was an increase in ST flow immediately after contraction for both groups breathing FI_{O_2} 0.21 and 0.40 (time 0 vs. 3, $p = 0.08$ and 0.02, respectively), which returned to resting values within five minutes after the contraction (time 0 vs. time 8, $p = 0.27$ and 0.22, respectively).

Table 11. Primary arteriolar blood flow parameters at baseline.

	Elastase	**Saline**	
FI_{O_2} 0.21			p value
Blood velocity (mm/sec)	3.4 (SD 1.7)	3.9 (SD 1.9)	0.68
Diameter (μm)	73 (SD 10.5)	84 (SD 28.0)	0.45
Blood velocity (mm/sec)	3.4 (SD 1.7)	3.9 (SD 1.9)	0.68
FI_{O_2} 0.40			
Blood flow (nl/sec)	18.3 (SD 11.1)	25.5 (SD 9.5)	0.32
Diameter (μm)	67 (SD 14.2)	79 (SD 21.8)	0.32
Blood velocity (mm/sec)	4.3 (SD 2.0)	4.9 (SD 1.3)	0.65

Table 12. Primary arteriolar blood flow parameters immediately post-contraction.

	Elastase	**Saline**	
FI_{O_2} 0.21			p value
Blood flow (nl/sec)	26.5 (SD 19.7)	49.5 (SD 17.7)	0.20
Diameter (μm)	97 (SD 15.7)	100 (SD 28.2)	0.84
Blood velocity (mm/sec)	3.1 (SD 1.9)	4.1 (SD 1.1)	0.52
FI_{O_2} 0.40			
Blood flow (nl/sec)	28.6 (SD 23.2)	37.8 (SD 9.1)	0.48
Diameter (μm)	88 (SD 15.0)	91 (SD 12.0)	0.69
Blood velocity (mm/sec)	3.7 (SD 2.2)	5.3 (SD 1.4)	0.25

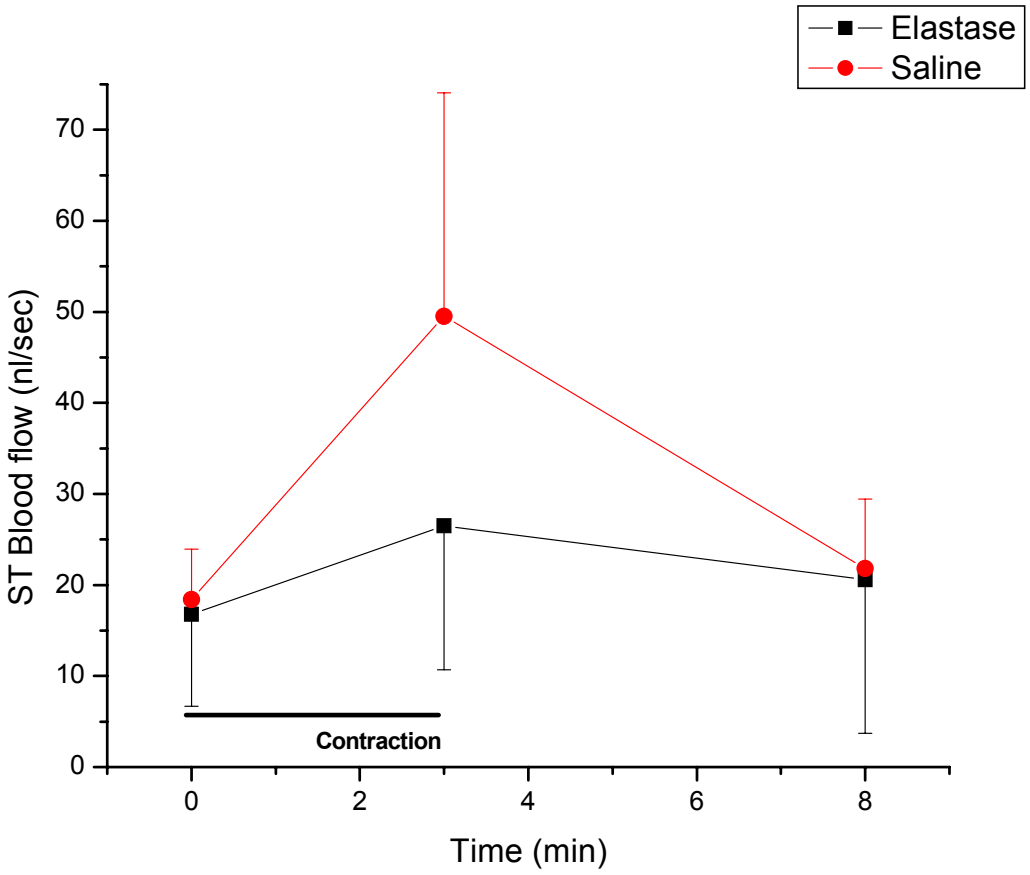

Figure 41. Arteriolar blood flow before (time = 0) and after a three-minute contraction (time = 3 and 8); FI_{O_2} = 0.21.

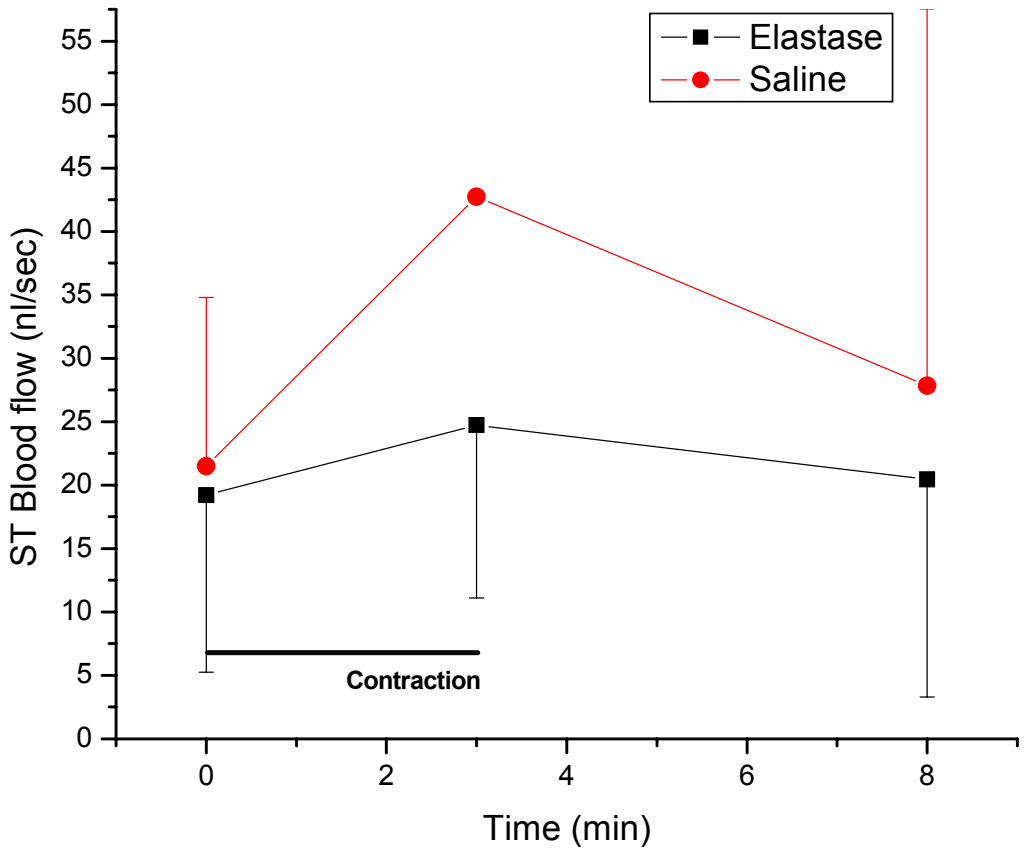

Figure 42. Venular blood flow before (time = 0) and after a three minute contraction (time = 3 and 8); FI_{O_2} = 0.21.

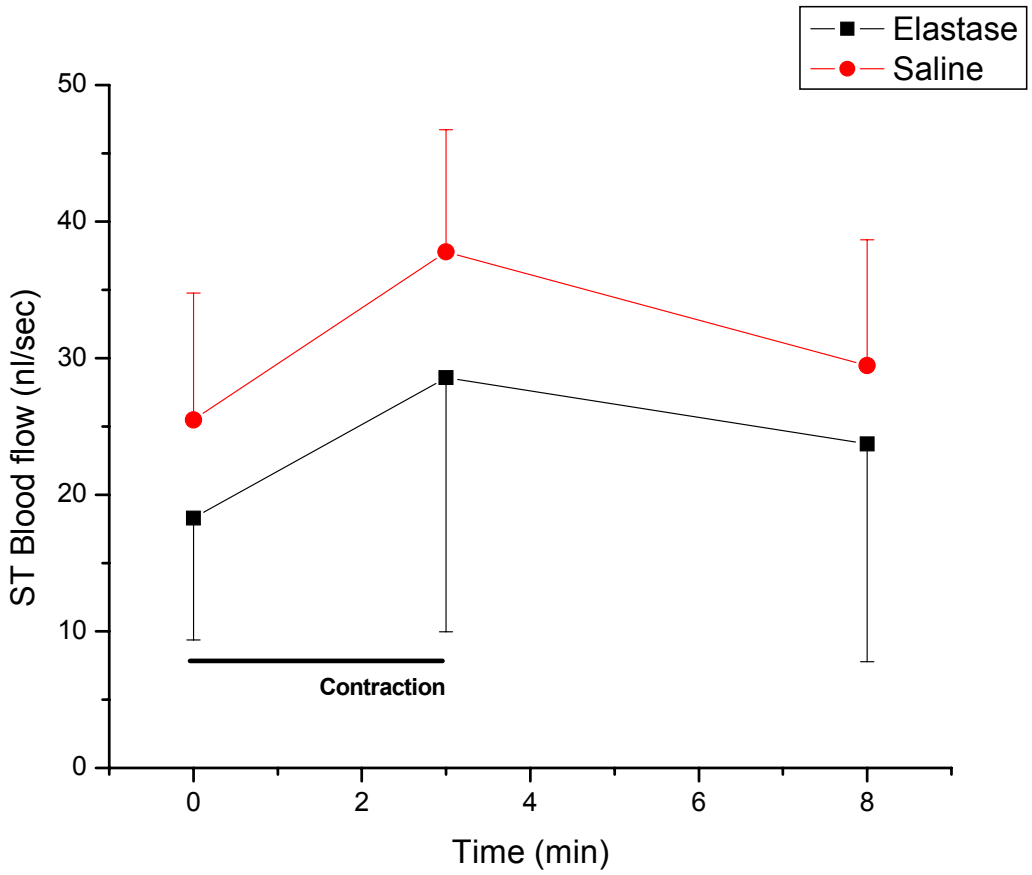

Figure 43. Arteriolar blood flow before (time = 0) and after a three minute contraction (time = 3 and 8); FI_{O_2} = 0.40.

Oxygen consumption

Spinotrapezius oxygen consumption ($\dot{V}_{O_2}^{ST}$) was calculated from spinotrapezius blood flow and arteriolar-venular oxygen difference (as previously described, page 10) and converted to μl of O_2 per min. $\dot{V}_{O_2}^{ST}$ was equivalent between elastase and saline animals across all time intervals and conditions (FI_{O_2}) (p = 0.18 to 0.86) (Figures 44 and 45). Although Figures 44 and 45 illustrate a trend towards increased $\dot{V}_{O_2}^{ST}$ immediately after contraction, a scatterplot of the data (Figure 46) reveals that a single outlier is primarily responsible for the elevated $\dot{V}_{O_2}^{ST}$ for the saline group immediately post contraction. When the data were analyzed to determine if there was an increase in $\dot{V}_{O_2}^{ST}$ with supplemental oxygen, only the final resting measurement on FI_{O_2} 0.40 (0.05 μl/min) was significantly higher than when breathing FI_{O_2} 0.21 (0.02 μl/min; p = 0.04 for time = 8, versus p = 0.28 and 0.36 for time 0 and 3, respectively).

Table 13 and Table 14 demonstrate the contributions of *blood flow* (convective oxygen delivery) and *oxygen extraction* (diffusive oxygen delivery) to $\dot{V}_{O_2}^{ST}$. Surprisingly, although not statistically significant, blood flow was greater in the saline group, while oxygen extraction was higher in the elastase group (Figures 47 and 48).

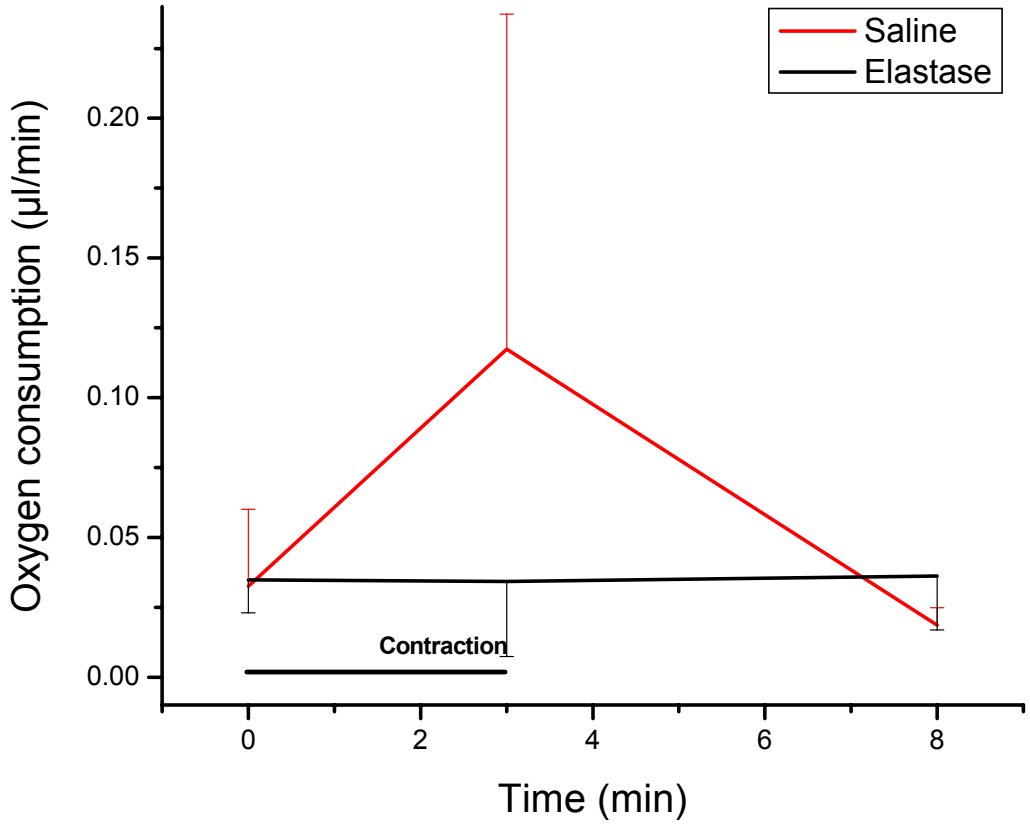

Figure 44. Spinotrapezius muscle oxygen consumption before (time = 0) and after a three-minute contraction (time = 3 and 8); $F_{I_{O_2}} = 0.21$.

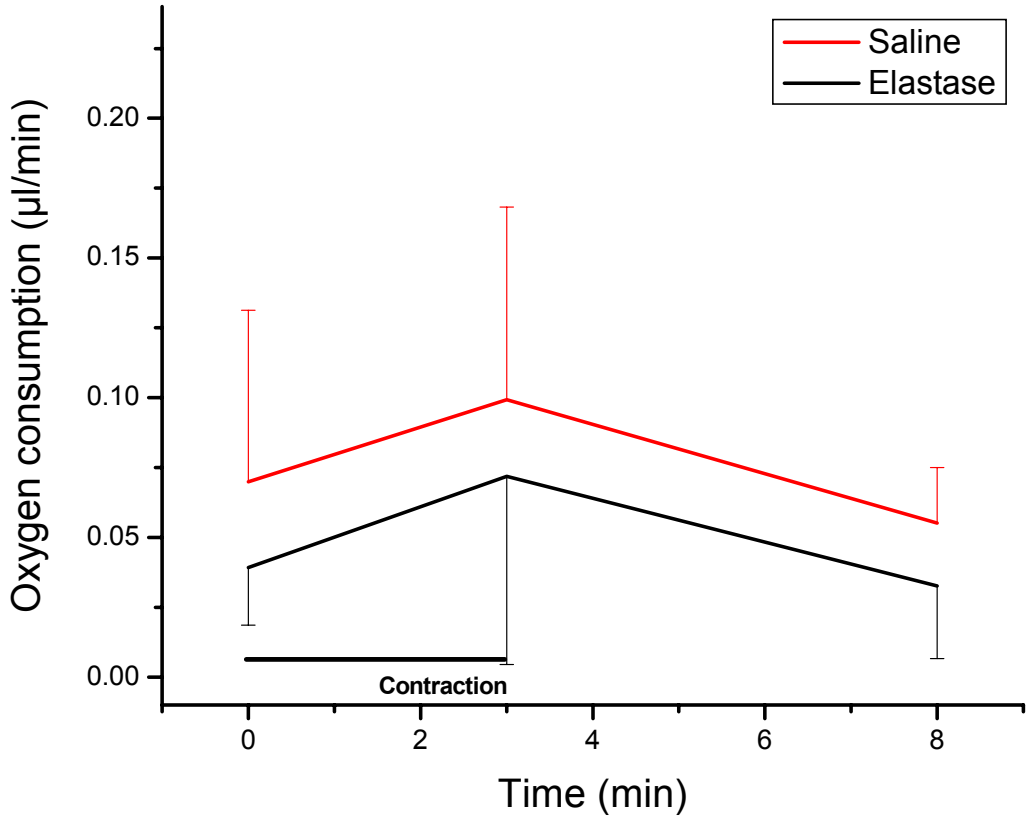

Figure 45. Spinotrapezius muscle oxygen consumption before (time = 0) and after a three-minute contraction (time = 3 and 8); $F_{I_{O_2}}$ = 0.40.

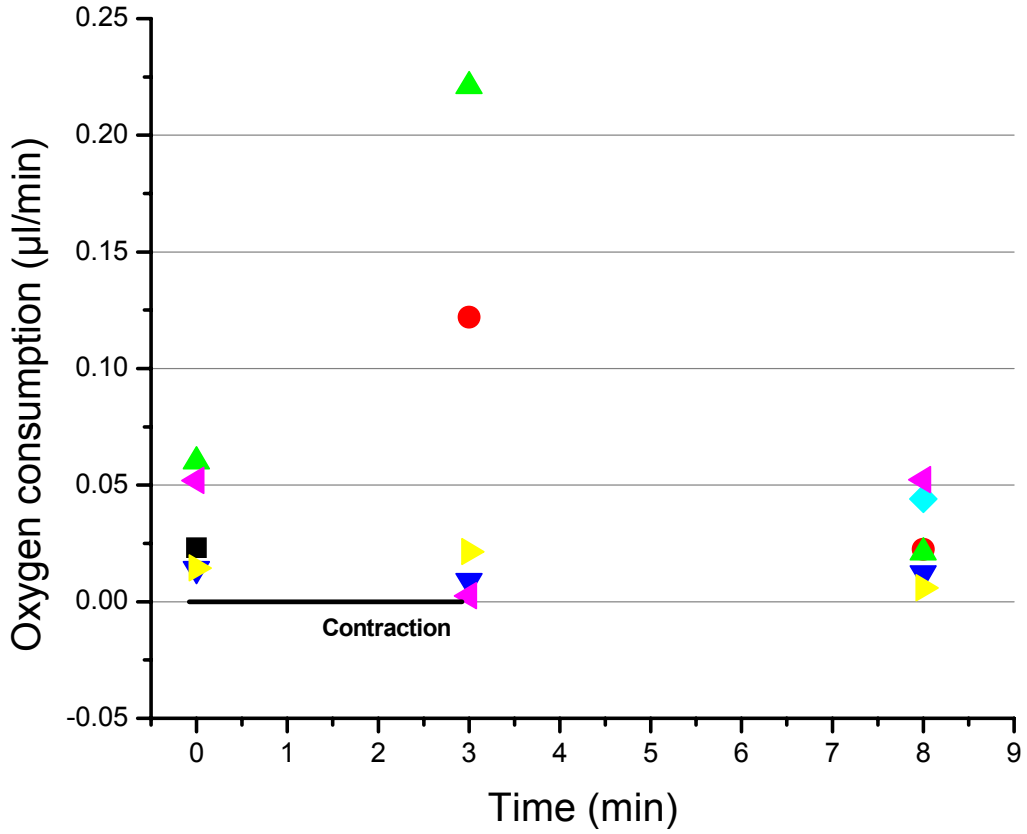

Figure 46. Scatterplot for oxygen consumption (FI_{O_2} = 0.21), indicating a single outlier at 0.22 µl/min.

Table 13. Baseline $\dot{V}_{O_2}^{ST}$ and the respective contributions of blood flow and O_2 extraction.

	Elastase	**Saline**	
FI_{O_2} 0.21			p value
$\dot{V}_{O_2}^{ST}$ (µl/min)	0.035 (SD 0.015)	0.032 (SD 0.024)	0.86
Blood flow (nl/sec)	16.8 (SD 12.6)	18.4 (SD 5.6)	0.82
O_2 extraction	0.51 (SD 0.16)	0.29 (SD 0.22)	0.06
FI_{O_2} 0.40			
$\dot{V}_{O_2}^{ST}$ (µl/min)	0.039 (SD 0.026)	0.070 (SD 0.054)	0.27
Blood flow (nl/sec)	18.3 (SD 11.1)	25.5 (SD 9.5)	0.32
O_2 extraction	0.35 (SD 0.21)	0.23 (SD 0.16)	0.29

Table 14. Immediate post-contraction $\dot{V}_{O_2}^{ST}$ and the respective contributions of blood flow and O_2 extraction.

	Elastase	**Saline**	
FI_{O_2} 0.21			p value
$\dot{V}_{O_2}^{ST}$ (µl/min)	0.034 (SD 0.027)	0.117 (SD 0.106)	0.18
Blood flow (nl/sec)	26.5 (SD 19.7)	49.5 (SD 17.7)	0.20
O_2 extraction	0.50 (SD 0.24)	0.29 (SD 0.16)	0.13
FI_{O_2} 0.40			
$\dot{V}_{O_2}^{ST}$ (µl/min)	0.072 (SD 0.077)	0.100 (SD 0.061)	0.62
Blood flow (nl/sec)	28.6 (SD 23.2)	37.8 (SD 9.1)	0.48
O_2 extraction	0.33 (SD 0.30)	0.23 (SD 0.08)	0.45

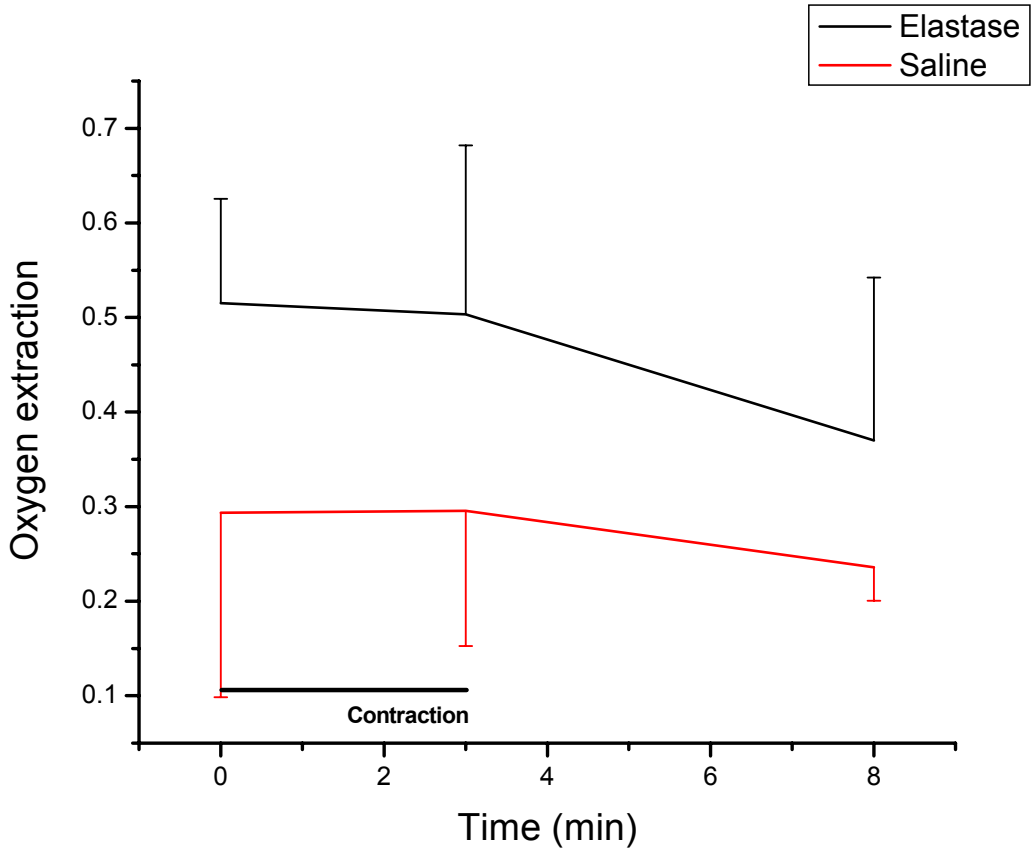

Figure 47. Oxygen extraction fraction of the spinotrapezius m.; $F_{I_{O_2}} = 0.21$.

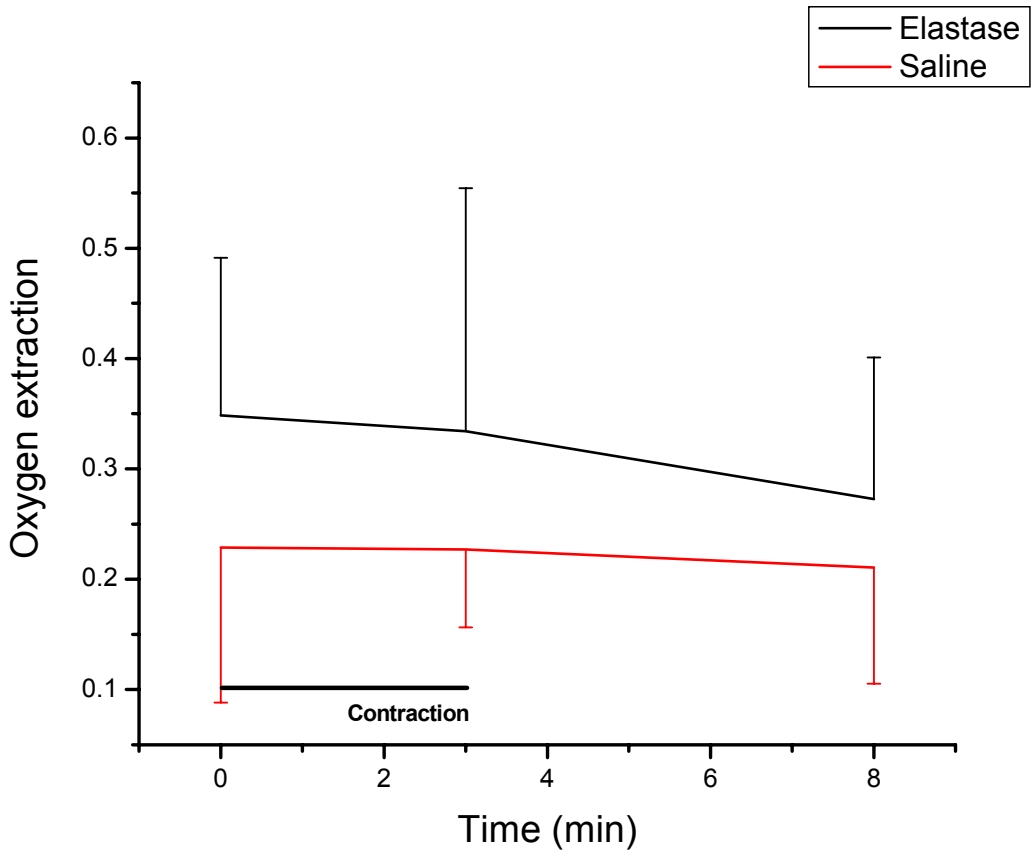

Figure 48. Oxygen extraction fraction of the spinotrapezius m.; $F_{I_{O_2}} = 0.40$.

Muscle performance

Although room air (FI_{O_2} 0.21) indices of muscle performance were statistically equivalent between groups (Table 15 and Figure 49), the saline group had consistently higher peak force, force-time integral, and fatigue index values. Although there was no statistical benefit when breathing supplemental oxygen (FI_{O_2} 0.40) on either the force-time integral or fatigue index ($p = 0.39$ and 0.85, respectively), the force time integral did increase ~18% for both groups.

There was a positive correlation between spinotrapezius muscle oxygen consumption and "muscle work," the force-time integral (Figure 50). Although no significant relationship between fatigue index (FI) and oxygen consumption (Figure 51), there was a trend toward less fatigue (higher FI) with lower $\dot{V}_{O_2}^{ST}$. There was also no relationship between the force-time integral and fatigue index ($p = 0.48$).

Table 15. Indices of ST muscle performance (Elastase vs. Saline).

	Elastase	**Saline**	
FI_{O_2} 0.21			p value
Force-time integral ($N \cdot s/cm^2$)	1.33 (SD 0.95)	2.38 (SD 1.21)	0.14
Fatigue index (%)	55 (SD 27)	62 (SD 19)	0.66
FI_{O_2} 0.40			
Force-time integral ($N \cdot s/cm^2$)	1.58 (SD 0.74)	2.79 (SD 0.99)	**0.05**
Fatigue index (%)	51 (SD 23)	67 (SD 19)	0.25
Mass (g)	0.37 (SD 0.04)	0.43 (SD 0.09)	0.12
Length (L_0, mm)	59 (SD 3.6)	61 (SD 3.3)	0.24
CSA (cm^2)	0.06 (SD 0.009)	0.07 (SD 0.013)	0.29

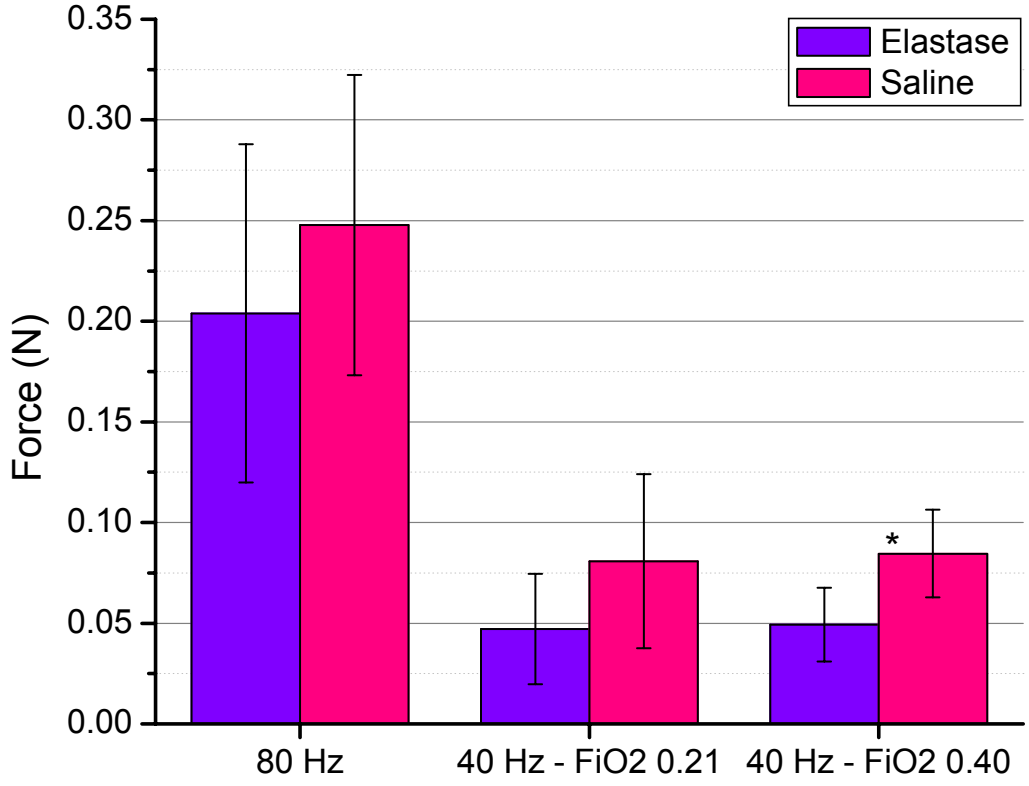

Figure 49. Spinotrapezius muscle force when stimulated at 80 Hz, and 40 Hz while breathing $F_{I_{O_2}}$ of either 0.21 or 0.40 (p = 0.47, 0.21, and 0.04, respectively).

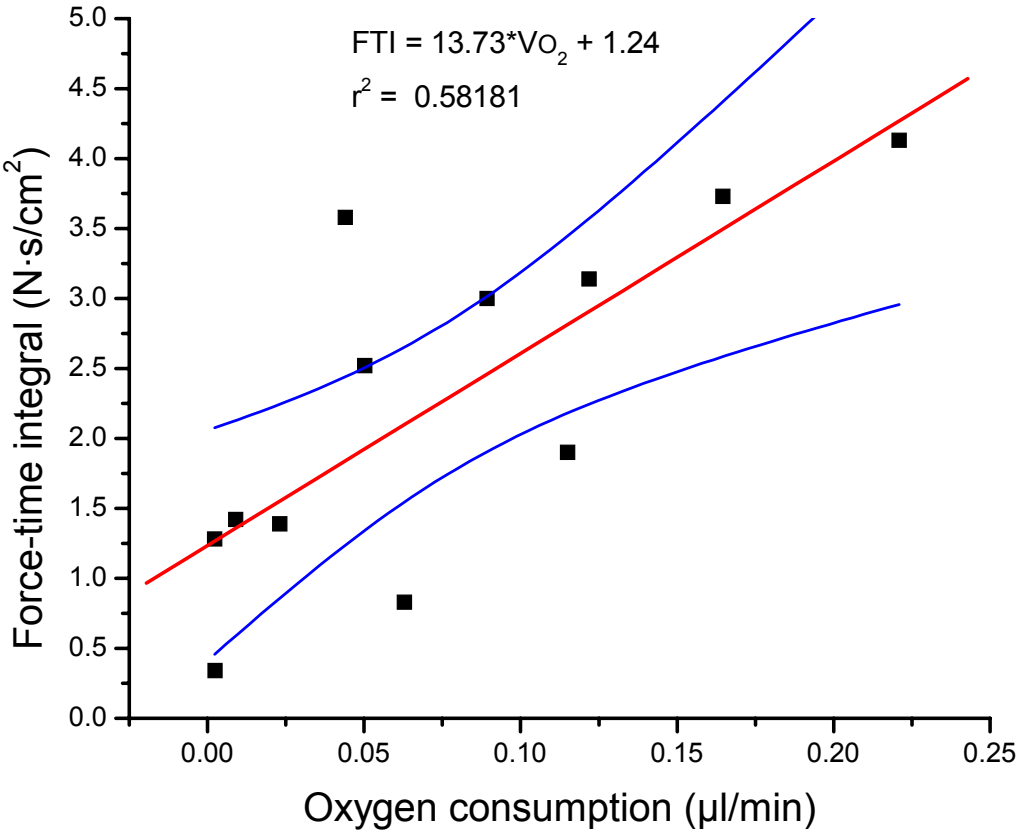

Figure 50. Relationship between oxygen consumption and muscle work, as measured by the force time integral (FTI) for all available points ($p < 0.01$; blue bands represent 95% confidence intervals).

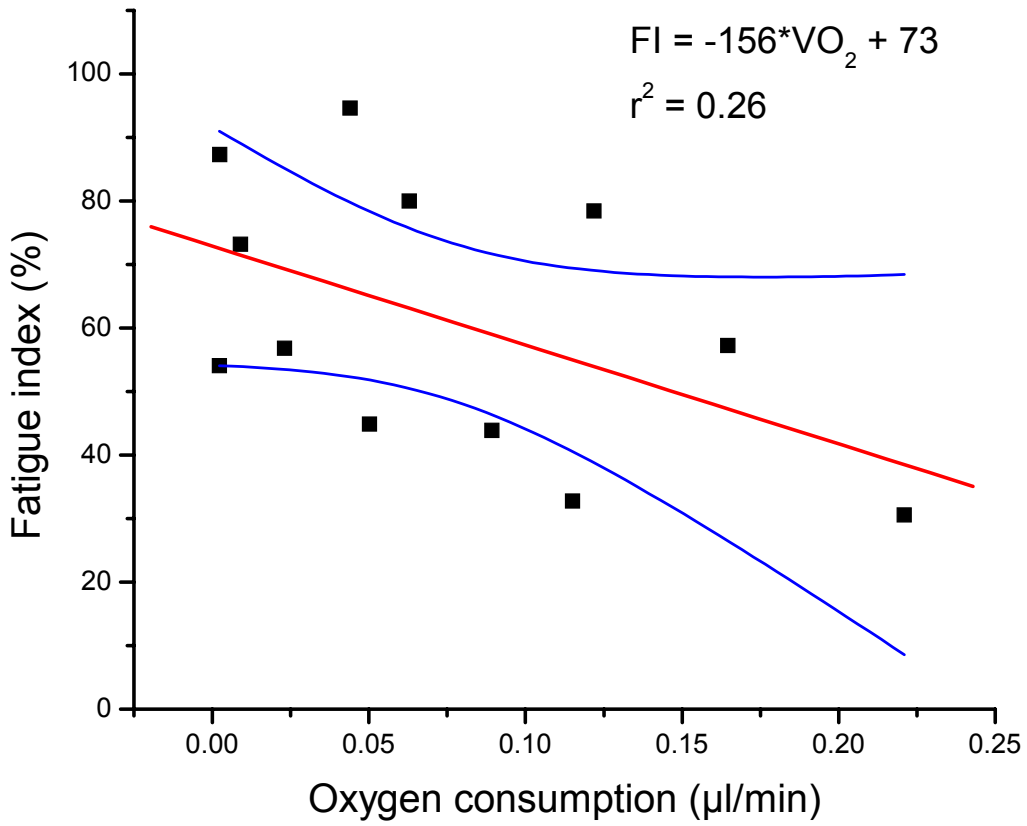

Figure 51. Relationship between oxygen consumption and fatigue index (p = 0.48; blue bands represent 95% confidence intervals), where lower fatigue index indicates more fatigue.

Discussion

Summary, limitations, and review of literature

Overall, the most obvious and concerning issue in the present set of studies is the lack of a "true" control group. The dependent groups in this study were the elastase and saline instilled animals. Although one of the primary purposes of these investigations was to validate an animal model of skeletal muscle dysfunction in COPD, based on the proposed hypothesis, alterations in muscle structure and function would purportedly be due to chronic hypoxemia, not necessary attributed to the elastase-induced emphysema. Thus, at the outset of the project, especially the phase II studies, it was expected that the elastase-induced emphysema (experimental) group would have significant hypoxemia, while the saline instilled group (control) would be normoxic; in the end, there was virtually no difference in Pa_{O_2} between groups when breathing room air (62 vs. 69 mmHg, respectively).

In addition to the possibly of a systemic viral respiratory infection, *Rat respiratory virus*, in most of my animals, other issues and limitations of this study include a possible *hypotension* related decrease in *blood flow* after administration of the FluoSpheres,

oxygen consumption values which are lower than predicted, as well as the wide variability in measures of *muscle performance.*

Rat respiratory virus

There is little-to-no publicly available information about Rat respiratory virus (RRV); what little that has been reported comes from the University of Missouri's Research Animal Diagnostic Laboratory's web site (Riley, Simmons et al. 2002) and a platform presentation from 2002 (Weisbroth 2002), which simply mentions RRV as an "emerging disease." Thus, whether the systemic hypoxemia found in my control animals is due to RRV, or some other infectious agent is not known; however, purportedly serological and histological data sent to the University of Missouri by VCU's Division of Animal Resources from two rats in phase I of this study were indicative of RRV.

RRV has purportedly been identified in research animals world wide. Information from the University of Missouri (Riley, Simmons et al. 2002) (see web address in "Bibliography") indicates that the pulmonary lesions peak at an age of 10-12 weeks, and by 18 weeks the lungs show signs of resolution. Arterial blood gas data from phase I of the present study (Figure 26, page 93) seem to be consistent with these observations: while Pa_{O_2} in the elastase group stayed $\leq$ 80 mmHg for all age groups, Pa_{O_2} was low at 14 at 18 weeks old (67 and 84 mmHg, respectively), by 22 weeks of age Pa_{O_2} had returned to normal (~100 mmHg). It appeared that over time, the hypoxemia resolved, possibly along with the virus and pulmonary lesions. In the meantime, VCU's Division of Animal

Resources began housing the animals in an isolated room with filter-top cages for each animal, in an attempt to prevent air-borne spread of the virus from animal-to-animal.

Thus, phase II in this series of investigations was initiated with the belief that 1) the filtered cages would minimize the spread and impact of the disease, 2) over time, systemic arterial P_{O_2} would remain divergent between the elastase and saline groups, as any infected animals would recover prior to the terminal experiment, and 3) the hypothesis that chronic hypoxemia effects skeletal muscle oxygen transport and muscle performance could adequately be tested. Unfortunately the gross necropsy and arterial blood gas results from phase II not only refute the contention that the animals get better, but rather it appears that their pulmonary infiltration worsens (sadly there are no pulmonary necropsy pictures from the phase I set of animals).

For the elastase group, it is impossible to say how much of the hypoxemia was the result of emphysema as opposed to RRV. However, it appears (Figures 34 and 35, pages 106 and 107) that the lungs of the elastase group have less infiltrate and consolidation than the saline group. While the Pa_{O_2}/FI_{O_2} ratio between groups was only slightly different (297 vs. 327 for the elastase and saline groups, respectively) when breathing room air, there was a significant difference when breathing supplemental oxygen (224 vs. 268). Perhaps this is due to more profound ventilation-perfusion mismatching in the emphysematous animals.

In addition to pulmonary infiltrates/consolidation, these animals seemed exquisitely sensitive to anesthesia. Prior to continuous arterial pressure monitoring at the beginning of the surgery, at least a half-dozen pilot study animals died during the surgery or experiment while receiving the lowest recommended does of i.v. Saffan (0.294 ml/hr). The average Saffan dose to maintain a proper plane of anesthesia and a stable systemic mean arterial pressure (95 to 105 mmHg) was (0.13); a similar sensitivity was also noted with gas anesthesia (Isoflurane).

MHC isoforms

The proportion of *soleus muscle* MHC type I increased with age, while type IIa decreased and type IIb oscillated up and down (Figure 30, page 99). The spinotrapezius muscle also demonstrated an increased proportion of MHC type I early on, but then a decrease to baseline by age 30 weeks, while MHC type IIa decreased early and stayed low, MHC type IIx increased, and type IIb oscillated up and down (Figure 31). Although contrary to my original hypothesis, which was that the muscle would shift toward less oxidative fiber-types over time due to chronic hypoxia, it is possible that concomitant muscle fiber atrophy also occurred, which would result in a decrease oxygen demand. However, there was no loss of muscle mass over time (Figure 21, page 87), and the muscle mass data were consistent with those of previous investigators in normal (Delp and Duan 1996) and chronically hypoxic rats (Deveci, Marshall et al. 2001).

Delp and Daun reported that the *spinotrapezius muscle* was composed of 41% type I fibers, 7% type IIa, 17% type IIx, and 35% type IIb (Delp and Duan 1996), which is in

general agreement with an earlier study that, using slightly different methods, reported 32% white fibers, 32% intermediate fibers, and 36% red fibers (Taylor and Calvey 1977). These prior data are somewhat consistent with the current results which found MHC isoforms I, IIa, IIx, and IIb in proportions of 16, 8, 45, and 30%, respectively (Table 7, page 98). Since the experimental and control animals in the current study were equally hypoxemic, and there were no differences in MHC isoforms, no definitive conclusions can be made regarding possible fiber-type transformation. However, it is possible that the hypoxemia experienced by both groups resulted in a shift towards more glycolytic fibers (IIa and IIx). In that case, a decrease in type I and increase in type IIx proportions would be concordant with the proposed hypothesis, and may help explain the discrepancy between the current and previously published data.

Of interest, and perhaps concern, is the fact that the values for *soleus* MHC type reported in Table 7 are drastically different than that of previous investigators in either normal rats (Delp and Duan 1996) or those exposed to short-term chronic hypoxia (Deveci, Marshall et al. 2001); these studies report that the soleus is composed of ~80% type I fibers as opposed the 9% found in the current study. It is possible that either: 1) the severity of hypoxia in the current group of animals was so severe that their muscles were composed almost entirely of type II muscle fibers, or 2) the bands thought to represent the various MHC isoforms on the SDS-PAGE were improperly identified; neither scenario seems unlikely. Deveci's animals were breathing a PI_{O_2} of ~85 mmHg, which should give a Pa_{O_2} of ~50 mmHg, at least as hypoxemic as the animals in the current study. In the

current SDS-PAGE analysis (Figures 28 and 29, page 97), if identification bands were shifted up (towards a higher molecular weight) three bands, so that the one currently labeled "IIx" would be MHC I, then the next, and only other significant, band would be MHC IIb, but there should be virtually no IIb in the soleus (Delp and Duan 1996). A Western blot, using antibodies specific for MHC I, IIa, and IIb, revealed that this could be a possibility, especially if one assumes that separation of bands above the "new" type I was incomplete due to a lower than usual current used for electrophoresis (3.75 mA/gel as opposed to 15 mA/gel). Of course, if this were the case, then it would also put the reasonable results of the spinotrapezius muscle into question, as the same scheme was used to evaluate both muscles.

One study reported finding developmental MHC in the diaphragm of both patients with severe emphysema and control subjects (Nguyen, Shrager et al. 2000). On a SDS-PAGE analysis, neonatal/embryonic MHC migrates intermediate to MHC I and MHC IIb, and could thus be a fifth band that could diminish the proportions of the other bands. However, this same study found that when normal protein concentrations were injected into each lane of the gel, there was not enough developmental MHC to produce a band with SDS-PAGE or to be stained during immunoblotting (Nguyen, Shrager et al. 2000); thus it is unlikely that there was a fifth band in the region of interest of the current study to confound the results.

Tween related hypotension

Despite numerous reports regarding the hypotensive effect of Tween (Marks and Kolmen 1971; Burnell and Maxwell 1974; Maxwell and Rencis 1974; Lorenz, Reimann et al. 1977; Millard, Baig et al. 1977; Eschalier, Lavarenne et al. 1988; Munoz, Karila et al. 1988), it is found in most fluorescent and radiolabeled microspheres which are marketed for blood flow measurements. In one of the first studies of the hemodynamic effects of Tween-20, Marks and Kolmen (1971) found an immediate ~70 mmHg drop in mean arterial pressure in dogs given 5 ml of Tween-20. In addition to hypotension, they also reported bradycardia and tachypnea, and found pretreatment with antihistamines prevented these effects. This present study confirms that even minute amounts (0.002%) of Tween-20 can result in immediate, profound hypotension, but without bradycardia. Virtually eliminating the Tween, decreasing its percentage to $\sim 5.6 \cdot 10^{-5}$, as described in Appendix V was a simple and effective way of preventing this anaphylactic-like reaction, without administering prophylactic antihistaminic agents.

Blood flow

Several studies (Musch and Poole 1996; Poole, Musch et al. 1997; Kano, Padilla et al. 2004) have measured ST blood flow by injecting 15-μm diameter radioactive microspheres with the animal at rest or during exercise, and then measuring the radioactivity of the ST after euthanization. Using this method, blood flow to the entire muscle was measured and made relative to muscle mass, and gave values in the range of 30 to 70 ml/min/100 g (Kano, Padilla et al. 2004).

Blood flow to the entire muscle was not measured in the current study, and thus flow was not reported in ml/min/100 g. The results of this study are more comparable to those which report *in vivo* resting ST blood flows using the same ST preparation as in the present study (Lash 1994; Lash 1995; Lash and Bohlen 1995; Smith, Barbee et al. 2004); these studies report flows in the range of 6-10 nl/sec. These values are approximately half of what the present study determined. Smith *et al*'s (2004) blood velocities (3.4 to 4.0 mm/sec) were virtual identical to the present study's (3.4 to 3.9 mm/sec), but they were in smaller diameter arterioles (52 μm vs. 79 μm); this would account for the larger flow values of the current study. Lash had similar size vessels (74 μm), but a different technique to measure velocity, dual-slit cross-correlation method, may have underestimated velocity in such large vessels (the method is traditionally used in venules, small arterioles, and capillaries). Thus, when comparing the current data with these previous studies, in which Pa_{O_2} was normal, chronic hypoxemia does not appear to have a detrimental effect on ST blood flow.

There are no known studies that have measured both arteriolar and venular flow concurrently, and thus no empirical data from which to predict this relationship. The present study measured velocity and diameter of both arterioles and venules at nearly the same time in order to provide a measure of internal validity for the novel method/equations developed to measure blood velocity. Figure 40 illustrated the relationship between arteriolar and venular flow. While the best-fit line (red, slope 0.61) is close to the identity line (green, slope = 1) ($r = 0.68$), theoretically one would predict that they should be the same. Several assumptions went into the derivation of Equations

17 and 18 (pages 71 and 72): 1) both vessels were perfectly cylindrical, 2) the velocity profile for both vessels was a Poiseuille parabolic profile (B = 1), and 3) all blood entering the ST muscle via the arteriole measured also left via the adjacent venule in which measurements were made.

Each of these assumptions may not be entirely correct. While the arterioles, which have a greater amount of smooth muscle, are likely cylindrical, the venules, which are more compliant, may assume a more elliptical cross section, which would affect diameter (d). This would lead to error in calculating both mean velocity (which uses W/d) and cross-sectional area ($\pi d^2/4$). Although the velocity profile (B) may be different in arterioles and venules of different sizes (as in the current study), both objective (Pittman and Ellsworth 1986) and subjective (Schmid-Schoenbein and Zweifach 1975) data suggest that the profiles are similar in arterioles and venules of similar diameter, of which they were not in this study. Of most concern is that there were two primary arterioles and venules in the spinotrapezius preparation used, thus allowing a different route for blood to enter or leave the muscle than from the measurement site. Due to fewer assumptions for the arterioles as well as a lower variability in measurements, arteriolar flow was used for $\dot{Q}^{ST}$ in all calculations and analyses.

Oxygen consumption

As seen in Table 16, the raw, un-normalized, values for spinotrapezius oxygen consumption in this study, 0.5 nl/sec, are consistent with those of a previous study from the same laboratory (Smith 2002). However, Marshall and Davies (1999), reported a

resting oxygen consumption in the rat hind limb of 0.004 ml/min/g after normalizing for predicted muscle mass. A nearly 20-fold lower value, 0.00026 ml/min/g, was calculated for spinotrapezius oxygen consumption when the current data were normalized to one-third of spinotrapezius muscle mass (an approximation of the perfused muscle mass supplied by the large arteriole from which blood flow and oxygen measurements were made in this study). Since there were two large arterioles in the field of view using the current preparation, in addition to the rostral feed artery and any vessels on the ventral surface of the preparation that are not observed, it is likely that the mass of tissue perfused in the current setup is much less than the one-third originally predicted (perhaps as little as one-sixth). Since there is no way to estimate the exact perfused tissue mass, the current setup does not lend itself to "normalization." This was also evident when attempting to normalize the current raw blood flow data to muscle mass (see Table 16).

Table 16. Resting systemic and tissue (spinotrapezius m.) parameters of oxygen delivery and consumption from the current study compared to reference values.

Parameter	Experimentally derived mean values	Reference values	Source for reference values
Ca_{O_2} (systemic) (ml O_2/dl of blood)	14.6 (SD 1.0)	20	(Richardson, Leek et al. 2003)
Ca_{O_2} (tissue) (ml O_2/dl of blood)	9.0 (SD 2.9)		
Cv_{O_2} (tissue) (ml O_2/dl of blood)	5.2 (SD 2.7)		
$Ca_{O_2} - Cv_{O_2}$ (tissue) (ml O_2/dl of blood)	3.9 (SD 2.4)	3.5 – 5.0	
O_2 extraction (tissue)			
rest	0.43 (SD 0.21)	0.20	(Nellis, Flaim et al. 1980)
exercise	0.42 (SD 0.23)	0.74 – 0.80	(Nellis, Flaim et al. 1980; Henderson, Wagner et al. 2002)
Blood flow (tissue) (dl of blood/min)	1.05E-05 (SD 6E-06)		
Blood flow (tissue) (ml/min/100 g)	0.800 (SD 0.50)	30	(Kano, Padilla et al. 2004)
		60	(Musch and Poole 1996)
Oxygen consumption (nl O_2/sec)	0.5 (SD 0.3)	0.05 – 2.0	(Smith 2002)
Oxygen consumption (ml O_2/min)	$3.4 \cdot 10^{-5}$ (SD $1.7 \cdot 10^{-5}$)		
Oxygen consumption (ml O_2/min/g of m.)	0.00026 (SD 0.00014)	0.004	(Marshall and Davies 1999)

Of interest is the fact that while blood flow and oxygen consumption were higher in the saline group, oxygen extraction was higher in the elastase group (Table 13, page 127). Although all three of these parameters were statistically equivalent, these differences were consistent across time (time = 0, 3, and 8 min) and condition ($F_{I_{O_2}}$ 0.21 vs. 0.40), indicating that the difference was more real, and not merely by chance. At rest the higher blood flow in the saline group was primarily due to larger diameter vessels, as blood velocity was equivalent (Table 11, page 119). However, immediately after contraction, the vessel diameters were equivalent, but the blood velocity was higher in the saline group (Table 12). Thus, the elastase group has both a more pronounced hyperemic response to exercise as well as having a higher degree of oxygen extraction, but blood velocity remained constant after exercise. Perhaps the elastase group developed some degree of right heart failure and cardiac output was impaired compared to the saline group, and in an effort to compensate, peripheral skeletal muscles became more efficient at extracting oxygen.

Based on Fick's principle, mass conservation of oxygen (Equation 22), ST *oxygen consumption* ($\dot{V}_{O_2}^{ST}$) is the product of ST *convective oxygen delivery* ($\dot{Q}^{ST} \cdot Ca_{O_2}$) and *diffusive oxygen delivery*, or oxygen extraction, ($Ca_{O_2} - Cv_{O_2} / Ca_{O_2}$).

Equation 22

$$\dot{V}_{O_2}^{ST} = \left(\dot{Q}^{ST} \cdot Ca_{O_2}\right) \cdot \left(\frac{Ca_{O_2} - Cv_{O_2}}{Ca_{O_2}}\right)$$

Although $\dot{V}_{O_2}^{ST}$ was still lower in the elastase group at all time points, it appears that while its convective oxygen delivery was diminished relative to the saline group, an enhanced diffusive oxygen delivery helped the elastase group maintain a level of work and oxygen consumption comparable to that of the saline group (Figure 52, page 148). Based on Equation 3, enhanced diffusive oxygen transport would be possible if there was either 1) an increase in area available for diffusion (A), or 2) a decrease in diffusion distance (Δr). Increased area available for diffusion could occur if there is an increase in capillary surface area due to increased capillarity of the muscle, while a decreased diffusion distance could occur if either capillarity truly increased, or if the muscle fibers were smaller. Unfortunately no histological measures were done on the animals from this study; however, given that muscle mass and calculated CSA were slightly smaller for the elastase group (Table 15, page 131), this may partially account for the higher oxygen extraction.

In a group of patients with COPD and activity matched controls, Richardson *et al* (2003) studied oxygen transport during a small-muscle mass exercise, similar to the present study, in which pulmonary function should not be a limiting factor. For an equal workload, they did not find a difference in oxygen extraction, nor did they find a difference in capillarity or aerobic enzyme activity. However, they did find a reduced capacity for muscular work that was associated with a reduced proportion of type I muscle fibers and an increase in type II, especially IIx.

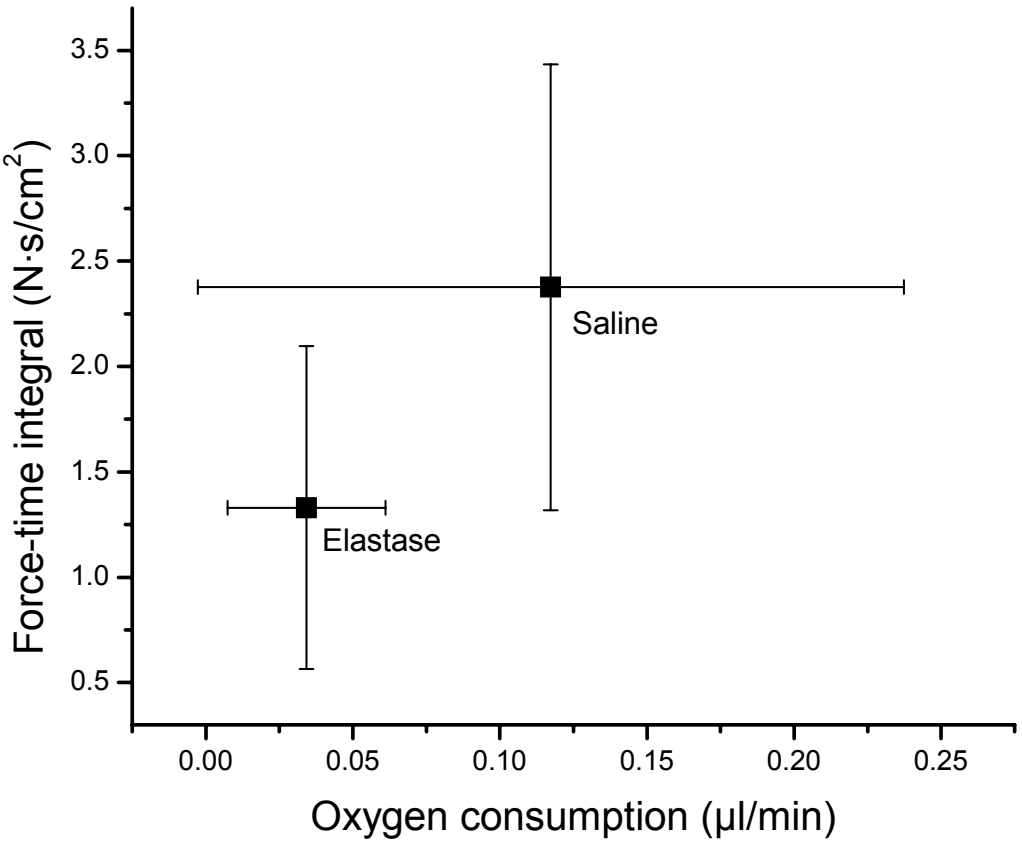

Figure 52. Relationship between ST muscle oxygen consumption and work (FTI).

Muscle performance

Only two other studies have measured muscle force of the spinotrapezius muscle. Both Taylor and Calvey (1977), and Suzuki *et al* (1995) demonstrated that muscle force was partially fused at 40 Hz and became fully fused by 80 Hz, producing a maximal force of ~0.44 N (45 g); data from the current study concur with these prior results (Figure 53). However, neither of these studies actually reports the raw force data or standard deviations from their experiments, but rather the value stated above was calculated from the representative force tracings in their figures.

The force data from the current study exhibited a large degree of variability (Figure 54); mean peak force of the spinotrapezius muscle for all data points, when stimulated at 40 Hz, was 51 mN (5.2 g) with a standard deviation of 36 mN (3.7 g); this variability is much greater than that reported by researchers in eye and tongue muscles (Goldberg, Wilson et al. 1997; Sutlive, Shall et al. 2000) as well as in the soleus muscle (Segal, Faulkner et al. 1986). However, when the single outlier is removed from the data set, the mean force only decreases only 9.8%, to 46 mN, but the standard deviation decreases 25%, to 27 mN. This is still a wide degree of variability. In an attempt to determine if this was due to the investigators inexperience at the beginning of the study, a scatterplot was done of all force data over time, Figure 54, which illustrates no learning effect of the investigator that resulted in less variable and/or increased force values over time. Despite this variability and no statistically significant differences between groups, the saline group outperformed the elastase group in every measure of muscle performance (peak force at 80 and 40 Hz, force-time integral, and fatigue index). As illustrated above,

Figure 52, $\dot{V}_{O_2}^{ST}$ was also concomitantly decreased; it would have been interesting to see how these relationships compared at a different work loads (*i.e.*, by increasing stimulation frequency > 40 Hz, or by increasing the pulse-train frequency > 1 Hz).

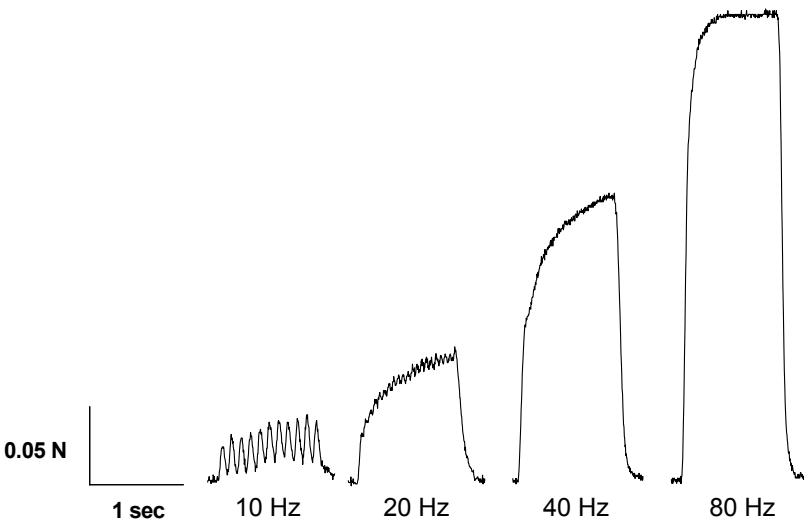

Figure 53. Representative isometric force profile of the spinotrapezius muscle stimulated at 10, 20, 40, and 80 Hz.

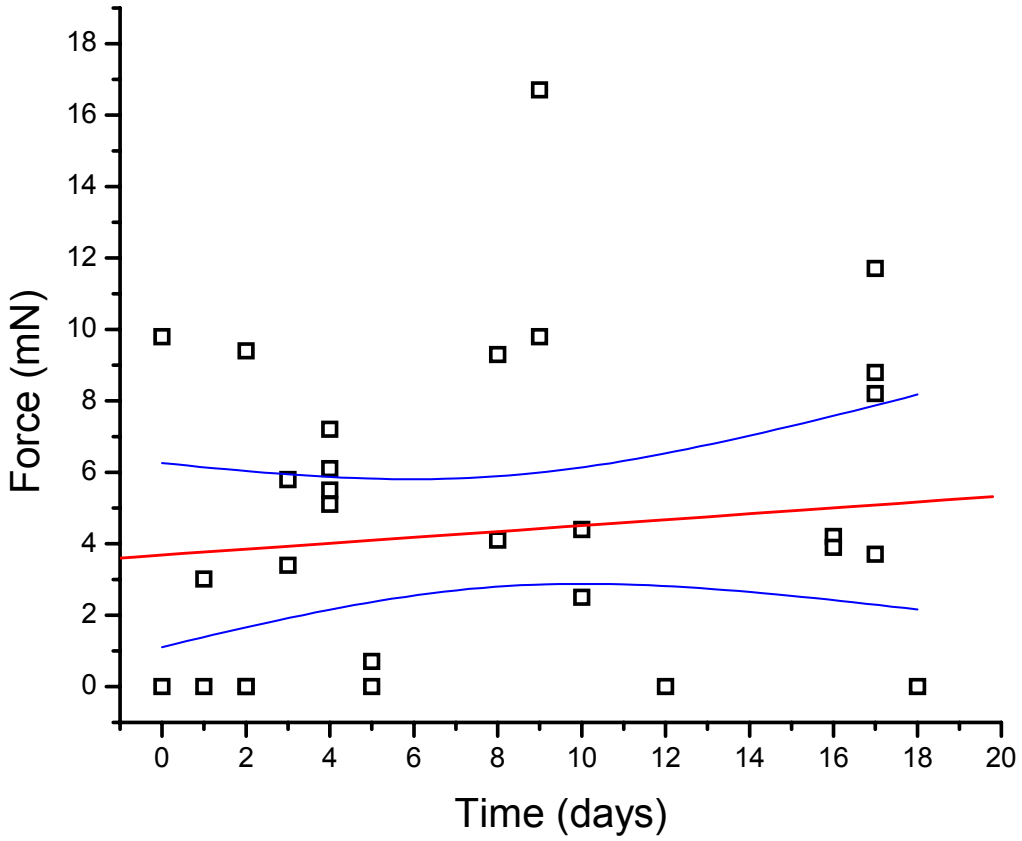

Figure 54. Scatterplot of force data over time, demonstrating no "learning effect" by the investigator (r = 0.12).

Suggestions for future research

Above all else, the viral agent responsible for RRV needs to be characterized, a relatively non-invasive way in which to test animals for RRV needs to be developed, and an effective systematic and comprehensive prevention and control procedure needs to be developed.

Due to the unknown effects of prolonged anesthesia as well as the variability in muscle force measures, it would be useful to know the intra-animal reliability of repeated measures of the course of an experiment under the same conditions in normal animals. In addition, it would be useful to determine intra-animal reliability of repeated measures of blood velocity and blood flow under both steady state and exercise conditions.

The stimulation protocol used did not result in a significant increase in $\dot{V}_{O_2}^{ST}$ immediately after contraction. A graded exercise protocol could help determine the relationship between ST $\dot{V}_{O_2}^{ST}$ and muscle work as well as possibly define $\dot{V}_{O_2\,\max}^{ST}$, so that future investigators would know more specifically what workload a given stimulation protocol would result in.

As noted above, characterization of the spinotrapezius muscle histochemically with regard to muscle-fiber types, fiber cross-sectional area, and capillarity would provide useful information in interpreting the findings from the present study

Conclusions

Due to a presumed Rat respiratory virus, which likely resulted in the control group (saline) being nearly as hypoxemic as the experimental group (elastase-induced emphysema), as well as a wide degree of variability in several independent measures, the present study was not able to definitively test the proposed hypothesis that chronic hypoxemia (due to emphysema) leads to both a diminished oxygen supply and demand in skeletal muscle.

Compared to previous studies, animals with elastase induced emphysema also appeared to have a dramatic transformation of muscle fiber types away from oxidative and toward more glycolytic, especially type IIb. However, these proportions were virtually the same as that seen in the control group which was normoxic 12 weeks after instillation, and increasing age actually lead to an small increase in MHC I (as seen in normal aging).

Although many of the results of the present study were not statistically significant, they were consistent over time and are likely of physiological significance. All measures of muscle performance were lower in the elastase group. In addition, spinotrapezius oxygen consumption and blood flow were lower in the elastase group. Only oxygen extraction was higher in the elastase group, likely due to diminished fiber cross-sectional area. The addition of supplemental oxygen during isolated, small-muscle mass exercise did improve the force-time integral ~18% in both groups, suggesting that muscle work in these hypoxemic animals may be limited by oxygen supply.

Thus, the data on muscle fiber type, oxygen consumption and muscle performance suggests that elastase-induced emphysema in rats does lead to a similar skeletal muscle dysfunction that is seen in humans with COPD, and indicates that it is a valid animal model of skeletal muscle dysfunction in COPD.

Bibliography

ALA (2001). Trends in chronic bronchitis and emphysema: morbidity and mortality, American Lung Association Epidemiology & Statistics Unit.

Anderson, R. (2001). Deaths: Leading causes 1999. *National Vital Statistics Reports*. Hyattsville, Maryland, National Center for Health Statistics. 49.

Aniansson, A., G. Grimby, M. Hedberg and M. Krotkiewski (1981). Muscle morphology, enzyme activity and muscle strength in elderly men and women. *Clinical Physiology* 1(1): 73-86.

Artigas, A., G. R. Bernard, J. Carlet, D. Dreyfuss, L. Gattinoni, L. Hudson, M. Lamy, J. J. Marini, M. A. Matthay, M. R. Pinsky, R. Spragg, P. M. Suter and t. C. Committee (1998). The American-European Consensus Conference on ARDS, Part 2. Ventilatory, Pharmacologic, Supportive Therapy, Study Design Strategies, and Issues Related to Recovery and Remodeling. *Am. J. Respir. Crit. Care Med.* 157(4): 1332-1347.

ATS/ERS (1999). Skeletal muscle dysfunction in chronic obstructive pulmonary disease. A statement of the American Thoracic Society and European Respiratory Society. *Am J Respir Crit Care Med* 159(4 Pt 2): S1-40.

Aw, T. Y. and D. P. Jones (1990). Intracellular Respiration. *The Lung: Scientific Foundations*. R. G. Crystal and J. B. West. New York, Raven Press, Ltd. 2: 1445-1453.

Bailey, J. K., C. A. Kindig, B. J. Behnke, T. I. Musch, G. W. Schmid-Schoenbein and D. C. Poole (2000). Spinotrapezius muscle microcirculatory function: effects of surgical exteriorization. *Am J Physiol Heart Circ Physiol* 279(6): H3131-3137.

Behnke, B. J., M. D. Delp, P. McDonough, S. A. Spier, D. C. Poole and T. I. Musch (2004). Effects of chronic heart failure on microvascular oxygen exchange dynamics in muscles of contrasting fiber type. *Cardiovasc Res* 61(2): 325-332.

Behnke, B. J., C. A. Kindig, T. I. Musch, S. Koga and D. C. Poole (2001). Dynamics of microvascular oxygen pressure across the rest-exercise transition in rat skeletal muscle. *Respir Physiol* 126(1): 53-63.

Behnke, B. J., C. A. Kindig, T. I. Musch, W. L. Sexton and D. C. Poole (2002). Effects of prior contractions on muscle microvascular oxygen pressure at onset of subsequent contractions. *J Physiol* 539(Pt 3): 927-934.

Berne, R. M. and M. N. Levy (1998). *Physiology*. St. Louis, Mosby.

Bio-Rad PROTEAN II xi Cell and PROTEAN II xi 2-D Cell Instruction Manual. 2004.

Bishop, J. J., P. R. Nance, A. S. Popel, M. Intaglietta and P. C. Johnson (2001). Effect of erythrocyte aggregation on velocity profiles in venules. *Am J Physiol Heart Circ Physiol* 280(1): H222-236.

Bishop, J. J., A. S. Popel, M. Intaglietta and P. C. Johnson (2002). Effect of aggregation and shear rate on the dispersion of red blood cells flowing in venules. *Am J Physiol Heart Circ Physiol* 283(5): H1985-1996.

Bradford, M. M. (1976). A rapid and sensitive method for the quantitation of microgram quantities of protein utilizing the principle of protein-dye binding. *Anal Biochem* 72: 248-254.

Brooke, M. H. and K. K. Kaiser (1970). Three "myosin adenosine triphosphatase" systems: the nature of their pH lability and sulfhydryl dependence. *J Histochem Cytochem* 18(9): 670-672.

Burke, R. E., D. N. Levine, P. Tsairis and F. E. Zajac, 3rd (1973). Physiological types and histochemical profiles in motor units of the cat gastrocnemius. *J Physiol* 234(3): 723-748.

Burke, R. E., D. N. Levine and F. E. Zajac, 3rd (1971). Mammalian motor units: physiological-histochemical correlation in three types in cat gastrocnemius. *Science* 174(10): 709-712.

Burnell, R. H. and G. M. Maxwell (1974). General and coronary haemodynamic effects of Tween 20. *Aust J Exp Biol Med Sci* 52(1): 151-156.

Busch, R. H., R. L. Buschbom and L. G. Smith (1984). Comparison of methods for evaluation of experimentally induced emphysema. *Environ Res* 33(2): 473-496.

Busch, R. H., K. E. Lauhala, S. M. Loscutoff and K. E. McDonald (1984). Experimental pulmonary emphysema induced in the rat by intratracheally administered elastase: morphogenesis. *Environ Res* 33(2): 497-513.

Cassin, S., R. D. Gilbert, C. E. Bunnell and E. M. Johnson (1971). Capillary development during exposure to chronic hypoxia. *Am J Physiol* 220(2): 448-451.

Costa, D. L., J. R. Lehmann, W. M. Harold and R. T. Drew (1986). Transoral tracheal intubation of rodents using a fiberoptic laryngoscope. *Lab Anim Sci* 36(3): 256-261.

Curran-Everett, D. and D. J. Benos (2004). Guidelines for reporting statistics in journals published by the American Physiological Society. *J Appl Physiol* 97(2): 457-459.

Curran-Everett, D., S. Taylor and K. Kafadar (1998). Fundamental concepts in statistics: elucidation and illustration. *J Appl Physiol* 85(3): 775-786.

Damon, E. G., J. L. Mauderly and R. K. Jones (1982). Early effects of intratracheal Instillation of elastase on mortality, Respiratory function, and pulmonary morphometry of F-344 rats. *Toxicol Appl Pharmacol* 64(3): 465-475.

Delp, M. D. and C. Duan (1996). Composition and size of type I, IIA, IID/X, and IIB fibers and citrate synthase activity of rat muscle. *J Appl Physiol* 80(1): 261-270.

Desplanches, D., H. Hoppeler, L. Tuscher, M. H. Mayet, H. Spielvogel, G. Ferretti, B. Kayser, M. Leuenberger, A. Grunenfelder and R. Favier (1996). Muscle tissue adaptations of high-altitude natives to training in chronic hypoxia or acute normoxia. *J Appl Physiol* 81(5): 1946-1951.

Deveci, D., J. M. Marshall and S. Egginton (2001). Relationship between capillary angiogenesis, fiber type, and fiber size in chronic systemic hypoxia. *Am J Physiol Heart Circ Physiol* 281(1): H241-252.

Eaton, T., J. E. Garrett, P. Young, W. Ferguson, J. Kolbe, S. Rudkin and Whyte (2002). Ambulatory oxygen improves quality of life in COPD patietns: a randomized controlled study. *Eur Respir J* 20(2): 306-312.

Eichelbronner, O., A. Sielenkamper, M. D'Almeida, C. G. Ellis, W. J. Sibbald and I. H. Chin-Yee (1999). Effects of FIO2 on hemodynamic responses and O2 transport during RSR13-induced reduction in P50. *Am J Physiol Heart Circ Physiol* 277(1): H290-298.

Engelson, E. T., G. W. Schmid-Schonbein and B. W. Zweifach (1985). The microvasculature in skeletal muscle. III. Venous network anatomy in normotensive and spontaneously hypertensive rats. *Int J Microcirc Clin Exp* 4(3): 229-248.

Engelson, E. T., G. W. Schmid-Schonbein and B. W. Zweifach (1986). The microvasculature in skeletal muscle. II. Arteriolar network anatomy in normotensive and spontaneously hypertensive rats. *Microvasc Res* 31(3): 356-374.

Engelson, E. T., T. C. Skalak and G. W. Schmid-Schonbein (1985). The microvasculature in skeletal muscle. I. Arteriolar network in rat spinotrapezius muscle. *Microvasc Res* 30(1): 29-44.

Eriksson, S. (1965). Studies in alpha 1-antitrypsin deficiency. *Acta Med Scand* 117(Suppl 432): 1-85.

Eschalier, A., J. Lavarenne, C. Burtin, M. Renoux, E. Chapuy and M. Rodriguez (1988). Study of histamine release induced by acute administration of antitumor agents in dogs. *Cancer Chemother Pharmacol* 21(3): 246-250.

Finlay, G. A., M. D. O'Donnell, C. M. O'Connor, J. P. Hayes and M. X. FitzGerald (1996). Elastin and collagen remodeling in emphysema. A scanning electron microscopy study. *Am J Pathol* 149(4): 1405-1415.

Fisher, A. J., N. W. Schrader and B. Klitzman (1992). Effects of chronic hypoxia on capillary flow and hematocrit in rat skeletal muscle. *Am J Physiol* 262(6 Pt 2): H1877-1883.

Goldberg, M. E. and C. W. Henry (2000). Guidelines of Acceptable Methods for Euthanasia of Animals, Virginia Commonwealth University Institutional Animal Care and Use Committee. (http://www.research.vcu.edu/dar/dar_guides/Acceptable_Methods_for_Euthanasia_of_Animals.pdf)

Goldberg, S. J., K. E. Wilson and M. S. Shall (1997). Summation of extraocular motor unit tensions in the lateral rectus muscle of the cat. *Muscle Nerve* 20(10): 1229-1235.

Golub, A. S. and R. N. Pittman (2003). Thermostatic animal platform for intravital microscopy of thin tissues. *Microvasc Res* 66(3): 213-217.

Golub, A. S., A. S. Popel, L. Zheng and R. N. Pittman (1997). Analysis of phosphorescence in heterogeneous systems using distributions of quencher concentration. *Biophys J* 73(1): 452-465.

Gray, S. D. (1973). Rat spinotrapezius muscle preparation for microscopic observation of the terminal vascular bed. *Microvasc Res* 5(3): 395-400.

Green, H. J., J. R. Sutton, A. Cymerman, P. M. Young and C. S. Houston (1989). Operation Everest II: adaptations in human skeletal muscle. *J Appl Physiol* 66(5): 2454-2461.

Green, H. J., J. R. Sutton, E. E. Wolfel, J. T. Reeves, G. E. Butterfield and G. A. Brooks (1992). Altitude acclimatization and energy metabolic adaptations in skeletal muscle during exercise. *J Appl Physiol* 73(6): 2701-2708.

Gross, P., M. Babjak, E. Tolker and M. Kaschak (1964). Enzymatically produced pulmonary emphysema: a preliminary report. *J Occup Med* 6: 481-4884.

Gross, P., E. Pfitzer, E. Tolker and e. al (1965). Experimental emphysema: Its production with papain in normal and silicotic rats. *Arch Environ Health* 11: 50-58.

Hall, F. G. (1966). Minimal utilizable oxygen and the oxygen dissociation curve of blood of rodents. *J Appl Physiol* 21(2): 375-378.

Hamilton, A., K. Killian, E. Summers and N. Jones (1995). Muscle strength, symptom intensity, and exercise capacity in patients with cardiorespiratory disorders. *Am J Respir Crit Care Med* 152: 2021-2031.

Hansen-Smith, F., A. S. Greene, A. W. Cowley, Jr. and J. H. Lombard (1990). Structural changes during microvascular rarefaction in chronic hypertension. *Hypertension* 15(6 Pt 2): 922-928.

Henderson, K. K., H. Wagner, F. Favret, S. L. Britton, L. G. Koch, P. D. Wagner and N. C. Gonzalez (2002). Determinants of maximal O(2) uptake in rats selectively bred for endurance running capacity. *J Appl Physiol* 93(4): 1265-1274.

Hildebrand, I. L., C. Sylven, M. Esbjornsson, K. Hellstrom and E. Jansson (1991). Does chronic hypoxaemia induce transformations of fibre types? *Acta Physiol Scand* 141(3): 435-439.

Honig, C. R., T. E. J. Gayeski and K. Groebe (1991). Myoglobin and Oxygen Gradients. *The Lung: Scientific Foundations*. R. G. Crystal and J. B. West. New York, Raven Press, Ltd. 2: 1489-1496.

Hoppeler, H., E. Kleinert, C. Schlegel, H. Claassen, H. Howald, S. Kayar and P. Cerretelli (1990). Morphological adaptations of human skeletal muscle to chronic hypoxia. *Int J Sports Med* 11(suppl 1): S3-S9.

Hoppeler, H. and M. Vogt (2001). Muscle tissue adaptations to hypoxia. *J Exp Biol* 204(Pt 18): 3133-3139.

Howald, H., D. Pette, J. Simoneau, A. Uber, H. Hoppeler and P. Cerretelli (1990). Effect of chronic hypoxia on muscle enzyme activities. *Int J Sports Med* 11: 510-514.

Hughes, R. L., H. Katz, V. Sahgal, J. A. Campbell, R. Hartz and T. W. Shields (1983). Fiber size and energy metabolites in five separate muscles from patients with chronic obstructive lung diseases. *Respiration* 44(5): 321-328.

Icochea, A., B. S. Cooper and C. Kuhn (1982). The effect of oxygen on Cor pulmonale in experimental emphysema induced by elastase or elastase and beta-aminopropionitrile in hamsters. *Am Rev Respir Dis* 126(5): 792-796.

Institute of Laboratory Animal Resources (U.S.). Committee on Care and Use of Laboratory Animals. (1996). *Guide for the Care and Use of Laboratory Animals*. Bethesda, Md., U.S. Dept. of Health and Human Services Public Health Service National Institutes of Health.

Itoh, K., T. Moritani, K. Ishida, C. Hirofuji, S. Taguchi and M. Itoh (1990). Hypoxia-induced fibre type transformation in rat hindlimb muscles. Histochemical and electro-mechanical changes. *Eur J Appl Physiol Occup Physiol* 60(5): 331-336.

Jakobsson, P., L. Jorfeldt and A. Brundin (1990). Skeletal muscle metabolites and fiber types in patients with advanced chronic obstructive pulmonary disease (COPD), with and without chronic respiratory failure. *Eur Respir J* 3: 192-196.

Jakobsson, P., L. Jorfeldt and J. Henriksson (1995). Metabolic enzyme activity in the quadriceps femoris muscle in patients with severe chronic obstructive pulmonary disease. *Am J Respir Crit Care Med* 151: 374-377.

Kano, Y., D. Padilla, K. S. Hageman, D. C. Poole and T. I. Musch (2004). Downhill running: a model of exercise hyperemia in the rat spinotrapezius muscle. *J Appl Physiol*: 00334.02004.

Kaplan, P. D., C. Kuhn and J. A. Pierce (1973). The induction of emphysema with elastase. I. The evolution of the lesion and the influence of serum. *J Lab Clin Med* 82(3): 349-356.

Kindig, C. A., T. I. Musch, R. J. Basaraba and D. C. Poole (1999). Impaired capillary hemodynamics in skeletal muscle of rats in chronic heart failure. *J Appl Physiol* 87(2): 652-660.

Kindig, C. A. and D. C. Poole (1998). A comparison of the microcirculation in the rat spinotrapezius and diaphragm muscles. *Microvasc Res* 55(3): 249-259.

Kindig, C. A. and D. C. Poole (1999). Effects of skeletal muscle sarcomere length on in vivo capillary distensibility. *Microvasc Res* 57(2): 144-152.

Kindig, C. A. and D. C. Poole (2001). Sarcomere length-induced alterations of capillary hemodynamics in rat spinotrapezius muscle: vasoactive vs passive control. *Microvasc Res* 61(1): 64-74.

Kindig, C. A., T. E. Richardson and D. C. Poole (2002). Skeletal muscle capillary hemodynamics from rest to contractions: implications for oxygen transfer. *J Appl Physiol* 92(6): 2513-2520.

Kindig, C. A., W. L. Sexton, M. R. Fedde and D. C. Poole (1998). Skeletal muscle microcirculatory structure and hemodynamics in diabetes. *Respir Physiol* 111(2): 163-175.

Kinirons, S. A. (2002). The effects of an altered activity level, via artificial rearing, on the developing rat tongue retractor musculature. *Anatomy/Physical Therapy*. Richmond, VCU: 115.

Kuhn, C., 3rd and F. Tavassoli (1976). The scanning electron microscopy of elastase-induced emphysema. A comparison with emphysema in man. *Lab Invest* 34(1): 2-9.

Kuhn, C., S. Y. Yu, M. Chraplyvy, H. E. Linder and R. M. Senior (1976). The induction of emphysema with elastase. II. Changes in connective tissue. *Lab Invest* 34(4): 372-380.

Kunert, M. P., J. F. Liard, D. J. Abraham and J. H. Lombard (1996). Low-affinity hemoglobin increases tissue PO2 and decreases arteriolar diameter and flow in the rat cremaster muscle. *Microvasc Res* 52(1): 58-68.

Lahiri, S. (1975). Blood oxygen affinity and alveolar ventilation in relation in body weight in mammals. *Am J Physiol* 229(2): 529-536.

Lash, J. M. (1994). Contribution of arterial feed vessels to skeletal muscle functional hyperemia. *J Appl Physiol* 76(4): 1512-1519.

Lash, J. M. (1995). Arterial and arteriolar contributions to skeletal muscle functional hyperemia in spontaneously hypertensive rats. *J Appl Physiol* 78(1): 93-100.

Lash, J. M. (1998). Exercise training enhances adrenergic constriction and dilation in the rat spinotrapezius muscle. *J Appl Physiol* 85(1): 168-174.

Lash, J. M. (1998). Training-induced alterations in contractile function and excitation-contraction coupling in vascular smooth muscle. *Med Sci Sports Exerc* 30(1): 60-66.

Lash, J. M. and H. G. Bohlen (1987). Perivascular and tissue PO2 in contracting rat spinotrapezius muscle. *Am J Physiol* 252(6 Pt 2): H1192-1202.

Lash, J. M. and H. G. Bohlen (1995). Excess oxygen delivery during muscle contractions in spontaneously hypertensive rats. *J Appl Physiol* 78(1): 101-111.

Laurell, C. and S. Eriksson (1963). The electrphoretic alpha1-globulin pattern of alpha1-anti-tyrpsin deficiency. *Scand J Clin Lab Invest* 15: 132-140.

Lieber, R. L. (1992). *Skeletal muscle structure and function : implications for rehabilitation and sports medicine*. Baltimore, Williams & Wilkins.

Lloyd, M. H. and S. E. Wolfensohn (1999). *Practical use of distress scoring systems in the application of humane endpoints*. Humane Endpoints in Animal Experiments for Biomedical Research: Proceedings of the International Conference, Zeist, The Netherlands, The Royal Society of Medicine Press: London, UK.

Lorenz, W., H. J. Reimann, A. Schmal, P. Dormann, B. Schwarz, E. Neugebauer and A. Doenicke (1977). Histamine release in dogs by Cremophor E1 and its derivatives: oxethylated oleic acid is the most effective constituent. *Agents Actions* 7(1): 63-67.

Lucey, E. C., J. Keane, P.-P. Kuang, G. L. Snider and R. H. Goldstein (2002). Severity of Elastase-Induced Emphysema Is Decreased in Tumor Necrosis Factor-{alpha} and Interleukin-1{beta} Receptor-Deficient Mice. *Lab Invest* 82(1): 79-85.

Lucey, E. C., J. J. O'Brien, Jr., W. Pereira, Jr. and G. L. Snider (1980). Arterial blood gas values in emphysematous hamsters. *Am Rev Respir Dis* 121(1): 83-89.

MacDougall, J. D., H. J. Green, J. R. Sutton, G. Coates, A. Cymerman, P. Young and C. S. Houston (1991). Operation Everest II: structural adaptations in skeletal muscle in response to extreme simulated altitude. *Acta Physiol Scand* 142(3): 421-427.

Maltais, F., P. LeBlanc, F. Whittom, C. Simard, K. Marquis, M. Belanger, M.-J. Breton and J. Jobin (2000). Oxidative enzyme activities of the vastus lateralis muscle and the functional status in patients with COPD. *Thorax* 55: 848-853.

Maltais, F., A. Simard, C. Simard, J. Jobin, P. Desgagnes and P. LeBlanc (1996). Oxidative capacity of the skeletal muscle and lactic acid kinetics during exercise

in normal subjects and in patients with COPD. *Am J Respir Crit Care Med* 153: 288-293.

Marks, L. and S. Kolmen (1971). Tween 20 shock in dogs and related fibrinogen changes. *Am J Physiol* 220(1): 218-221.

Marshall, J. M. and W. R. Davies (1999). The effects of acute and chronic systemic hypoxia on muscle oxygen supply and oxygen consumption in the rat. *Exp Physiol* 84(1): 57-68.

Mathieu-Costello, O., C. G. Ellis, R. F. Potter, I. C. MacDonald and A. C. Groom (1991). Muscle capillary-to-fiber perimeter ratio: morphometry. *Am J Physiol* 261(5 Pt 2): H1617-1625.

Mattson, J. P. and D. C. Poole (1998). Pulmonary emphysema decreases hamster skeletal muscle oxidative enzyme capacity. *J Appl Physiol* 85(1): 210-214.

Maxwell, G. M. and V. Rencis (1974). The effect of burimamide, an H-2 receptor antagonist, upon the general and coronary haemodynamics of intact dogs and upon histamine release by Tween 20. *Aust J Exp Biol Med Sci* 52(5): 825-832.

McDonough, P., B. J. Behnke, C. A. Kindig and D. C. Poole (2001). Rat muscle microvascular PO2 kinetics during the exercise off-transient. *Exp Physiol* 86(3): 349-356.

Millard, R. W., H. Baig and S. F. Vatner (1977). Cardiovascular effects of radioactive microsphere suspensions and Tween 80 solutions. *Am J Physiol* 232(3): H331-334.

Moller, P., K. Hellstrom and I. L. Hermansson (1984). Myoglobin content in leg skeletal muscle in patients with chronic obstructive lung disease. *Respiration* 45(1): 35-38.

Munoz, A., P. Karila, P. Gallay, F. Zettelmeier, P. Messner, M. Mery and R. Grolleau (1988). A randomized hemodynamic comparison of intravenous amiodarone with and without Tween 80. *Eur Heart J* 9(2): 142-148.

Musch, T. I. and D. C. Poole (1996). Blood flow response to treadmill running in the rat spinotrapezius muscle. *Am J Physiol* 271(6 Pt 2): H2730-2734.

Narici, M. V. and B. Kayser (1995). Hypertrophic response of human skeletal muscle to strength training in hypoxia and normoxia. *Eur J Appl Physiol Occup Physiol* 70(3): 213-219.

NCHS (1999). Ambulatory care visits to physician offices, hospital outpatient departments and emergency departments: United States, 1997. *Vital Health Stat* Series No 13 (143).

Nellis, S. H., S. F. Flaim, K. M. McCauley and R. Zelis (1980). alpha-Stimulation protects exercise increment in skeletal muscle oxygen consumption. *Am J Physiol Heart Circ Physiol* 238(3): H331-339.

Nguyen, T., J. Shrager, L. Kaiser, L. Mei, M. Daood, J. Watchko, N. Rubinstein and S. Levine (2000). Developmental myosin heavy chains in the adult human diaphragm: coexpression patterns and effect of COPD. *J Appl Physiol* 88(4): 1446-1456.

NOTTG (1980). Continuous or nocturnal oxygen therapy in hypoxemic chronic obstructive lung disease: a clinical trial. Nocturnal Oxygen Therapy Trial Group. *Ann Intern Med* 93(3): 391-398.

Nusz, D. J., D. C. White, Q. Dai, A. M. Pippen, M. A. Thompson, G. B. Walton, C. J. Parsa, W. J. Koch and B. H. Annex (2003). Vascular rarefaction in peripheral skeletal muscle after experimental heart failure. *Am J Physiol Heart Circ Physiol* 285(4): H1554-1562.

O'Brien, J. J., Jr., E. C. Lucey and G. L. Snider (1979). Arterial blood gases in normal hamsters at rest and during exercise. *J Appl Physiol* 46(4): 806-810.

Peter, J. B., R. J. Barnard, V. R. Edgerton, C. A. Gillespie and K. E. Stempel (1972). Metabolic profiles of three fiber types of skeletal muscle in guinea pigs and rabbits. *Biochemistry* 11(14): 2627-2633.

Pierson, D. J. (2000). Pathophysiology and clinical effects of chronic hypoxia. *Respir Care* 45(1): 39-51; discussion 51-33.

Pittman, R. N. (2000). Oxygen supply to contracting skeletal muscle at the microcirculatory level: diffusion vs. convection. *Acta Physiol Scand* 168(4): 593-602.

Pittman, R. N. (2004). Calculation of mean arteriolar velocity using FluoSpheres. J. D. Lowman, Jr. Richmond.

Pittman, R. N. (2004). Calculation of mean venular blood velocity using FluoSpheres. J. D. Lowman, Jr. Richmond, VA.

Pittman, R. N. and M. L. Ellsworth (1986). Estimation of red cell flow microvessels: consequences of the Baker-Wayland spatial averaging model. *Microvasc Res* 32(3): 371-388.

Poole, D. C. (2002). Reagrding elastase. J. D. Lowman, Jr.

Poole, D. C., T. I. Musch and C. A. Kindig (1997). In vivo microvascular structural and functional consequences of muscle length changes. *Am J Physiol* 272(5 Pt 2): H2107-2114.

Powell, R. J., G. W. Machiedo, B. F. Rush, Jr. and G. Dikdan (1991). Oxygen free radicals: effect on red cell deformability in sepsis. *Crit Care Med* 19(5): 732-735.

Richardson, R. S. (1999). Skeletal muscle dysfunction vs. muscle disuse in patients with COPD. *J Appl Physiol* 86(5): 1751-1753.

Richardson, R. S., B. T. Leek, T. P. Gavin, L. J. Haseler, S. R. D. Mudaliar, R. Henry, A. L. Ries, O. D. Mathieu-Costello and P. D. Wagner (2003). Reduced mechancial efficiency in COPD, but normal peak VO2 with small muscle mass exercise. *Am. J. Respir. Crit. Care Med.*: 200305-200627OC.

Richardson, T. E., C. A. Kindig, T. I. Musch and D. C. Poole (2003). Effects of chronic heart failure on skeletal muscle capillary hemodynamics at rest and during contractions. *J Appl Physiol* 95(3): 1055-1062.

Richmond, K. N., R. D. Shonat, R. M. Lynch and P. C. Johnson (1999). Critical PO(2) of skeletal muscle in vivo. *Am J Physiol* 277(5 Pt 2): H1831-1840.

Riley, L. K., J. H. Simmons, G. Purdy, R. S. Livingston, C. L. Franklin, C. L. Besch-Williford and R. J. Russell (2002). Rat Respiratory Virus (RRV). Research

Update: Idiopathic Lung Lesions in Rats. (http://www.radil.missouri.edu/RADILinfo/research/ResearchRRV.asp).

Rome, L. C. and M. J. Kushmerick (1983). Energetics of isometric contractions as a function of muscle temperature. *Am J Physiol Cell Physiol* 244(1): C100-109.

Rovainen, C. M., D. B. Wang and T. A. Woolsey (1992). Strobe epi-illumination of fluorescent beads indicates similar velocities and wall shear rates in brain arterioles of newborn and adult mice. *Microvasc Res* 43(2): 235-239.

Russ, D. W., M. A. Elliott, K. Vandenborne, G. A. Walter and S. A. Binder-Macleod (2002). Metabolic costs of isometric force generation and maintenance of human skeletal muscle. *Am J Physiol Endocrinol Metab* 282(2): E448-457.

Russell, J. A., C. A. Kindig, B. J. Behnke, D. C. Poole and T. I. Musch (2003). Effects of aging on capillary geometry and hemodynamics in rat spinotrapezius muscle. *Am J Physiol Heart Circ Physiol* 285(1): H251-258.

Saltzman, D., F. A. DeLano and G. W. Schmid-Schonbein (1992). The microvasculature in skeletal muscle. VI. Adrenergic innervation of arterioles in normotensive and spontaneously hypertensive rats. *Microvasc Res* 44(3): 263-273.

Sato, S., S. Kato, Y. Arisaka, H. Takahashi and H. Tomoike (1994). Pulmonary haemodynamics in awake rats following treatment with endotracheal pancreatic elastase. *Eur Respir J* 7(7): 1294-1299.

Sato, S., S. Kato, H. Takahashi, Y. Arisaka and K. Takahashi (1990). Dose dependency of intratracheal elastase-induced changes in pressure volume curve and morphometry in rat lungs. *Tohoku J Exp Med* 161(2): 101-110.

Satta, A., G. Migliori, A. Spanevello, M. Neri, R. Bottinelli, M. Canepari, M. Pellegrino and C. Reggiani (1997). Fiber types in skeletal muscles of chronic obstructive pulmonary disease patients related to respiratory function and exercise tolerance. *Eur Respir J* 10: 2853-2860.

Schenkman, K. A., D. R. Marble, D. H. Burns and E. O. Feigl (1997). Myoglobin oxygen dissociation by multiwavelength spectroscopy. *J Appl Physiol* 82(1): 86-92.

Schmid-Schoenbein, G. W. and B. W. Zweifach (1975). RBC velocity profiles in arterioles and venules of the rabbit omentum. *Microvasc Res* 10(2): 153-164.

Schmid-Schonbein, G. W., G. Firestone and B. W. Zweifach (1986). Network anatomy of arteries feeding the spinotrapezius muscle in normotensive and hypertensive rats. *Blood Vessels* 23(1): 34-49.

Schumacker, P. T. (1991). Systemic Effects of Hypoxia. *The Lung: Scientific Foundations*. W. J. Crystal Rg. New York, Raven Press, Ltd. 2: 1534-1551.

Segal, S. S., J. A. Faulkner and T. P. White (1986). Skeletal muscle fatigue in vitro is temperature dependent. *J Appl Physiol* 61(2): 660-665.

Serres, I., V. Gautier, A. Varray and C. Prefaut (1998). Impaired skeletal muscle endurance related to physical inactivity and altered lung function in COPD patients. *Chest* 113: 900-905.

Severinghaus, J. W. (1966). Blood gas calculator. *J Appl Physiol* 21(3): 1108-1116.

Sexton, W. L. and D. C. Poole (1998). Effects of emphysema on diaphragm blood flow during exercise. *J Appl Physiol* 84(3): 971-979.

Sheridan, R. L., W. M. Zapol, R. H. Ritz and R. G. Tompkins (1999). Low-dose inhaled nitric oxide in acutely burned children with profound respiratory failure. *Surgery* 126(5): 856-862.

Sillau, A. H., L. Aquin, M. V. Bui and N. Banchero (1980). Chronic hypoxia does not affect guinea pig skeletal muscle capillarity. *Pflugers Arch* 386(1): 39-45.

Skalak, T. C. and G. W. Schmid-Schonbein (1986). The microvasculature in skeletal muscle. IV. A model of the capillary network. *Microvasc Res* 32(3): 333-347.

Slayter, E. M. (1970). *Optical Methods in Biology*. New York, Wiley-Interscience.

Smith, K. and J. M. Marshall (1999). Physiological adjustments and arteriolar remodelling within skeletal muscle during acclimation to chronic hypoxia in the rat. *J Physiol* 521 Pt 1: 261-272.

Smith, L., M. H. Tiba, M. E. Goldberg and R. W. Barbee (2004). Chronic implantation of transit-time flow probes on the ascending aorta of rodents. *Lab Anim* 38(4): 362-370.

Smith, L. M. (2002). Oxygen delivery to the skeletal muscle of the spontaneously hypertensive rat. *Physiology*. Richmond, Virginia Commonwealth University: 144.

Smith, L. M., R. W. Barbee, K. R. Ward and R. N. Pittman (2004). Prolonged reduction of tissue PO2 in the spinotrapezius muscle of spontaneously hypertensive rats following contraction. *Am J Physiol Heart Circ Physiol*: 00980.02002.

Smith, L. M., R. W. Barbee, K. R. Ward and R. N. Pittman (2004). Prolonged tissue PO2 reduction after contraction in spinotrapezius muscle of spontaneously hypertensive rats. *Am J Physiol Heart Circ Physiol* 287(1): H401-407.

Smith, L. M., A. S. Golub and R. N. Pittman (2002). Interstitial PO(2) determination by phosphorescence quenching microscopy. *Microcirculation* 9(5): 389-395.

Snider, G. L., E. C. Lucey and P. J. Stone (1986). Animal models of emphysema. *Am Rev Respir Dis* 133(1): 149-169.

Snider, G. L. and C. B. Sherter (1977). A one-year study of the evolution of elastase-induced emphysema in hamsters. *J Appl Physiol* 43(4): 721-729.

Snider, G. L., C. B. Sherter, K. W. Koo, J. B. Karlinsky, J. A. Hayes and C. Franzblau (1977). Respiratory mechanics in hamsters following treatment with endotracrael elastase or collagenase. *J Appl Physiol* 42(2): 206-215.

Streiner, D. L. (1996). Maintaining standards: differences between the standard deviation and standard error, and when to use each. *Can J Psychiatry* 41(8): 498-502.

Sutlive, T. G., M. S. Shall, J. R. McClung and S. J. Goldberg (2000). Contractile properties of the tongue's genioglossus muscle and motor units in the rat. *Muscle Nerve* 23(3): 416-425.

Suzuki, H., D. C. Poole, B. W. Zweifach and G. W. Schmid-Schonbein (1995). Temporal correlation between maximum tetanic force and cell death in postischemic rat skeletal muscle. *J Clin Invest* 96(6): 2892-2897.

Swain, D. P. and R. N. Pittman (1989). Oxygen exchange in the microcirculation of hamster retractor muscle. *Am J Physiol* 256(1 Pt 2): H247-255.

Takahashi, H., K. Kikuchi and H. Nakayama (1992). Effect of chronic hypoxia on skeletal muscle fiber type in adult male rats. *Ann Physiol Anthropol* 11(6): 625-630.

Talmadge, R. J. and R. R. Roy (1993). Electrophoretic separation of rat skeletal muscle myosin heavy-chain isoforms. *J Appl Physiol* 75(5): 2337-2340.

Tangelder, G. J., D. W. Slaaf, A. M. Muijtjens, T. Arts, M. G. oude Egbrink and R. S. Reneman (1986). Velocity profiles of blood platelets and red blood cells flowing in arterioles of the rabbit mesentery. *Circ Res* 59(5): 505-514.

Taylor, K. and T. N. Calvey (1977). Histochemical characteristics and contractile properties of the spinotrapezius muscle in the rat and the mouse. *J Anat* 123(1): 67-76.

Teisseire, B. P., C. D. Soulard, L. J. Teisseire, R. A. Herigault and D. N. Laurent (1984). Induced low P50 in anesthetized rats: blood gas, circulatory and metabolic adjustments. *Respir Physiol* 58(3): 335-344.

Termin, A., R. S. Staron and D. Pette (1989). Myosin heavy chain isoforms in histochemically defined fiber types of rat muscle. *Histochemistry* 92(6): 453-457.

van Ekeren, G. J., R. C. Sengers and A. M. Stadhouders (1992). Changes in volume densities and distribution of mitochondria in rat skeletal muscle after chronic hypoxia. *Int J Exp Pathol* 73(1): 51-60.

Vovenko, E. P., A. S. Golub and R. N. Pittman (2002). Oxygen tension and blood velocity measurements in single cortical microvessels during normovolemic hemodilution. *Journal of Vascular Research* 39(S1): 71.

Wang, X. N., T. J. Williams, M. J. McKenna, J. L. Li, S. F. Fraser, E. A. Side, G. I. Snell, E. H. Walters and M. F. Carey (1999). Skeletal muscle oxidative capacity, fiber type, and metabolites after lung transplantation. *Am J Respir Crit Care Med* 160(1): 57-63.

Waynforth, H. B. and P. A. Flecknell (1992). *Experimental and Surgical Technique in the Rat*. San Diego, Academic Press.

Weibel, E. R. (1984). *The Pathway for Oxygen: Structure and Function in the Mammalian Respiratory System*. Cambridge, Mass., Harvard University Press.

Weibel, E. R. (2000). *Symmorphosis: On Form and Function in Shaping Life*. Cambridge, Mass., Harvard University Press.

Weisbroth, S. H. (2002). *Emerging Diseases of Laboratory Rodents*. Tribranch, American Association for Laboratory Animal Science Annual Meeting, Philadelphia, PA.

West, J. B. (1997). *Pulmonary pathophysiology--the essentials*. Baltimore, Md., Williams & Wilkins.

West, J. B. (1998). *Pulmonary pathophysiology--the essentials*. Baltimore, Md., Williams & Wilkins.

Whittom, F., J. Jobin, P. Simard, P. LeBlanc, C. Simard, S. Bernard, R. Belleau and F. Maltais (1998). Histochemical and morphological characteristics of the vastus lateralis muscle in patients with chronic obstructive pulmonary disease. *Med Sci Sports Exerc* 30: 1467-1474.

Zattara-Hartmann, M., M. Badier, C. Guillot, C. Tomei and Y. Jammes (1995). Maximal force and endurance to fatigue of respiratory and skeletal muscles in chronic hypoxemic patients: the effects of oxygen breathing. *Muscle Nerve* 18: 495-502.

Zhang, K. M., L. D. Wright, P. Hu, J. A. Spratt, A. S. Wechsler and F. N. Briggs (1997). Induction of molecular and mechanical transformations in canine skeletal muscle by chronic neuromuscular stimulation. *J Muscle Res Cell Motil* 18(1): 81-90.

Zheng, L., A. S. Golub and R. N. Pittman (1996). Determination of PO2 and its heterogeneity in single capillaries. *Am J Physiol* 271(1 Pt 2): H365-372.

Zinchuk, V. V. and L. V. Dorokhina (2002). Blood Oxygen Transport in Rats under Hypothermia Combined with Modification of the -Arginine-NO Pathway. *Nitric Oxide* 6(1): 29-34.

Appendix I.

Thermostatic animal platform

A thermostatic animal platform for intravital microscopy (Figures 55 and 56) was modified from one originally designed, built, and described by Aleksander S. Golub (Golub and Pittman 2003). The current device was specifically designed for the spinotrapezius muscle, and incorporates a force transducer and tension adjuster for contractile measurement in skeletal muscle. This device allows both transmission and episcopic illumination of thin tissues while maintaining both the animal and tissue at a physiologic temperature. In addition, it allows muscle contractile measures to be made while the muscle is at its physiologic length and temperature; this is important, because muscle blood flow, contractile performance and metabolism decrease in response to sub-physiologic temperatures. A disclosure was made with the VCU Office of Technology Transfer, the device was assigned to the VCU-Intellectual Property Foundation, and it has been protected and is currently being marketed to potential licensees. The following are the photographs, bill of materials, and detailed drawings of the device.

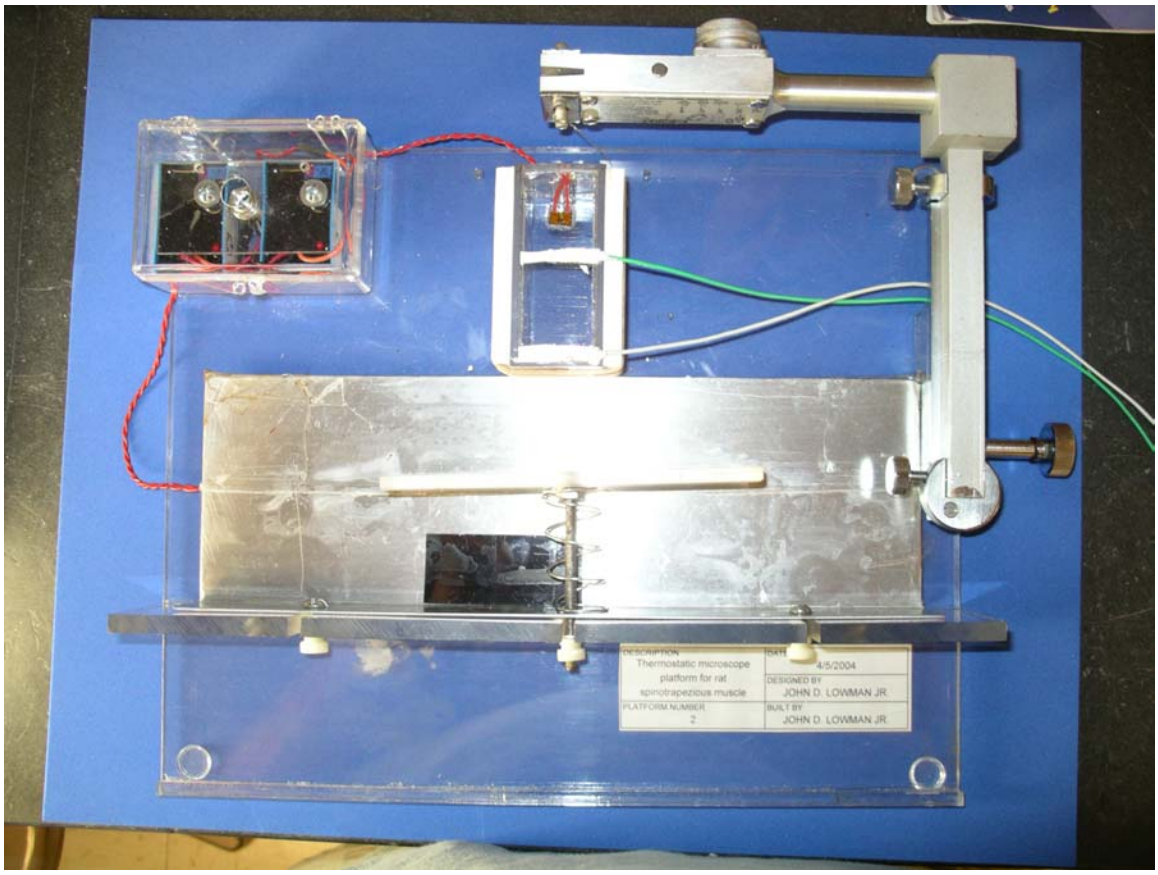

Figure 55. Thermostatic animal platform with force transducer and tension adjuster.

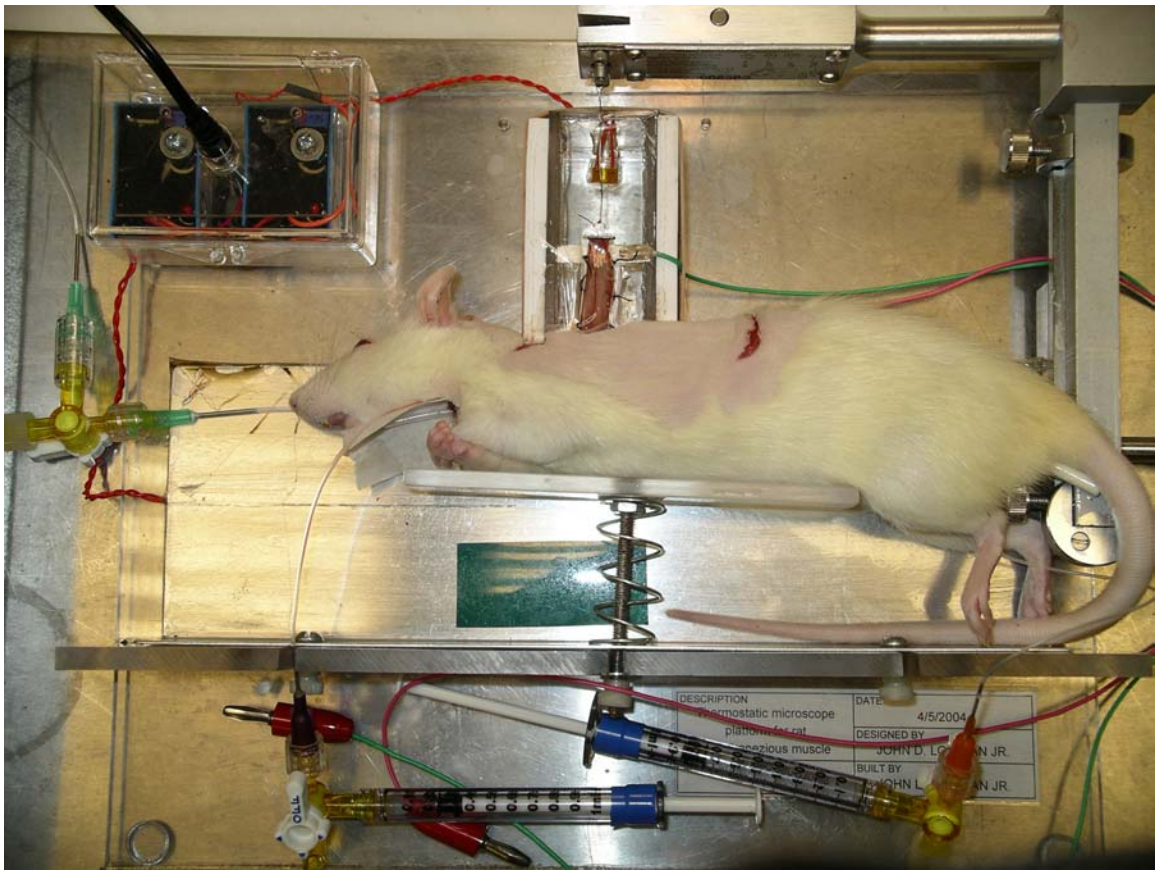

Figure 56. Rat on thermostatic animal platform with spinotrapezius muscle connected to force transducer.

Bill of materials

I. Platform (Figure 57)

A. Polymer Plastics Corp., http://www.polymerplastics.com/transparents_lexan.shtml

1. Clear Lexan sheets

a. Base (Figure 58)

i. 11 x 9 x .250" (280 x 230 x 6mm) +/-0.010-0.029 $28.17

b. Upright (Figure 59)

i. 11 x 1.97 x .250" (280 x 50 x 6mm) +/-0.010-0.029 $18.66

c. Window box (Figure 60)

i. 1.260 x 10" (32 x 254.0mm), 0.093 +/-0.010-0.029 $17.85

ii. 1.260 x 3" (32 x 76.2mm), 0.060 +/-0.010-0.029 $17.17

iii. 1.220 x 8" (31 x 203.2mm), 0.030, +/-0.010-0.029 $27.28

II. Animal heating tray

A. VCU Custom Design and Fabrication

1. L-shaped 1 mm thick aluminum, 80 x 250mm/30 x 250mm $15.00

II. Animal heater:

A. Minco Products, Inc., http://www.minco.com

1. Standard Kapton heater

a. 3 x 9", 14.2Ω, 12" lead, PSA backing, no UL marking

b. Part # HK5472R14.2L12B $129.10

2. Heaterstat controller for standard Kapton heater# 1 above

a. Part # CT698-1005T39CL1

3. Neoprene foam insulation for #1 above

a. Part # IN5176N1B(-) $5.00

4. Window heater:

a. Standard Thermal Clear Heater
b. 0.9 x 2", 43.3Ω, PSA backing, 12" lead
c. Part # H6702R43.3L12B $117.75

5. Heaterstat controller for window heater

a. Part # CT698-1010T37CL1

III. Optical window:

A. Edmund Scientific, http://www.edmundoptics.com

1. Window Glass 25 x 63.5 x1mm AR CTD

a. Stock # NT32-739, Part # 32739 $14.90

IV. Power supply

A. Elpac Power Systems, http://www.elpac.com

1. Power supply

a. 100-120V AC input, 15.0V, 1.20A, 18W max output
b. Part # WM1815/1.2-76 $42.09

V. Other

A. Miscellaneous size screws, thumb nuts, DC power connector, plastic box to contain electronics, 5 x 5mm acrylic rod, spring for width adjuster, E6000 Industrial Strength Adhesive ((clear) Eclectic Products, Inc.), and foam for pedestal insulation ≈ $30.00

Total cost ≈ $**460.00**

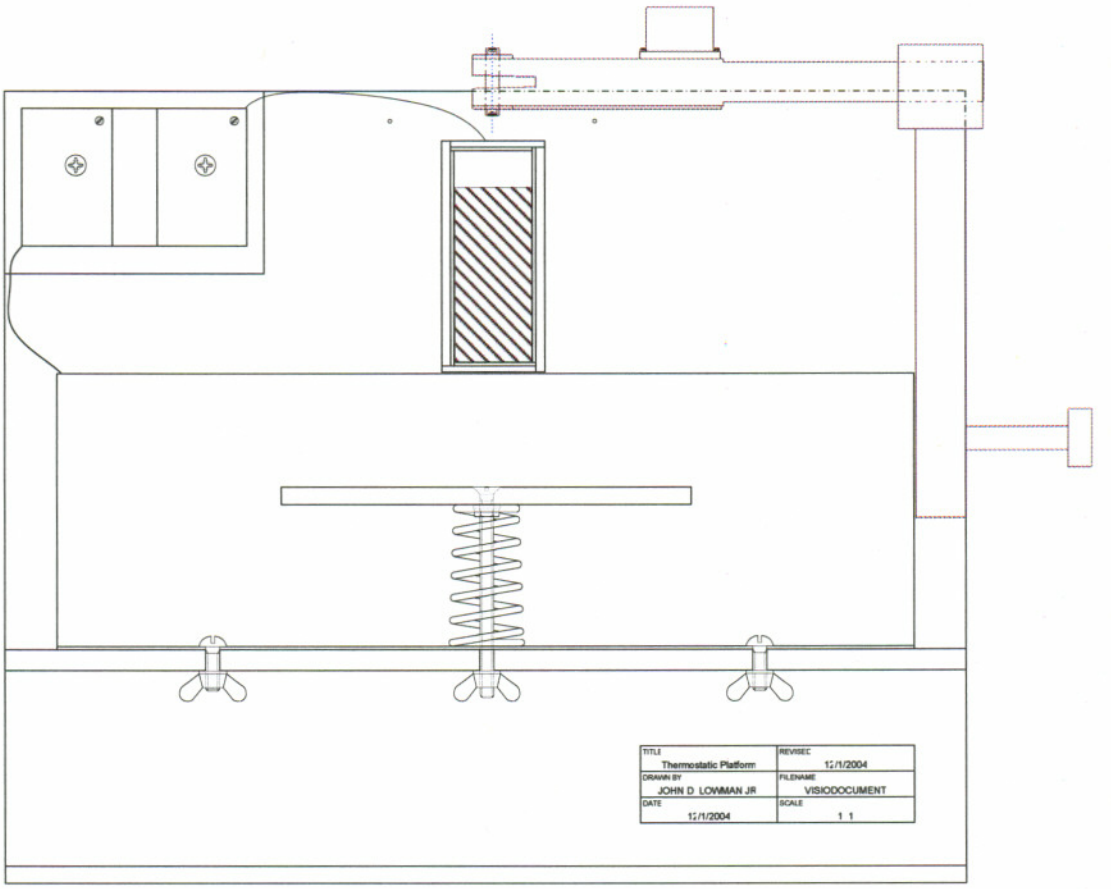

Figure 57. Thermostatic animal platform drawing.

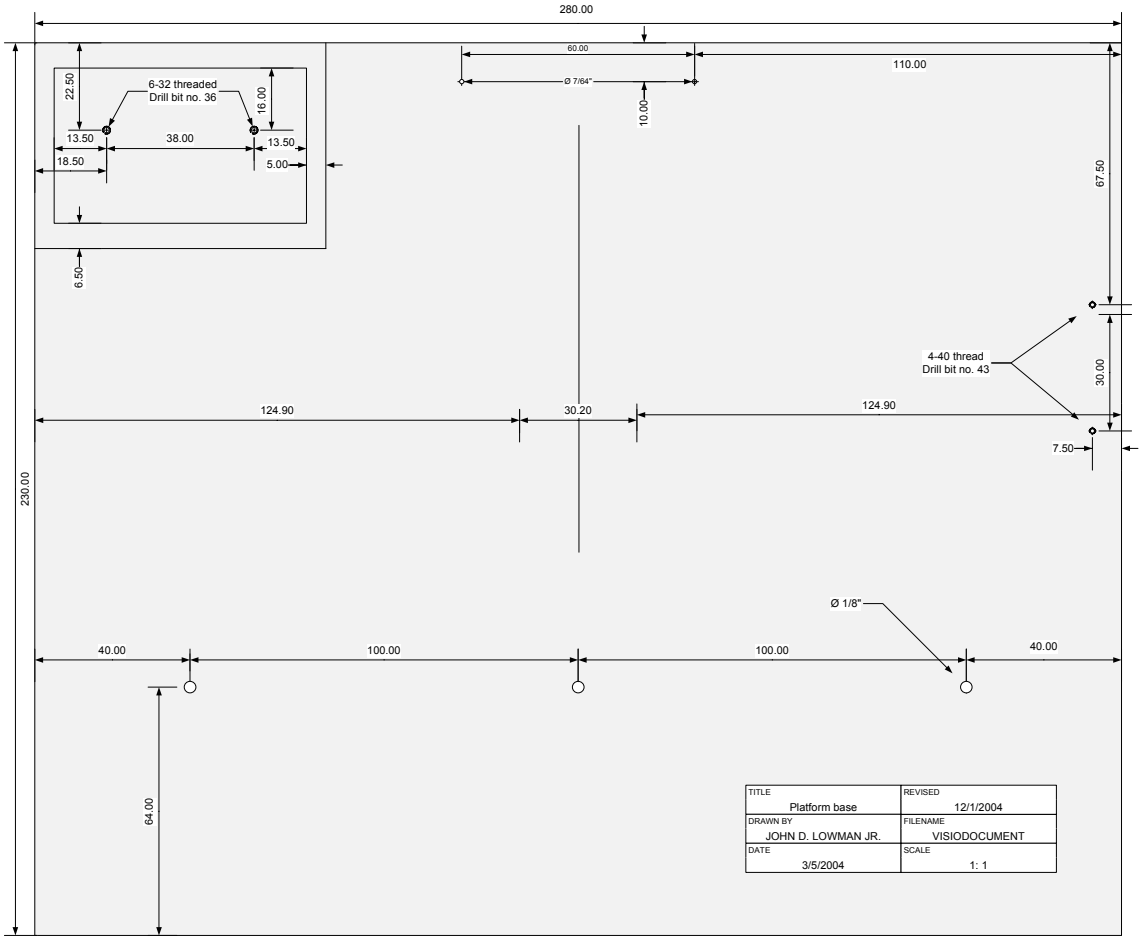

Figure 58. Platform base

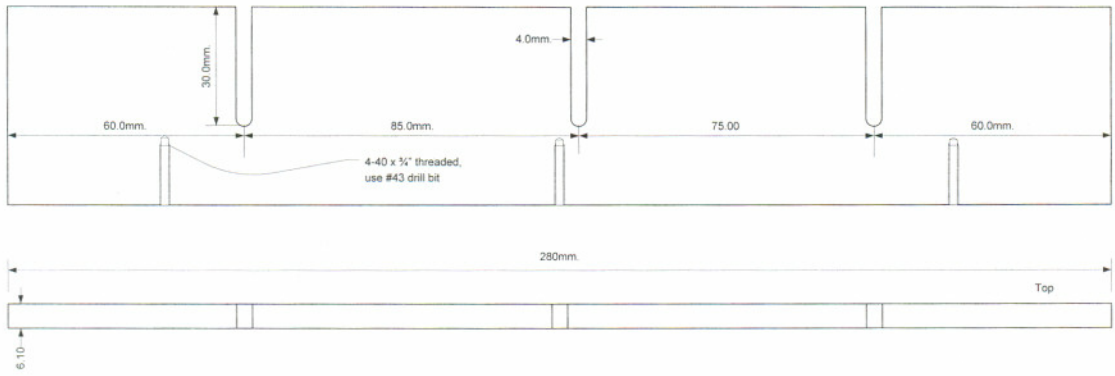

Figure 59. Platform upright.

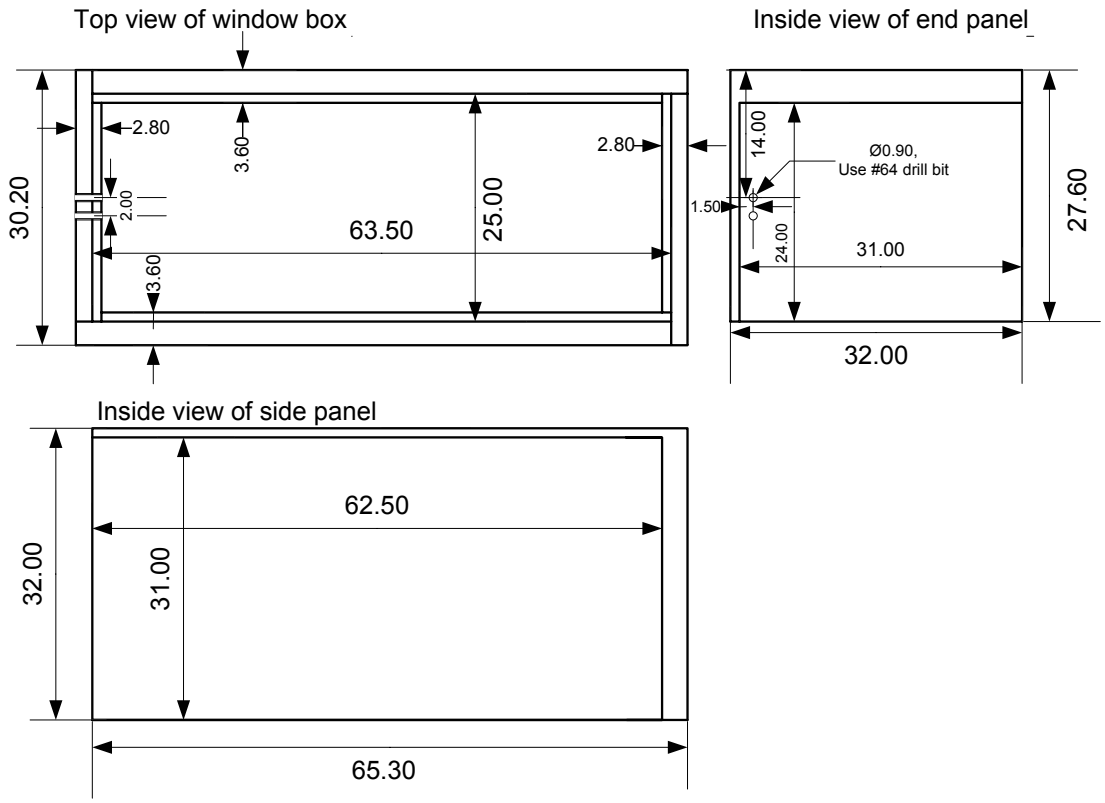

Figure 60. Platform window box for transmission illumination of the spinotrapezius muscle.

Appendix II.

Distress scoring sheet

Table 17. Distress scoring sheet. Adapted from Lloyd and Wolfensohn's work (1999), validating this distress scoring system with respiratory parameters with the elastase-induced emphysema model in the rat.

Parameter	Descriptive characteristic	Score
Appearance	Normal	0
	General lack of grooming	1
	Piloerection, fresh ocular and nasal discharges	2
	Piloerection, hunched up	3
	Above and eyes half closed	4
Natural behavior	Normal	0
	Minor changes	1
	Less mobile and isolated, but alert	2
	Restless or very still, not alert	3
Hydration status	Normal	0
	Abnormal skin pinch test	5
Clinical signs	Normal Respiratory rate and pattern	0
	Slight changes, increased rate only	1
	Increased rate with abdominal breathing	2
	Decreased rate with abdominal breathing	3
	Marked abdominal breathing and cyanosis	4
Provoked behavior	Normal	0
	Minor depression or exaggerated response	1
	Moderate change in expected behavior	2
	Very weak and precomatose	3
Total		0-19
Animals scoring ≥ 12/19 will be euthanized		

Appendix III.

Preparation of Albumin-bound Pd-porphyrin phosphorescence probe

General precautions

Use proper personal protective equipment and procedures: 1) respirator, when using powdered chemicals, 2) safety glasses, 3) gloves, and 4) wash any skin thoroughly if contaminated.

Solubilization of Pd-porphyrin

Table 18. Ingredients for 20 ml phosphorescence probe (10 mg/ml)

Item	Quantity
Tris base	1 g
BSA	1.32 g
Pd-MTCPP	200 mg
DMSO	4-5 ml
Deionized H_2O	100 ml, divided

Table 19. Solubilization – equipment and supplies

Scale	10 ml beaker	Mortar & pestle
pH meter	30 ml beaker	Mug (“don’t”)
Stirrer & micro stirring bar	25 ml graduated cylinder	Parafilm
Spatula & small weigh boats	Glass pipette & bulb	Aluminum foil

1. Prepare 2.75 M Tris base solution:
    a. Dissolve ***Tris*** into 3 ml of deionized H_2O in 10 ml beaker.
    b. Cover with parafilm.

2. Prepare 1 mM BSA solution:
    a. Poor 20 ml of deionized H_2O into a 30 ml beaker with micro-stir bar.
    b. With beaker on stirrer, use spatula to *slowly* add small portions of ***BSA*** (just sprinkle enough to cover the surface, letting each application dissolve). This takes at least 60 minutes.
    c. Use pipette to add a few drops of Tris base as needed to keep pH between 7.3 and 7.7.
    d. Color should gradually turn a clear yellow by the completion of this step.
3. In meantime, gently crush granules of ***Pd-MTCPP*** into mortar with pestle until you have a fine powder (*wear respirator*).
4. *Slowly* add small portions of Pd-MTCPP to BSA solution on the stirrer (just sprinkle enough to cover the surface, letting each application dissolve).
    a. This will take ~30 minutes.
    b. Protect solution from light, wrap beaker with aluminum foil.
    c. Rinse excess Pd-MTCPP from mortar and pestle with few drops of ***DMSO***, and poor into beaker; rinse a second time.
    d. Maintain pH between 7.3 and 7.7 with drops of Tris base.
    e. Cover with “don’t” mug and leave Pd-porphyrin solution on stirrer overnight.

Dialysis of Pd-porphyrin

Table 20. Ingredients for 1 L of dialysis solution

Item	Quantity
PBS	1 packet
PVP	55 g
Deionized H_2O	1 L

Table 21. Dialysis – equipment and supplies

Large weigh boats	10 ml beaker
Large stir bar	3 Spectra/Por® 4 membranes, 10 cm long
1 L beaker	Spectra/Por® clamps (3 white, 3 orange)
600 ml beaker	Plastic forceps & small needle
Two 100 ml beakers with deionized H_2O	Large glass syringe with Teflon needle

1. Prepare 1 mM dialysis solution:
    a. Dissolve ***PBS*** into 1 L of deionized H_2O.
    b. Fill 10 ml beaker with PBS (for volume restoration)
    c. Heat remaining PBS buffer solution to approximately 50° C on stirrer.
    d. *Slowly* add ***PVP*** to PBS buffer solution (*wear respirator*). It takes ~60 minutes to dissolve completely.
2. Poor 500 ml of dialysis solution into 600 ml beaker, and cover remaining beaker with parafilm.
3. Prepare dialysis bags:
    a. Place one ***Spectra/Por® 4 membrane*** into 100 ml beaker with deionized H_2O, let sit for 5 minutes.
    b. In meantime, withdraw Pd-porphyrin solution into syringe.
    c. Clamp one end of membrane with white/weighted clamp.

d. Open other end gently with small needle, and inject ~8 ml of Pd-porphyrin solution using glass syringe with Teflon needle.
e. Place orange clamp on other end of membrane, while leaving some air at top.
f. Rinse in a separate 100 ml beaker with deionized H_2O.
g. Place "bag" into dialysis solution.
h. Repeat for 2^{nd} and 3^{rd} membrane

4. Cover beaker on stirrer with aluminum foil, and let dialyze overnight (18 to 20 hours).
5. Remove bags from beaker and replace "old" dialysis solution with remaining dialysis solution.
6. Leave solution on stirrer for 4 – 6 hours, or longer.

Final processing

Table 22. Final processing – equipment and supplies

100 ml beaker with deionized H_2O	Vacuum pump
Two 50 ml beakers	50 – 0.5 ml microcentrifuge tubes with cap
25 ml graduated cylinder	Pipette and sterile pipette tip
115-ml sterilization filter unit	Dewar and 4" liquid N_2
< 10 ml PBS (from "Dialysis," step 1b)	

1. Remove dialysis bags from solution, rinse in 100 ml beaker with deionized H_2O, and dry with Kimwipe.
2. Unclamp dialysis bag and pour contents into 50 ml beaker, and squeeze remaining solution out.
3. Measure volume of solution in graduated cylinder.
4. Using vacuum pump, filter solution through sterilization filter unit, and return to a clean 50 ml beaker.
5. Rinse the graduated cylinder, original beaker, and filter unit with enough PBS to increase to volume measured in step 3 to 20 ml.
6. Pipette out 0.5 ml of solution into microcentrifuge tubes and close cap tightly.
7. Drop into liquid N_2 filled dewar.
8. Store in -80° C freezer, room 3-012.

Usage

Table 23. Usage – equipment and supplies

20-G needle, 22 mm long with blunt tip
1 ml empty syringe with Luer-Lok tip
One 0.5 ml microcentrifuge tube of probe
1 ml syringe filled with PBS

1. Remove a 0.5 ml microcentrifuge tube of Pd-porphyrin phosphorescence probe from freezer and thaw at room temperature.
2. Using 20-G needle and syringe, *slowly* withdraw solution from microcentrifuge tube (avoid bring any air bubbles into solution).
3. Inject into animal via stopcock and catheter
4. Flush "probe" syringe with 0.5 ml PBS, then inject into animal.
5. Flush catheter with 0.3 to 0.4 ml PBS.

Bill of materials

Table 24. Pd-porphyrin – bill of materials for 20 ml of probe

Item	Product number	Common abbreviation	Supplier	MW	Quantity
Oxyphor R0 (Pd-meso-tetra (4-carboxylphenyl) porphyrin)		Pd-MTCPP	Oxygen Enterprises, Ltd., Philadelphia, PA	896	200 mg
Trizma ® base $(CH_2OH)_3CNH_2$	T-1503	Tris	Sigma-Aldrich, Inc., St. Louis, MO	121.14	1 g
Dimethyl sulfoxide $(CH_3)_2SO$	D-8779	DMSO	Sigma-Aldrich, Inc., St. Louis, MO	78.13	4-5 ml
Albumin bovine serum, Fraction V	A-9647	BSA	Sigma-Aldrich, Inc., St. Louis, MO	66,000	1.32 g
Polyvinylpyrrolidone	856568	PVP	Sigma-Aldrich, Inc., St. Louis, MO	55,000	55 g
Phosphate buffered saline (0.01 M), pH 7.4	P-3813	PBS	Sigma-Aldrich, Inc., St. Louis, MO		1 packet
Spectra/Por ® 4 dialysis membrane	132700		Spectrum Laboratories, Inc., Rancho Dominquez, CA		3, 10 cm long
Spectra/Por ® closures	132751		Spectrum Laboratories, Inc., Rancho Dominquez, CA		3 white/ 3 orange
115-ml sterilization filter unit	121-0020		NALGENE Co., Rochester, NY		1

Appendix IV.

Molecular biology solutions and mixtures

Agents used in the electrophoresis procedures were electrophoretic grade (Bio-Rad).

MHC extraction solution

The MHC extraction solution (pH 6.5) had a final composition of 0.3 M NaCl, 0.15 M Na_2HPO_4 and 10 mM EDTA, and was stored at 4° C.

SDS-polyacrylamide gels

The 8% separating gel was composed of the following stock solutions: 68.16% glycerol, 29% acrylamide-bis (2%C), 1.5 M Tris (pH 8.8), 1 M glycine, 10% SDS, which were degassed for 15 minutes prior to initiation of polymerization with 10% ammonium persulfate (made fresh) and *N,N,N',N'*-tetramethylethylenediamine (TEMED).

The 4% stacking gel was composed of the following stock solutions: 68.16% glycerol, 29% acrylamide-bis (2%C), 0.5 M Tris (pH 6.8), 100 mM EDTA, 10% SDS, as well as deionized water, which were degassed for 15 minutes prior to initiation of polymerization with 10% ammonium persulfate (made fresh) and TEMED.

Buffer solutions

The sample buffer (2x Laemli) was composed of the following solutions: 0.5 Tris-HCl base, 10% SDS, 68.16% glycerol, 2 β-mercaptoethanol, and 0.05% bromophenol blue dye.

The upper running buffer had a final composition of 100 mM Tris base, 150 mM glycine, and 0.1% SDS in deionized water; the lower running buffer was half as concentrated as the upper. Both solutions were made immediately before gel electrophoresis and were stored at 4° C.

Staining procedure solutions

The fixative enhancer solution had a final composition of 50% methanol, 10% acetic acid, 10% fixative enhancer concentrate (Bio-Rad), and 30% deionized, distilled water.

The staining solution was made with 1) silver complex solution, 2) reduction moderator solution, 3) image development reagent, and 4) development accelerator solution (Silver Stain Plus, Bio-Rad).

Appendix V.

Preparation of FluoSpheres

Dilution of FluoSpheres

The 2.0 μm diameter FluoSpheres (F-8823, Carboxylate-Modified Microspheres, Molecular Probes, Inc., Eugen OR) had an original concentration of $4.5 \cdot 10^9$ particles/ml in an aqueous suspension with 0.02% Tween-20 and 2 mM sodium azide. The goal concentration for injection was $4.5 \cdot 10^8$ particles/ml. In addition to a 10-fold dilution, due to the histaminergic properties of Tween, the particles were "washed" as described below to yield 3-ml of solution (enough for 2-3 experiments). This is best done immediately prior to an experiment, no more than 48 hours before.

1. With the lid on tight, place the vial of FluoSpheres in an ultrasonic water bath for five minutes.
2. Put micro-stir bar in vial, place vial on stirrer for at least five minutes (cover to protect from light).
3. Pipette 0.3 ml of the probe into a small translucent plastic bottle and then add 2.7 ml of normal saline.
4. Centrifuge for 20 minutes at 3,600 rpm (~1,000 g).
5. Withdraw 2.5 ml of supernatant and replace it with normal saline.
6. Centrifuge again for 20 minutes at 3,600 rpm (~1,000 g).

7. Withdraw 2.5 ml of supernatant and replace it with normal saline.
8. Place back on stirrer or in vortex mixer to re-suspend the particles

This should reduce the Tween-20 concentration to ~$5.6 \cdot 10^{-5}$%, while maintaining a particle concentration of ~$4.5 \cdot 10^{8}$ per ml.

Usage

Prior to use in an experiment:

1. Place the vial of diluted solution in the ultrasonic bath for five minutes.
2. Use vortex mixer to re-suspend particles
3. Withdraw 0.6 to 1.0 ml of solution into a 1-ml syringe, and cap (leaving some room for air).
4. Immediately prior to injecting into the animal, briefly place the syringe in the vortex mixer.

Vita

John D. Lowman Jr. was born in Radford, Virginia (Va.), U.S.A., August 3, 1971. John graduated from Pulaski County High School, Dublin, Va. in 1989. He was a Cum Laude and Commonwealth Scholar Graduate of Virginia Polytechnic Institute and State University (Va. Tech), Blacksburg, Va., earning his *Bachelor of Science in Education* in 1993, and was named the College of Education's Outstanding Senior of the Year. Prior to matriculating in the Graduate Program in Physical Therapy at Duke University, Durham, North Carolina (N.C.), in 1993, John spent the summer as an adjunct instructor at New River Community College, Dublin, Va. He graduated with a *Master of Science* from the Graduate School and a *Certificate of Physical Therapy* from the School of Medicine, Duke University in 1995.

John received his physical therapy license from the N.C. Board of Physical Therapy Examiners August 11, 1995. He subsequently began working as a physical therapist for Hillhaven (now Vencor) in Durham and Greensboro, N.C. In 1996, he left Vencor and began working in the Department of Physical and Occupational Therapy, Duke University Hospital, Durham, N.C., where his primary responsibility was the evaluation and treatment of inpatient adult medical patients especially those with cardiac and respiratory disorders; in addition, he served as a clinical instructor for five physical therapy students, and gave several lectures each year to students in Duke University's Graduate Program in Physical Therapy. He became a Board-Certified Clinical Specialist in Cardiovascular and Pulmonary Physical Therapy April 26, 1999.

In 2000, John matriculated into the Department of Physiology's graduate program, Medical College of Virginia Campus, Virginia Commonwealth University, Richmond, Va., under the mentorship of Dr. Roland N. Pittman, who trained him in microcirculatory and respiratory physiology. While at Virginia Commonwealth University, he completed the Preparing Future Faculty in the Professions' certificate program, was awarded both the University's Outstanding Leadership and Service Awards, and was also awarded a $15,000 scholarship from the Foundation for Physical Therapy. During this time, John served his profession as a member of both the American Board of Physical Therapy Specialties' Specialization Academy of Content Experts, and the Federation of State Boards of Physical Therapy's Physical Therapist Assistant Examination Construction and Review Committee. Throughout his studies, John continued to work part-time as a physical therapist at Duke University Hospital.

John has been married to Mary E. (Beth) Lindsay since August 17, 1996; they are godparents to three of their nieces.